AN INVESTIGATION OF THE STATIC STABILITY OF CORRUGATED RECTANGULAR PLATES LOADED IN PURE SHEAR

by

David E. McFarland
B.S., Wichita State University, 1961
M.S., Wichita State University, 1964

Submitted to the Department of Mechanics and Aerospace Engineering and the Faculty of the Graduate School of the University of Kansas in partial fulfillment of the requirements for the degree of Doctor of Philosophy.

Advisory Committee:

Redacted Signature

Chairman

Redacted Signature

Redacted Signature

January, 1967

ACKNOWLEDGMENTS

The author wishes to take this opportunity to express his appreciation to the many people who have contributed of their time and energy to this investigation. The author is especially indebted to Dr. John T. Easley for the guidance and encouragement he provided throughout this investigation, and to Dr. Kenneth H. Lenzen for his continued assistance to the author's educational program. The author would also like to thank the Butler Manufacturing Company for the financial assistance provided and in particular, John D. Wright, James W. Martin and Lloyd G. Jackson of the Butler Manufacturing Company for the many hours invested in the experimental portion of this investigation. In addition, the author wishes to acknowledge the assistance which was provided to this investigation by the use of the University of Kansas Computation Center 7040 I.B.M. computer. The author is also deeply indebted to his wife Marcia for her patience and unending assistance to the author in his work on this investigation in particular, and his seemingly unending educational program in general.

TABLE OF CONTENTS

TABLE OF CONTENTS (continued)

CHAPTER I

INTRODUCTION

The purpose of this dissertation is to study the buckling behavior of a corrugated panel of arbitrary cross-section subjected to in-plane shear loads. A typical corrugated panel is formed from a flat sheet of thin metal. Sample sections from three typical corrugated panels are shown in Figure 1.

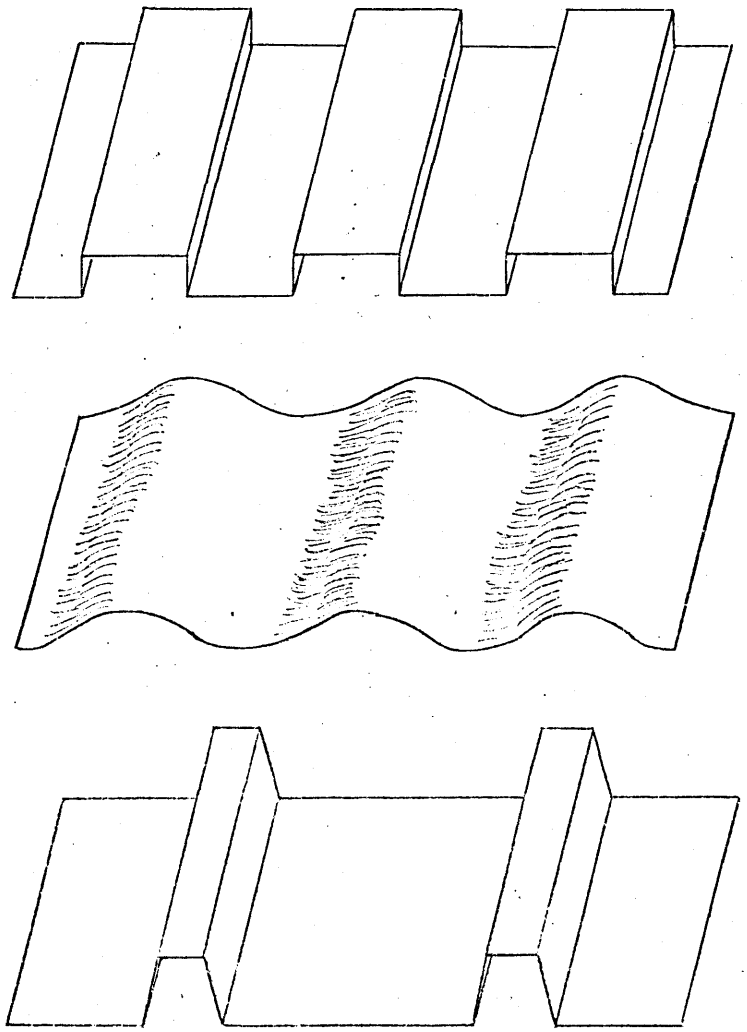

Figure 1

An understanding of this topic is of considerable importance because of the wide spread use of these types of panels in building construction. In particular, interest has developed in the analysis of corrugated panels which are designed to act as shear diaphrams, i.e. roof, wall, or floor panels in a building which act in shear to resist wind loadings without the aid of diagonal framing members. Also, light-weight, high-strength structures can be made from this type of panel which could conceivably play an important role in future construction in space.

Very few previous investigations have been made of this type panel. The few investigators who have completed analyses related to the problem of corrugated panels in shear have been primarily interested in aircraft structures, and hence, in long narrow flat plates to which identically spaced, equal ribs have been attached.[1] and [2]* This type of panel is similar to a corrugated panel, although its behavior is different. A corrugated panel is considerably the more flexible of the two types of panels due to the bending of the thin components of the corrugations which occur as a result of load perpendicular to the corrugations.

---

*Numbers in square brackets refer to references listed at the end of this work.

Timoshenko[3], presents an analysis of a corrugated plate in shear, but the plate is assumed to be a standard orthotropic plate, and the analysis is directed only toward determining the buckling load by means of the standard differential equation for an orthotropic plate. Hence, very little insight into the problem is provided. In addition, very little has been done to specialize even this limited information to make it applicable to an arbitrary corrugated panel.

In order to clarify the specific problem of buckling of a corrugated panel in shear, a considerably more thorough analysis than has previously been conducted is presented in this paper. In this analysis, equations are derived which define the buckling load, the buckled shape and the post buckling behavior of an arbitrary corrugated panel in shear.

The solution is obtained by first replacing the corrugated panel with an equivalent special orthotropic flat plate for which the appropriate material properties are derived. These material properties depend upon the particular corrugated shape and must be derived for a specific corrugated plate. Then, assuming that this orthotropic plate is acted upon by bending moments, twisting moments and membrane forces, a general equation for the potential energy of the system is derived in terms of displacements. From this equation for the potential

energy, expressions describing the buckling behavior of the plate are developed using techniques of calculus of variations and the Ritz energy method.

In conjunction with the theoretical study, a number of tests were conducted on corrugated panels of building construction size with various cross-sections to measure their buckling loads and observe their general behavior. The test data obtained from tests of panels of three different corrugation shapes is used to verify and supplement the theoretical analysis presented herein.

CHAPTER II

DEFINING THE MODEL OF THE CORRUGATED PLATE

The first and most crucial step in this analysis of corrugated plates in shear is to choose a model which most closely represents the corrugated plate. Once the model is selected and carefully defined, the appropriate mathematical tools can be applied to obtain a solution.

The model chosen is an orthotropic plate which has material constants equaling the average material constants of the corrugated panel. The orthotropic model seems to be a good choice for this analysis since the interest here is in over-all plate buckling, and not local buckling or stresses. This choice is substantiated by the buckled patterns created in the panels tested during the experimental portion of this investigation. In these tests, the buckles occur diagonally across the plate, and appear to be independent of local shapes of the corrugation. (See Figure 58).

To determine the material constants and corresponding load deflection relations of the orthotropic model, an element from the corrugated panel is analyzed. A square element is chosen with sides equal in length to the distance between repeating cross-sections of the corrugation. This element is illustrated in Figure 2.

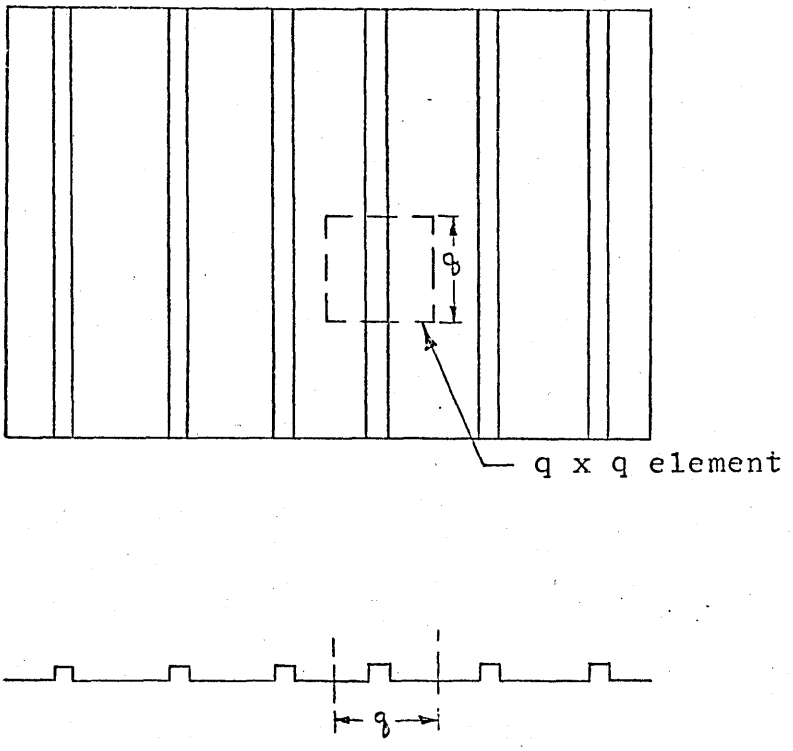

Figure 2

The components of the element contribute in varying ways to its load-deflection relations, and therefore the total load-deflection relations are viewed as indicators of the average material constants for the panel. It is then these average values that in this report are assumed to apply to an infinitesimal element from an orthotropic plate.

Before load-deflection relations can be derived, it is necessary to estimate the nature of the internal loads acting on the element and to decide which loads are pertinent to the analysis. The loads to be considered are indicated in the following sketch which shows only the loads on positive faces.

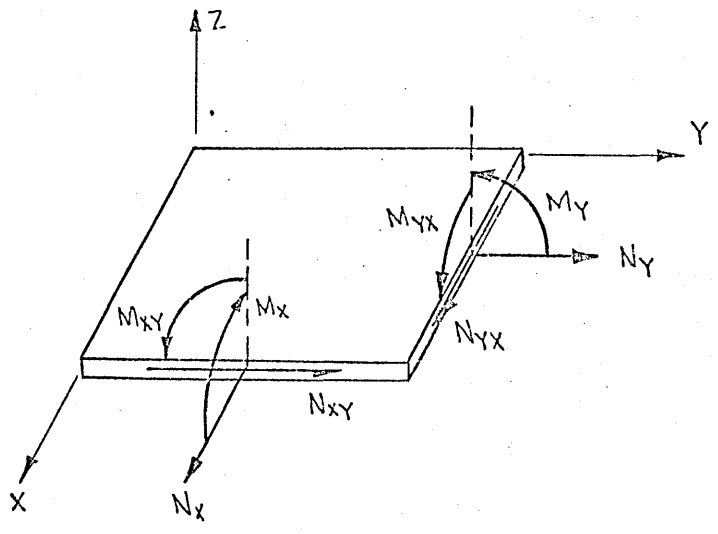

Figure 3

The membrane forces N_x, N_y and N_{xy} are given in units of pounds per inch and the moments M_x, M_y and M_{xy} are given in units of inch pounds per inch.

It should be noted that transverse shear has been omitted from the forces considered to be acting on the element. It is easily visualized that on the faces parallel to the corrugations, the contribution of transverse shear to deflection compared to the deflection due to bending can be neglected as is commonly done in the theory of thin plates. However, on the planes perpendicular to the corrugation, where the cross section can be relatively deep, it would seem possible that transverse shear might play a major role in deflection. Pursuing this further, it is observed that if the span-depth ratio of a beam is of the order of magnitude of fifteen or more, the transverse shear deflection is negligible when compared to bending deflection.[4] The

panels tested as a part of this investigation are considered to be typical corrugated panels, and their span-depth ratios vary from approximately twenty-five to one hundred and seventy-five, thus making it reasonable to assume that the effects of transverse shear are also negligible on the faces perpendicular to the corrugations.

When the loads acting on the qxq element have been defined the equations relating these loads to the deflections and the corresponding material constants can be derived. In doing so however, it is necessary to define the coordinate system which is used throughout the analysis. The x and y coordinates are placed in the plane of the plate in the following manner.

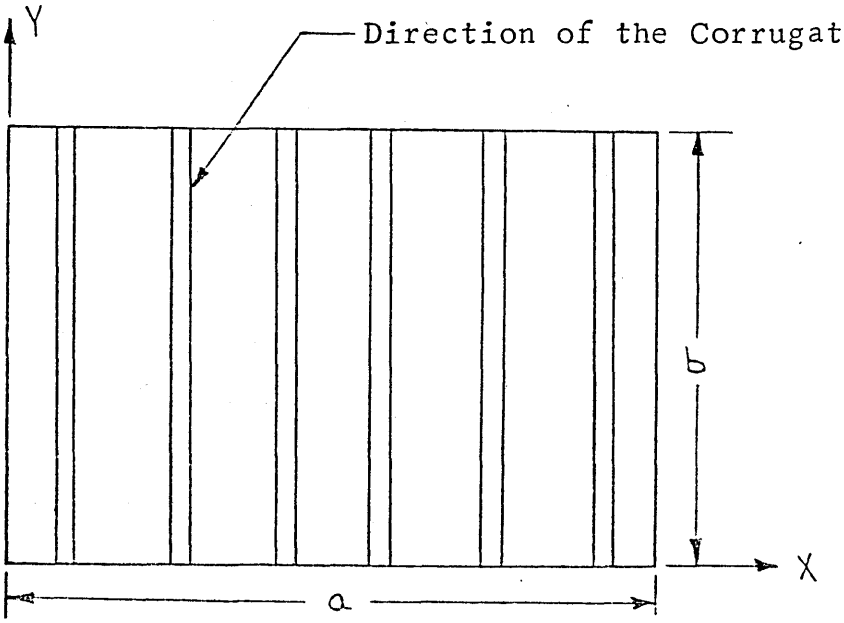

Figure 4

The geometry of the corrugated plate is defined by the following symbols.

a = plate dimension in the x direction

b = plate dimension in the y direction

h = corrugated plate thickness (base metal)

s = actual rolled out material length contained in the plate portion for which q is the projected length (i.e. actual material length of the repeating cross-section)

$\bar{I}$ = moment of inertia of one repeating cross-section about its neutral axis

Now, using the preceeding symbols and coordinate system the relation between load in the y direction and deflection in the y direction is considered. The force $N_y q$ is assumed to act on the q x q element as shown.

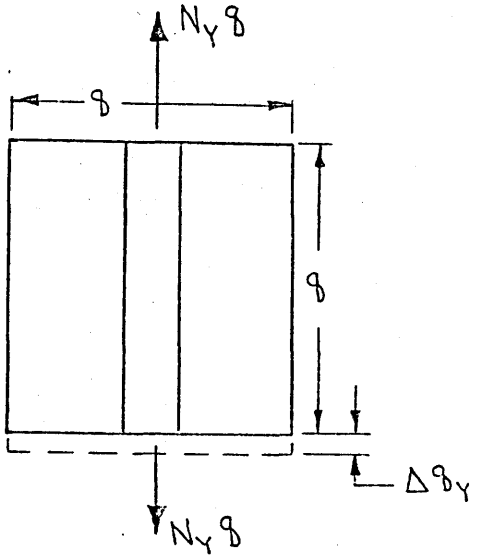

Figure 5

Then by definition

$$\epsilon_Y = \Delta q_Y / q = \sigma_Y / E_Y$$

in which Δq_y = the change in q in the y direction due to N_y

$\sigma_y = N_y q/hs$

$E_y = E$ = Young's modulus of elasticity for the particular material

which gives

$$\epsilon_Y = \frac{N_Y q}{E h S} \qquad (1)$$

Next, the load-deflection relation for loads and deflections in the x direction is derived. The following element is considered:

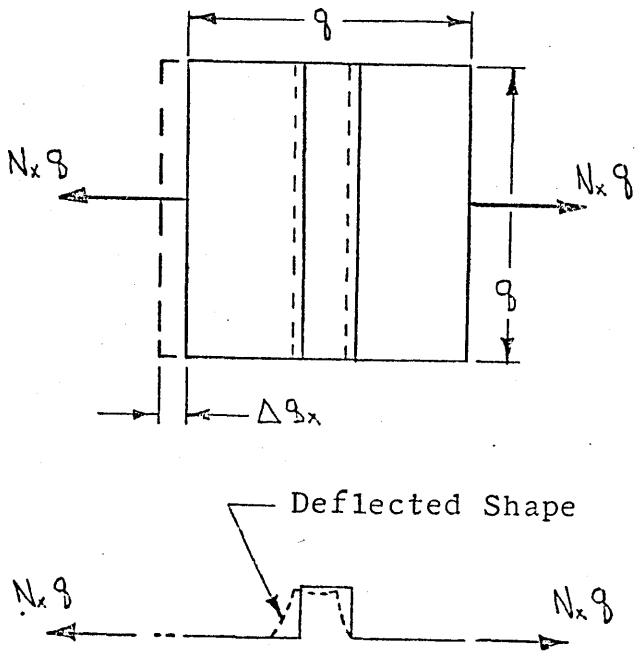

Figure 6

Again, strain is

$$\epsilon_x = \Delta q_x / q = \sigma_x / E_x$$

Then in this case, it is obvious that ϵ_x is not the strain that is normally visualized, since it does not represent the strain at any particular point in the panel. Instead, it merely represents the average deflection per unit length across the element. Therefore, this relation gives an indication of the behavior of the plate as a whole, but certainly has no meaning applied to an arbitrary area or point in the panel.

Now, since $\sigma_x = N_x/h$, the average material constant E_x is equal to the slope of the N_x/h versus $\Delta q_x/q$ curve. The resulting equation becomes

$$\epsilon_x = \frac{N_x}{E_x h} \qquad (2)$$

It is illustrated later in this report that the actual value of E_x is not needed for this analysis; however, if for some reason the magnitude of E_x is desired, it can be obtained by test or by using Castigliano's Theorem. General equations which can be used to compute E_x for most corrugated shapes are given in Appendix A. It is interesting to note that E_x will be much smaller than the actual Young's modulus of elasticity associated with the particular material.

After equations (1) and (2) are derived for uniaxial loading in each case, it is necessary to write expressions for biaxial loading. Utilizing equations (1) and (2), the following equations can be listed:

$$\epsilon_y = \frac{N_y \varphi}{E h s} - \nu_x \frac{N_x}{E_x h} \tag{3}$$

$$\epsilon_x = \frac{N_x}{E_x h} - \nu_y \frac{N_y \varphi}{E h s} \tag{4}$$

in which

ν_x = lateral deflection in the y direction due to an axial deflection in the xidirection

ν_y = lateral deflection in the x direction due to an axial deflection in the y direction

As with E_x, the actual values of ν_x and ν_y are not needed in this analysis. When needed, they are best obtained by conducting appropriate experiments with an actual section of the panel in question. Approximations for ν_x and ν_y have been obtained theoretically and are presented in Appendix A.

The final relations needed must give N_x and N_y as functions of ϵ_x and ϵ_y. Therefore, solving equations (1) and (2) simultaneously,

$$N_x = k_1 E_x (\epsilon_x + \nu_y \epsilon_y) \tag{5}$$

$$N_Y = \frac{k_1 E S}{g}(\epsilon_Y + \nu_X \epsilon_X) \qquad (6)$$

in which

$$k_1 = \frac{h}{(1-\nu_X \nu_Y)}$$

In order to complete the load-deflection analysis of the membrane forces, shearing stresses and shearing strains are examined. The assumption that body forces are zero leads to the basic equality that

$$N_{xy} = N_{yx}$$

The load-displacement relation is

$$\frac{N_{XY}}{h} = \frac{N_{YX}}{h} = G_{XY}\gamma_{XY} = G_{XY}\gamma_{YX} \qquad (7)$$

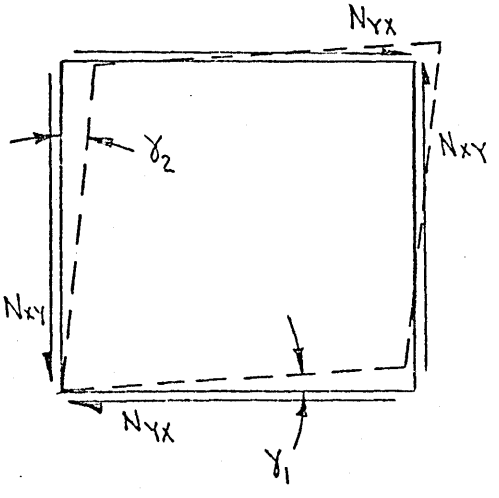

Figure 7

in which

$$\gamma_1 + \gamma_2 = \gamma_{XY} = \gamma_{YX}$$

The constant G_{xy} can best be determined by an experimental analysis, although it can also be determined analytically. Just as with several of the other constants, the value of G_{xy} is not important in this analysis, but a theoretical approximation for G_{xy} is given in Appendix A.

This completes the load-displacement relations for the membrane forces, and leads to consideration of similar relations for bending and twisting moments.

Just as was done with the membrane forces N_x and N_y, each of the bending moments are analyzed separately before considering situations in which both act simultaneously. If the moments are treated separately the following relations are defined:

$$M_Y = H_Y \Theta_Y \tag{8}$$

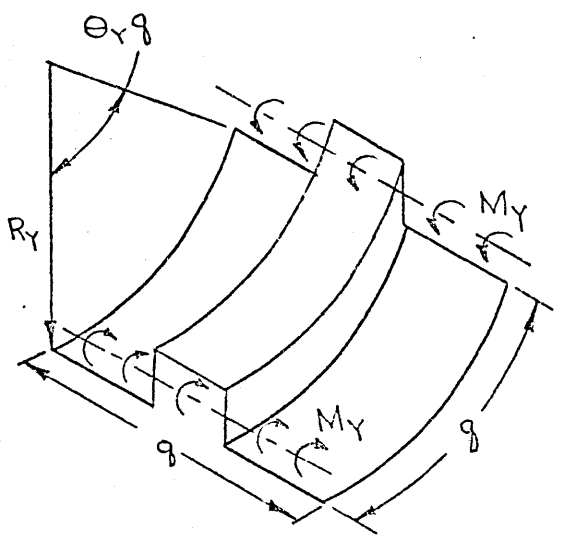

Figure 8

$$M_x = H_x \theta_x \tag{9}$$

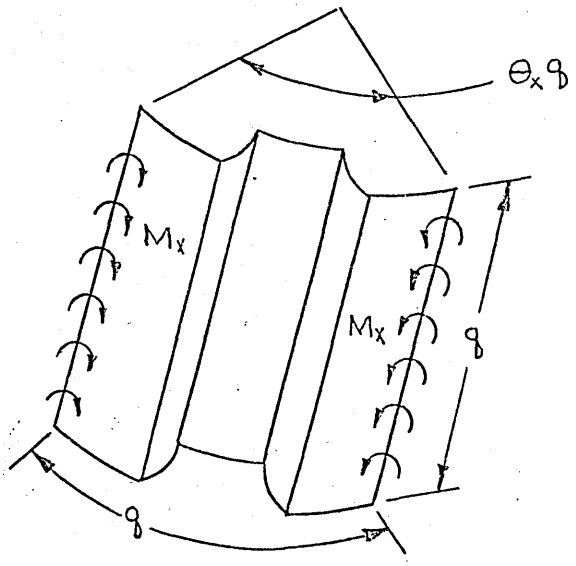

Figure 9

The constants H_y and H_x are an important part of the final results presented in this report, and are therefore examined in more detail at this time. It is observed, that when M_Y alone is applied, the plate behaves as a beam with a constant cross-section. Consequently, using basic strength of materials techniques, the following result is obtained:[4]

$$\theta_Y = \frac{1}{R_Y} = \frac{M_Y q}{E \bar{I}} \tag{10}$$

Now by equating θ_y from equations (8) and (10) H_y is seen to be

$$H_Y = \frac{E \bar{I}}{q} \tag{11}$$

To compute H_x it is assumed that all angles formed at the junctions of the various components of the corrugation remain constant under load. Then, using Castigliano's Theorem, and noting the total moment (M) is given by

$$M = M_x q$$

the total angle ($\theta_x q$) is found to be

$$\theta_x q = \int_0^S \frac{M \frac{\partial M}{\partial (M_x q)}}{EI} ds = \frac{MS}{EI} \qquad (12)$$

where

$$I = q h^3 / 12$$

Simplifying equation (12) by substituting in the above equations for M and I, the expression for θ_x becomes

$$\theta_x = \frac{12 M_x S}{q h^3 E} \qquad (13)$$

Now from equations (9) and (13) H_x is derived as

$$H_x = \frac{E h^3 q}{12 S} \qquad (14)$$

At this point it is necessary to determine whether any significant effect is made on θ_y by M_x or on θ_x by M_y. It is first noted that the actual values of H_x and H_y

which were computed for the panels used in the experimental portion of this investigation, show the difference in magnitude of H_y and H_x to be of the order

$$H_Y / H_X = 10^4$$

The assumption is made that Θ_x and Θ_y are of the same order of magnitude, and observation of the panels which were tested shows this assumption to be reasonable. Therefore, comparing equations (8) and (9) and using the fact that $H_x >> H_y$, it is concluded that $M_y >> M_x$.

With the preceeding information in mind, M_x is now applied to the q x q element.

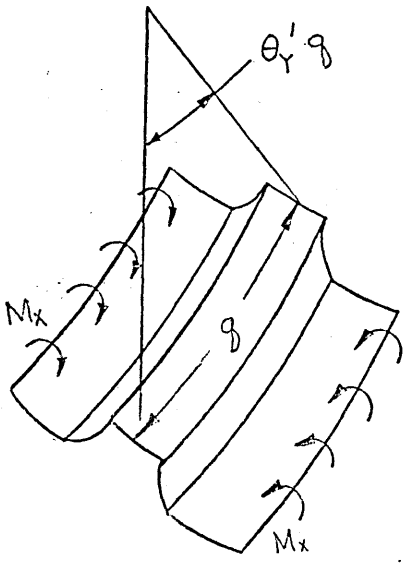

Figure 10

It is reasonable to assume that the Poisson effect will cause some type of curvature $\theta'_Y q$ in addition to $\Theta_x q$. It is also clear that M_x will have a different effect on the Θ_y of each leg of the corrugation which will in some

way depend on the shape and location of the leg. The overall effect on θ_y will be a complicated function of the geometry of the corrugated shape. Fortunately, this does not appear to be a problem since M_y has been shown to be much greater than M_x, and therefore the relatively small moment M_x should have little effect on θ_y compared to the contribution from M_y. Consequently, equation (8) is assumed to be applicable when M_x and M_y are applied simultaneously.

The effect of M_y on θ_x can be observed by looking again at a section of an arbitrary corrugated panel with the moment M_y applied.

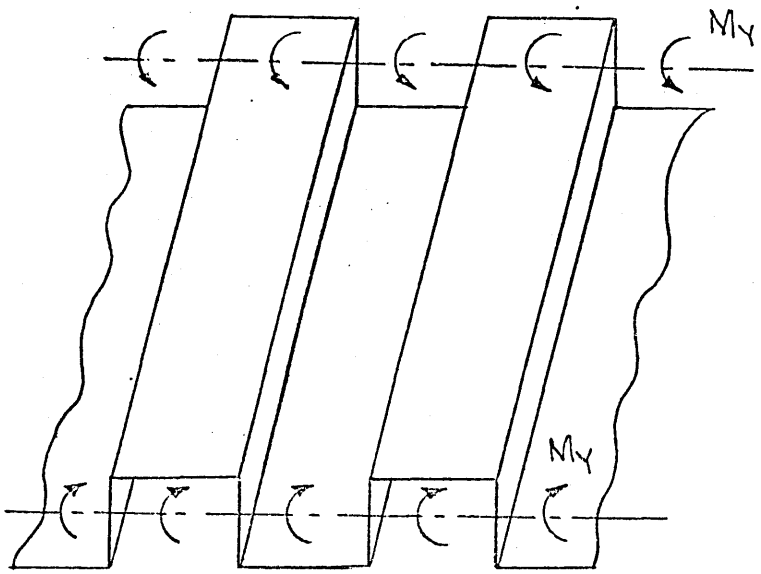

Figure 11

From an end view of the cross-section, the following approximate displacements are found to occur due to the Poisson effect.

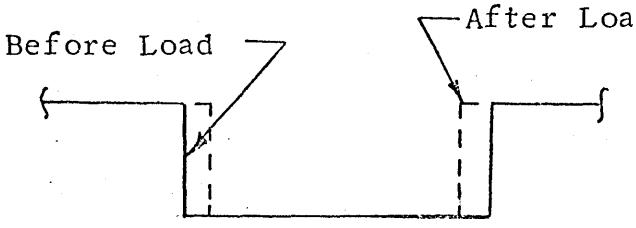

Figure 12

It is noted that the Poisson effect caused the upper surface to lengthen and lower surface to shorten with a net change in geometry but no change in θ_x. It is then assumed that equation (9) which shows M_y to have no effect on θ_x is correct in the form presented.

This completes the analysis of bending moments and leads to the final step in the analysis of load deflection relations, that of relating twisting moments to the angles of twist. Again the relations are first defined by examining both M_{xy} and M_{yx} individually

$$H_{XY} = M_{XY} / \theta_{1XY} \qquad (15a)$$

$$H_{YX} = M_{YX} / \theta_{2YX} \qquad (15b)$$

It is now possible to demonstrate that H_{xy} must equal H_{yx}. M_{xy} is first applied to a square element. M_{yx} is added to the same element, and the total external work is computed as shown.

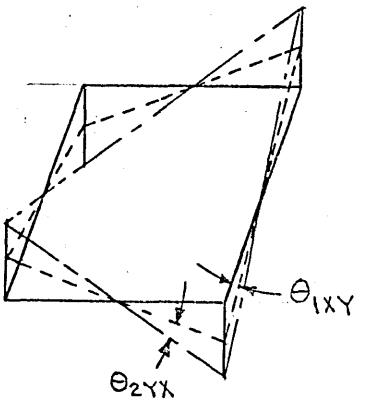

Figure 13

In the preceeding figure θ_{1xy} is caused by the application of M_{xy} and θ_{2yx} is caused by the application of M_{yx}. The resulting external work (W_1) is

$$W_1 = \frac{1}{2} M_{xy} \theta_{1xy} + \frac{1}{2} M_{yx} \theta_{2yx} + M_{xy} \theta_{2yx}$$

In a similar manner, the moments are applied in reverse order and the work (W_2) is given as

$$W_2 = \frac{1}{2} M_{yx} \theta_{2yx} + \frac{1}{2} M_{xy} \theta_{1xy} + M_{yx} \theta_{1xy}$$

Using the equality

$$W_1 = W_2$$

gives

$$\theta_{2yx} M_{xy} = \theta_{1xy} M_{yx}$$

and by inserting the relations listed in (15a) and (15b) it is shown that

$$H_{xy} = H_{yx}$$

Then, realizing that with both twisting moments applied

$$\theta_{1XY} + \theta_{2YX} = \theta_{XY} = \theta_{YX} \tag{16}$$

and substituting (15a) and (15b) into (16), the final equation is obtained as follows,

$$M_{XY} + M_{YX} = H_{XY}\,\theta_{XY} \tag{17}$$

The constant H_{xy} can be determined theoretically or experimentally. If the q x q element is treated as a shaft of non-circular cross section it follows that [4]

$$H_{XY} = \frac{G h^3 S}{3 q} \tag{18}$$

This completes the derivation of load-deflection relations. The resulting set of equations are summarized below.

$$\left.\begin{aligned} N_X &= k_1 E_X (\epsilon_X + \nu_Y \epsilon_Y) \\ N_Y &= \frac{k_1 E S}{q} (\epsilon_Y + \nu_X \epsilon_X) \\ N_{XY} &= G_{XY}\, h\, \gamma_{XY} \\ M_Y &= H_Y \theta_Y \\ M_X &= H_X \theta_X \\ (M_{XY} + M_{YX}) &= H_{XY}\,\theta_{XY} \end{aligned}\right\} \tag{19}$$

It is realized that as the load is increased and the buckled pattern forms, the shape of the corrugation begins to distort. Therefore, the terms E_x, G_{xy}, H_x, H_y and H_{xy}, which depend on the geometry of the corrugated cross-section, will change. From observation of the tests, it does not appear that this effect is significant until very large lateral deflections are reached. As is explained in detail in the section pertaining to large deflections, the large deflection analysis in this investigation was performed to obtain an indication of the load versus lateral deflection pattern in the immediate area of the bifurcation point, and the theory developed herein is not intended to pertain to deflections which are large enough to cause significant distortion of the cross-section. Consequently, the average material constants are assumed, as the name implies, to remain constant with variations in load and the corresponding deflections. Throughout the remainder of this analysis, the corrugated plate will be replaced by the orthotropic model. Then the response of the infinitesimal element, which becomes the basis of the analysis later in this investigation, is controlled by the load-displacement relations given in (19). Having defined the plate which is to be analyzed, a discussion of the mathematical techniques which are to be used in obtaining the final solutions defining the buckling of an arbitrary corrugated panel will follow.

CHAPTER III

INTRODUCING THE STABILITY CRITERIA BY MEANS OF CALCULUS OF VARIATIONS

In this investigation, the desired insight into the problem of buckling of a corrugated plate in shear is obtained by applying some of the techniques of calculus of variations to the orthotropic model of the corrugated plate. Therefore, it is necessary to outline the applicable calculus of variations, and to briefly illustrate how this method leads to a solution of the problem.

Before deriving the criteria which specify the equilibrium of a conservative system and define the stability of the system, the terms virtual work, virtual displacement and potential energy must be defined. It is noted, that any system whether in equilibrium or not, can be imagined to be held in a fixed position by adding the necessary additional forces to that system; it is also noted that this system can be moved from one configuration to another. With the imaginary displacement and correspoding set of forces in mind, the displacement is defined as a virtual displacement, the necessary forces are virtual forces, and the work done by the virtual forces during the virtual displacement is termed virtual work. Virtual displacement is imagined to take place at an infinitesimal speed, so that the particles of the system remain in

equilibrium under the action of the real and imaginary forces. It is observed that the virtual work will be the negative of the work of the real system.

As a system is moved from configuration X_1 to another configuration X the virtual work is expressed as $V(X_1,X)$; and $V(X_1,X)$ is in turn called the potential energy of the system in the X configuration. Later, it will be shown that the only interest this analysis has in the potential energy is the changes that occur in it as the corresponding system moves from one configuration to another. Since changes in the potential energy from the potential energy in configuration X are independent of the reference point X_1, the potential energy is expressed merely as V(X). It is also convenient to separate the potential energy into two components such that

$$V = \Omega + U$$

in which Ω is the potential energy of the applied loads and U is the internal strain energy of the system.

With this background, the role that calculus of variations plays in the solution of a stability problem is most easily understood by considering a conservative system with one degree of freedom. For this system, the potential energy is defined as V = V(y) where y is the coordinate that defines the configuration of the system. If V(y) and its derivatives are continuous in the interval $y_1 < y < y_2$,

and the points c and $c+\epsilon$ are included in this interval, then the potential energy of the system in the configuration $(c+\epsilon)$ can be represented as a function of the potential energy of that system and its derivatives in the configuration c by Taylor's expansion theorem as follows:

$$V(c+\epsilon) = V(c) + \epsilon V'(c) + \frac{\epsilon^2}{2} V''(c) + \cdots + \frac{\epsilon^{m-1}}{(m-1)!} V^{m-1}(c) + \frac{\epsilon^m}{m!} V^m(d)$$

in which d is some point which lies between c and $(c+\epsilon)$

The quantity ϵ can be viewed as a virtual displacement of the system from point c. It is obvious that the change in the potential energy of the system during the virtual displacement is

$$\Delta V = V(c+\epsilon) - V(c) = \epsilon V'(c) + \frac{\epsilon^2}{2!} V''(c) + \cdots + \frac{\epsilon^{m-1}}{(m-1)!} V^{m-1}(c) + \frac{\epsilon^m}{m!} V^m(d) \qquad (21)$$

Now from the well-known condition which states that potential energy must be a minimum it is necessary that

$$\lim_{\epsilon \to 0} \frac{\Delta V}{\epsilon} = 0$$

for equilibrium to exist. This shows the criteria for the

existence of an equilibrium configuration at c to be $V'(c) = 0$.

Then, under the condition that $V'(c) = 0$, the condition which specifies the stability of equilibrium can also be obtained. To do this, it must be realized that if ϵ is sufficiently small, equation (21) is a converging series, and the first non-zero term will determine the sign of ΔV. The importance of the sign of ΔV is made clear by recalling that only conservative systems are being considered, and noting therefore that a negative change in the potential energy of a system during a virtual displacement indicates an increase in the kinetic energy of the system. This implies a tendency for the system to diverge from its position, and thereby shows that a negative ΔV from an equilibrium configuration indicates an unstable equilibrium configuration. Similarly, a tendency to return to an equilibrium positive, i.e. stable equilibrium, is shown by a positive ΔV.

Therefore, the stability of a single-degree-of-freedom system in a particular equilibrium configuration can be determined by imagining an arbitrary infinitesimal virtual displacement from that configuration, and by then examining the subsequent sign of the first non-zero term in equation (21). Later in this report, when considering the orthotropic plate in shear with infinite degrees of

freedom, an expression analagous to V''(c) for the single-degree-of-freedom system is developed which is a function of the external load (Py). This expression can be positive, negative, or zero for different values of Py. If it is postulated that for the single-degree-of-freedom system V'' is a function of Py, and can be positive, negative, or zero depending on the magnitude of Py, then it is apparent that an equilibrium configuration is stable if Py is of such a nature that V'' is positive, unstable if Py is such that V'' is negative and neutral if Py is such that V'' = 0. To physically interpret a neutral equilibrium configuration, it is pointed out that after an infinitesimal displacement from this configuration, the system will remain in the new configuration, i.e. it will neither attempt to return to the old configuration nor diverge to a new one. To determine then, the external load at which the transition from stable to unstable equilibrium occurs, i.e. neutral equilibrium, the condition V''(c) = 0 must be examined.

Basically, the same procedures are followed in cases with more than one degree of freedom, although the mechanics of the solution become more complex. In cases with more than one degree of freedom, the standard notation for equation (21) becomes;

$$\Delta V = \delta V + \frac{\delta^2 V}{2!} + \frac{\delta^3 V}{3!} + \cdots + \frac{\delta^{m-1} V}{(m-1)!} + \text{REMAINDER} \qquad (22)$$

in which δV is defined as the first variation of V,
$\delta^2 V$ is defined as the second variation of V.
etc.

Using the notation of equation (22), it is then stated that the necessary condition for equilibrium is that $\delta V = 0$ for any infinitesimal virtual displacement consistent with the constraints. Similarly, the condition that $\delta^2 V = 0$ specifies neutral equilibrium, and it is from this condition that the critical buckling load, i.e. load just before buckling, can be obtained.

This completes the summary of the basic mathematical tool to be used in this analysis, and it is now necessary to develop the equation for the potential energy of the corrugated plate.

CHAPTER IV

DEVELOPING THE EQUATION FOR POTENTIAL ENERGY

The method chosen to solve the buckling problem of corrugated plates in shear involves applying virtual displacements to the plate; and examining the resulting change in the potential energy. It is thus necessary to derive a general expression for the equation of potential energy.

At this point, the corrugated plate has been replaced by an orthotropic plate. An infinitesimal element of the plate is shown in the following figure, and the internal forces acting on the element are indicated on the positive faces. With the figure as a guide, the differential change in strain energy due to a virtual displacement from a zero stress is

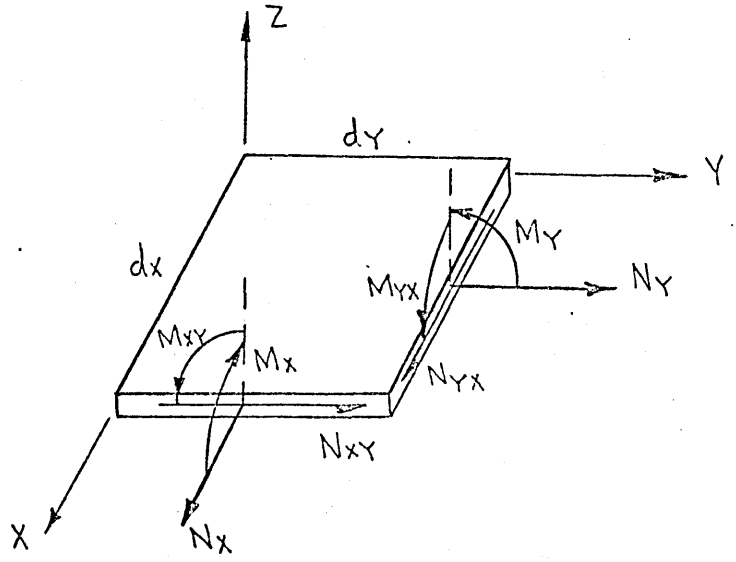

Figure 14

$$dU = \frac{1}{2}\left[N_x\epsilon_x + N_y\epsilon_y + N_{xy}\gamma_{xy} + M_x\theta_x + M_y\theta_y + M_{xy}\theta_{xy} + M_{yx}\theta_{yx}\right]dy\,dx \tag{23}$$

Now, substituting the load-deflection relations given in (20) into equation (23),

$$dU = \frac{1}{2}\left[k_1 E_x\epsilon_x^2 + \left(\nu_y k_1 E_x + \frac{\nu_x k_1 ES}{9}\right)\epsilon_x\epsilon_y + k_1\frac{SE}{9}\epsilon_y^2 + hG_{xy}\gamma_{xy}^2 + H_x\theta_x^2 + H_y\theta_y^2 + H_{xy}\theta_{xy}^2\right]dy\,dx \tag{24}$$

Eventually it will be necessary to determine the effects of specific displacements on the potential energy; therefore, the potential energy must be obtained in terms of displacements. If u, v and w represent the displacements in the x, y and z directions respectively, the strain displacement relations to be used are, [5] and [6]

$$\begin{aligned}
\epsilon_x &= u_x + \frac{1}{2}w_x^2 \\
\epsilon_y &= v_y + \frac{1}{2}w_y^2 \\
\gamma_{xy} &= u_y + v_x + w_x w_y \\
\theta_x &= w_{xx} \\
\theta_y &= w_{yy} \\
\theta_{xy} &= w_{xy}
\end{aligned} \tag{25}$$

in which each subscript on a displacement indicates a partial derivative of the displacement with respect to the subscript.

It is pointed out that quite often the terms involving derivatives of w are omitted from ϵ_x, ϵ_y and γ_{xy} when considering a small deflection theory. These terms are included in this analysis to account for the fact that w_x^2, w_y^2 and $w_x w_y$ are not small in this case compared to u_x, v_y, u_y and v_x even though w is small, and are not intended to indicate the consideration of large deflections, i.e. large w. [3]

Substituting the strain displacement relations given in (25) into equation (24), and integrating the resulting equation over the plate, the final expression for the total strain energy of the plate in terms of displacements is

$$U = \frac{1}{2}\int_0^a \int_0^b \Big\{ k_1 E_x (u_x + \tfrac{1}{2}w_x^2)^2 + \frac{k_1 S E}{9}(v_y + \tfrac{1}{2}w_y^2)^2$$

$$+ (\nu_y k_1 E_x + \frac{\nu_x k_1 E S}{9})(u_x + \tfrac{1}{2}w_x^2)(v_y + \tfrac{1}{2}w_y^2)$$

$$+ h G_{xy}(u_y + v_x + w_x w_y) + H_x w_{xx}^2 \qquad (26)$$

$$+ H_y w_{yy}^2 + H_{xy} w_{xy}^2 \Big\}\, dy\, dx$$

The potential energy, which is given by equation (20), contains the potential of the applied loads as well as the internal strain energy. Therefore, to complete the derivation of the total potential energy, the potential energy of the applied loads must be computed. In the experimental portion of this investigation, the plate was loaded as indicated in the following sketch.

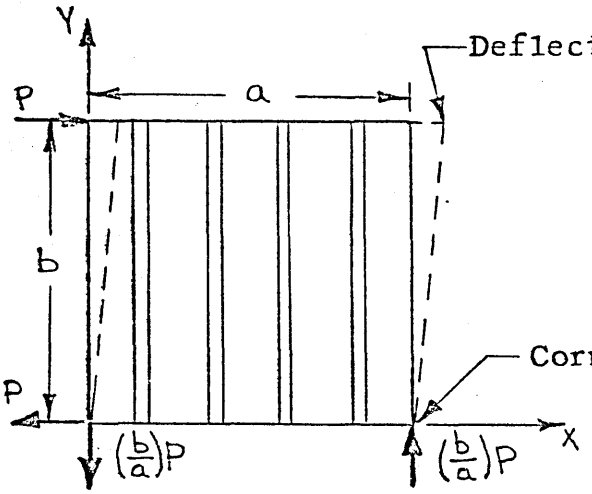

Figure 15

In a general analysis, where movement is also allowed at corner A of Figure 15, the external potential energy of the applied load is found to be

$$\Omega = -\int_0^a \int_0^b P_Y (u_Y + v_x)\, dy\, dx \qquad (27)$$

in which $P_Y = P/a$

However, when equation (27) is reduced to match the particular loading corresponding to the tests included as a part of

this analysis, i.e. setting $V_x = 0$, the external potential energy reduces to

$$\Omega = -\int_0^a\int_0^b P_Y u_Y \, dy\, dx \tag{27a}$$

The term V_x, shown in equation (27), will be included in the general expression and set equal to zero later in the derivation.

Combining equations (26) and (27) the equation for the total potential energy of the system corresponding to a virtual displacement from a zero stress configuration to an arbitrary state of stress becomes

$$\begin{aligned} V = \frac{1}{2}\int_0^a\int_0^b \Big\{ & k_1 E_x (u_x + \tfrac{1}{2}w_x^2)^2 + \frac{k_1 S E}{9}(v_y + \tfrac{1}{2}w_y^2)^2 \\ & + (\nu_y k_1 E_x + \frac{\nu_x k_1 E S}{9})(u_x + \tfrac{1}{2}w_x^2)(v_y + \tfrac{1}{2}w_y^2) \\ & + h G_{xy}(u_y + v_x + w_x w_y)^2 + H_x w_{xx}^2 + H_x w_{yy}^2 \\ & + H_{xy} w_{xy}^2 - 2P_y(u_y + v_x)\Big\} dy\, dx \end{aligned} \tag{28}$$

Having developed the general equation for potential energy, the next step becomes one of applying virtual displacements to various plate configurations, and then carefully examining the first and second variations of the potential energy to determine buckling loads, buckled patterns and load deflection curves.

This analysis is based on the assumption that the corrugated plate is loaded in pure shear. In reality, a corrugated plate fastened rigidly to frame members on all four sides, and loaded as shown in the preceeding sketch, is not in pure shear, but the actual loading condition is closely approximated by pure shear. Before proceeding to the derivation of the small deflection theory it is necessary to explain this.

The fact that the panel is not in pure shear is illustrated by considering a corrugation with the following cross-section:

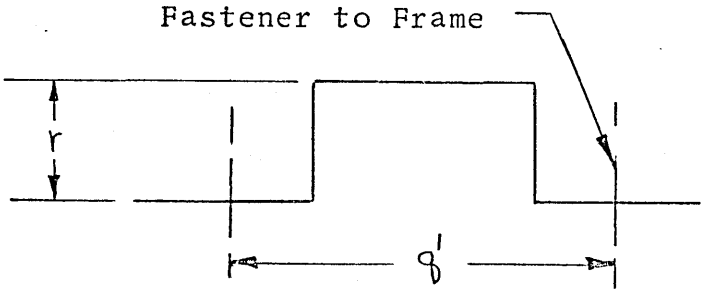

Figure 16

Then a plan view of the above corrugation in a deflected form is examined. The solid lines indicate the general shape which the corrugation must maintain due to the restraint of the frame, and the dotted lines show the configuration the corrugation would assume if it were in pure shear.

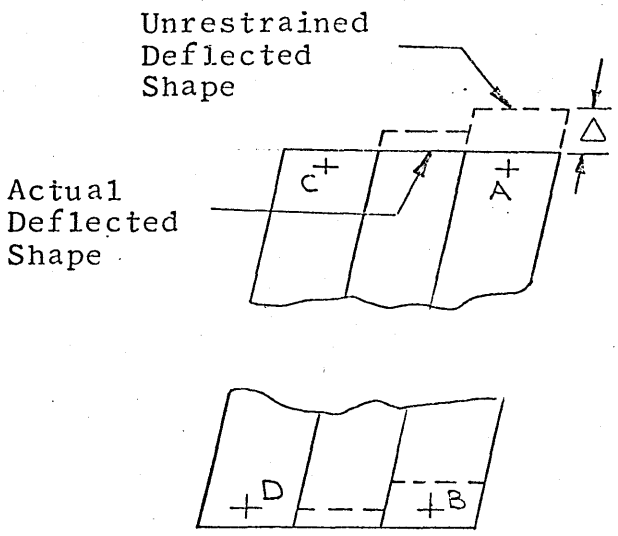

Figure 17

It is obvious from the figure that when the above corrugation is in pure shear, shear jumps will occur at the vertical components. It is also noted that regardless of the shape of the corrugations between fasteners, a corrugated panel which is imagined to be in pure shear will deflect farther than is actually permitted by the attachment to a rigid frame.

Since fastening the panel to a rigid frame prevents the panel from deflecting to the configuration it would assume under pure shear, it is then obvious that the panel is not in pure shear. This implies that normal forces are imposed upon the panel in order to force it to maintain the shape of the frame.

A rough estimate of the order of magnitude of the effect on buckling strength caused by restraining the shear jumps is obtained by assuming that the plate is unrestrained, and then adding the necessary forces at the

fastener locations which are needed to push the panel into the configuration consistent with the frame.

First, it is noted that the unrestrained panel deflects the amount Δ as indicated in the preceeding figure. The deflection Δ is

$$\Delta = 2r\gamma_{xy} = \gamma_{xy}(s' - q') \tag{29}$$

In equation (29) s' is the actual material length between fasteners, and q' is the projected distance as given in Figure 16.

Next it is assumed that equal forces (F/2) are applied at the fasteners A and B in order to push the corrugation back into a position which matches the frame. It is also assumed that the forces (F/2) are immediately distributed as shear down the length of the corrugation.

Now γ'_{xy}, the necessary strain to force the panel back into its actual shape, is

$$\gamma'_{xy} = \Delta / s' = \gamma_{xy}(s' - q') / s'$$

which gives

$$F = \frac{hbG_{xy}\gamma_{xy}(s' - q')}{s'} \tag{30}$$

The change in strain energy between the two fasteners is, therefore, given by

$$\frac{1}{2} F\Delta = \frac{hbG_{xy}\gamma_{xy}^2 (s' - q')^2}{2s'} \tag{31}$$

To obtain the total change in strain energy for one repeating cross-section, equation (31) must be computed for each section of the panel between two fasteners in the repeating cross-section. Then the total energy for the repeating cross-section (W') becomes

$$W' = \frac{hbG_{xy}\gamma_{xy}^2}{2} \sum_{i}^{\circ} \frac{(s_i' - q_i')^2}{s_i'} \tag{32}$$

in which i denotes each section separated by a fastener across one repeating cross-section

If the strain energy is assumed to be distributed uniformly over the panel, the additional differential strain energy becomes

$$dU' = \frac{hG_{xy}\gamma_{xy}^2}{2g} \sum_{i}^{\circ} \frac{(s_i' - q_i')^2}{s_i'} dy\, dx \tag{33}$$

Admittedly, this is a crude approximation, but as noted before, it gives an idea of the order of magnitude of the change in strain energy due to the restraint placed on the shear jumps.

It is noted that if equation (33) is added to the equation for internal strain energy it merely means changing the coefficient of $hG_{xy}\gamma^2_{xy}$ in equation (24) from 1 to $\left[1 + \frac{1}{2q}\sum_i \frac{(s_i' - q_i')^2}{s_i'}\right]$. This change in the coefficient of $hG_{xy}\gamma^2_{xy}$ was computed for the Butlerib, which was one of the primary panels tested in shear as part of this investigation, and the coefficient was found to change approximately one percent. Therefore, it is concluded that the effect of restrained shear jumps is negligible, and the arbitrary corrugated panel is assumed to be in pure shear. Consequently, equation (28) remains as the final equation for the potential energy. It is now possible to proceed to the derivation of the small deflection theory.

CHAPTER V

SMALL DEFLECTION THEORY

The work thus far in this paper has been concerned with the preparation of a foundation upon which to develop a solution to the problem of the buckling of a corrugated panel in shear. Having accomplished this, the analysis moves on to the obtaining of a solution. The first solution examined in this paper is essentially a small deflection analysis. It is designed to yield the buckling load as well as insight into the corresponding buckled pattern of an arbitrary corrugated panel.

To begin, recall that if a virtual displacement is taken from an equilibrium configuration, then the second variation ($\delta^2 V$) defines the stability of the equilibrium configuration. It is also known at this point that the straight-loaded form of the corrugated plate is an equilibrium configuration. Therefore, to obtain the desired solution, a virtual displacement will be taken from the straight-loaded configuration, and an expression for the second variation will be obtained as a function of the external load P. Consequently, the critical buckling load, i.e. the largest possible value of P before the system becomes unstable, can be obtained from the expression $\delta^2 V = 0$. Proceeding in the manner just described, the displacements in the straight-loaded form are found to be

$$\left.\begin{aligned} u &= u(Y) \\ V &= 0 \\ W &= 0 \end{aligned}\right\} \quad (34a)$$

which are directly followed by

$$V_X = V_Y = u_X = W_X = W_Y = W_{XX} = W_{YY} = W_{XY} = 0 \quad (34b)$$

If the plate is then given a virtual displacement from the loaded form such that the displacement components become

$$\begin{aligned} u &\longrightarrow u + \epsilon\xi \\ v &\longrightarrow \epsilon\eta \\ w &\longrightarrow \epsilon\zeta \end{aligned} \quad (35)$$

then (28), (34) and (35) lead to the following expression for the change in potential energy

$$\begin{aligned} \Delta V &= (V + \Delta V) - V \\ &= \frac{1}{2}\int_0^a\int_0^b \Big\{ k_1 E_X \left(\epsilon\xi_X + \tfrac{1}{2}\epsilon^2\zeta_X^2\right)^2 + \frac{k_1 SE}{q}\left(\epsilon\eta_Y + \tfrac{1}{2}\epsilon^2\zeta_Y^2\right)^2 \\ &\quad + k_1\left(\nu_Y E_X + \frac{\nu_1 S\Xi}{q}\right)\left(\epsilon\xi_X + \tfrac{1}{2}\epsilon^2\zeta_X^2\right)\left(\epsilon\eta_Y + \tfrac{1}{2}\epsilon^2\zeta_Y^2\right) \\ &\quad + hG_{XY}\left(u_Y + \epsilon\xi_Y + \epsilon\eta_X + \epsilon^2\zeta_X\zeta_Y\right)^2 \end{aligned} \quad (36)$$

(continued on next page)

(continued from previous page)

$$+ H_x \epsilon^2 \zeta_{xx}^2 + H_y \epsilon^2 \zeta_{yy}^2 + H_{xy} \zeta_{xy}^2$$

$$- 2P_y(u_y + \epsilon \xi_y + \epsilon \eta_x)\} dy\, dx \qquad (36)$$

$$- \frac{1}{2}\int_0^a \int_0^b (hG_{xy} u_y^2 - 2P_y u_y) dy\, dx$$

When equation (36) is expanded, and the terms containing ϵ raised to the same powers are grouped together, the form of ΔV is found to be similar to the form of equation (21). In this manner ΔV becomes

$$\Delta V = \epsilon\int_0^a \int_0^b \{hG_{xy}\xi_y u_y + hG_{xy}\eta_x u_y$$

$$- P_y\eta_x - P_y\xi_y\}\, dy\, dx$$

$$+ \frac{\epsilon^2}{2}\int_0^a \int_0^b \{k_1 E_x \xi_x^2 + \frac{k_1 S E}{q}\eta_y^2$$

$$+ k_1(\nu_y E_x + \frac{S\nu_x E}{q})\xi_x \eta_y$$

$$+ 2hG_{xy} u_y \zeta_x \zeta_y + hG_{xy}\xi_y^2 + hG_{xy}\eta_x^2 \qquad (37)$$

$$+ 2hG_{xy}\xi_y \eta_x + H_x \zeta_{xx}^2 + H_y \zeta_{xy}^2$$

$$+ H_{xy}\zeta_{xy}^2\}\, dy\, dx$$

$$+ \epsilon^3 \int_0^a \int_0^b \{\ *\ \}\, dy\, dx$$

$$+ \epsilon^4 \int_0^a \int_0^b \{\ *\ \}\, dy\, dx$$

* These expressions are not given since they are not pertinent to the analysis.

From equation (37), δV is identified as

$$\delta V = \epsilon \int_0^a \int_0^b \{hG_{xy} u_y - P_y\} \xi_y \, dy \, dx + \epsilon \int_0^a \int_0^b \{hG_{xy} u_y - P_y\} \eta_x \, dy \, dx \tag{38}$$

Since the condition for equilibrium requires that $\delta V = 0$, and it is known that the straight form in an equilibrium configuration, equation (38) must equal zero. Both integrals are equal to zero for arbitrary ξ and η only if

$$hG_{xy} u_y - P_y = 0 \tag{39}$$

Recalling that in the straight configuration γ_{xy} is defined such that

$$\gamma_{xy} = P_y / hG_{xy} = u_y$$

it is seen that equation (39) is automatically satisfied. Thus the first variation is indeed equal to zero when the plate is in a straight configuration.

Now the stability of the plate in the straight form must be determined, and to do this the second variation of the potential energy must be examined. From equation (39) $\delta^2 V$ is found to be

$$\delta^2 V = \epsilon^2 \int_0^a \int_0^b \left\{ \frac{k_1}{2} E_x \xi_x^2 + \frac{k_1 S E}{2\vartheta} \eta_Y^2 \right.$$

$$+ \frac{k_1}{2}\left(\nu_Y E_x + \frac{S\nu_x E}{\vartheta}\right)\xi_x \eta_Y + hG_{xY} U_Y \zeta_x \zeta_Y$$

$$+ \frac{1}{2} hG_{xY} \xi_Y^2 + hG_{xY} \xi_Y \eta_x + \frac{1}{2} hG_{xY} \eta_x^2 \qquad (40)$$

$$\left. + \frac{H_x}{2} \zeta_{xx}^2 + \frac{H_Y}{2} \zeta_{YY}^2 + \frac{H_{xY}}{2} \zeta_{xY}^2 \right\} dY\, dx$$

It will be shown that the contribution from ξ and η to $\delta^2 V$ is always equal to or greater than zero, and therefore ξ and η can be set equal to zero. First, suppose that the contribution to $\delta^2 V$ from ξ and η for all possible choices of ξ and η is equal to or greater than zero, and that this part of $\delta^2 V$ is called t. Then, when the system is unstable, the contribution to $\delta^2 V$ from ζ must be negative and is designated by λ, in which λ is a negative number. It is also noted that when the system is in an unstable equilibrium configuration the inequality

$$|\lambda| > t$$

must be satisfied. It will be shown later, that for any virtual displacement, the magnitude of $|\lambda|$ decreases as the applied load decreases, and hence the virtual displacement which will allow the smallest possible load to buckle the panel must be of such a nature that t equals zero.

The obvious choice which makes t equal zero is $\xi = \eta = 0$, and thus it is shown that if the contribution to $\delta^2 V$ from ξ and η is always equal to or greater than zero, then ξ and η can be set equal to zero.

To demonstrate that indeed the contribution of ξ and η to $\delta^2 V$ is always equal to or greater than zero, the terms containing ξ and η are examined. The following expression represents the total contribution of ξ and η to $\delta^2 V$.

$$\frac{k_1 E_x}{2}\xi_x^2 + \frac{k_1 S E}{2 g}\eta_Y^2 + \frac{k_1}{2}\left(\nu_Y E_x + \frac{S \nu_x E}{g}\right)\xi_x \eta_Y + \frac{h G_{xy}}{2}(\xi_Y + \eta_x)^2 \tag{41}$$

The last term in (41) is obviously equal to or greater than zero for all choices of ξ and η, and to show that the sum of the first three terms is equal to or greater than zero it is first observed that the expression

$$\left(\sqrt{\frac{k_1 E_x}{2}}\,\xi_x + \sqrt{\frac{k_1 S E}{2 g}}\,\eta_Y\right) = \frac{k_1 E_x}{2}\xi_x^2 + \frac{k_1 S E}{2 g}\eta_Y^2 + k_1\sqrt{\frac{S E E_x}{g}}\,\xi_x \eta_Y \tag{42}$$

is always equal to or greater than zero. From equation (42) it is apparent that the first three terms of expression (41) will be equal to or greater than zero if

$$k_1\sqrt{\frac{SEE_x}{\rho}} \geq \frac{k_1}{2}\left(\nu_y E_x + \frac{S\nu_x E}{\rho}\right)$$

which reduces to

$$E/E_x \geq \frac{\rho}{4S}\left(\nu_y + \frac{S\nu_x E}{\rho E_x}\right)^2 \qquad (43)$$

To examine this inequality, the estimated values of v_y and v_x derived in Appendix A are

$$\nu_y = \nu$$

$$\nu_x = \frac{E_x}{E}\nu$$

These substitutions further reduce equation (43) to

$$E/E_x \geq \frac{\rho\nu^2}{4S}\left(1 + \frac{S}{\rho}\right)^2 \qquad (44)$$

Since in general E/E_x is of the order of magnitude of 10^4 and $\frac{\rho\nu^2}{4S}\left(1 + \frac{S}{\rho}\right)^2$ is most often less than one, it is certainly safe to assume that equation (44) is satisfied, and therefore that the first three terms of equation (41) are positive.

Thus the assertion that the contribution to $\delta^2 V$ from ξ and η is always positive is verified, and it is possible to eliminate the variables ξ and η. The problem of determining at what point $\delta^2 V$ becomes negative is now reduced to

the consideration of the single variable ζ. The modified form of $\delta^2 V$ becomes

$$\delta^2 V = \epsilon^2 \int_0^a \int_0^b \{2hG_{xy} U_x \zeta_x \zeta_y + H_x \zeta_{xx}^2 + H_y \zeta_{yy}^2 + H_{xy} \zeta_{xy}^2\} dy\, dx \tag{45}$$

Noting that the relation $P_y = hG_{xx} \gamma_{xx} = hG_{xx} U_y$ remains constant during lateral displacement and setting $\delta^2 V = 0$, the equation which defines the critical buckling load is now defined as

$$\int_0^a \int_0^b \{2P_y \zeta_x \zeta_y + H_x \zeta_{xx}^2 + H_y \zeta_{yy}^2 + H_{xy} \zeta_{xy}^2\} dy\, dx = 0 \tag{46}$$

An approximate solution of equation (46) is then obtained by applying the Ritz method. Before an explanation of this method can be discussed, it must be noted that the exact solution for the buckling load (P_{cr}) results in a value of P_y below which the system has no deflected equilibrium configurations. This critical buckling load corresponds to the particular buckling pattern which results in the minimum strain energy of the panel. It is, then, evident that if the system is forced to buckle into some other pattern, but is still required to satisfy the forced boundary conditions, the strain energy and corresponding buckling load will be higher than P_{cr}. The Ritz method

involves assuming a buckled pattern which satisfies the forced boundary conditions, and then calculating the corresponding buckling load. Therefore, the buckling load computed by the Ritz method will always be higher than the exact solution for the buckling load, but if the buckled shape is closely approximated, then the corresponding buckling load will be closely approximated.

In this investigation the panels are assumed to be simply supported, and the desired solutions are obtained using each of the two choices given below to approximate the buckled configuration

$$\zeta = \sum_{M=1}^{\infty} \sum_{N=1}^{\infty} A_{MN} \sin\frac{M\pi x}{a} \sin\frac{N\pi y}{b}$$

and

$$\zeta = A \sin\frac{\pi y}{b} \sin\frac{m\pi}{a}(x-\alpha y)$$

The double Fourier sine series representation of ζ is selected since it is obvious that if enough terms are used, ζ can be closely approximated, and therefore a very accurate prediction of the buckling load can be obtained. The form $\zeta = A \sin\frac{\pi y}{b} \sin\frac{m\pi}{a}(x-\alpha y)$ is chosen since the buckled pattern of actual corrugated plates in shear appear to follow this form as can be observed from Figure 58. This approximation of ζ, although not as accurate as the infinite series approximation, is the more desirable of the two approximations because the use of it allows the

geometry of the buckled pattern to be more easily studied, and the single term is considerably more manageable than an infinite series, particularly in the derivation of a large deflection theory. Therefore, later in this paper the Fourier sine series approximation of ζ is used to verify the accuracy obtained by the single term approximation, and thereafter only the single term approximation is considered.

a) Obtaining the Criticial Buckling Load by Approximating the Lateral Deflections With an Infinite Series.

The condition which specifies the critical buckling load is given in equation (46), and as it has been previously discussed, the Ritz method is used to obtain an approximate solution to this equation. The orthotropic plate is assumed to be simply supported, and therefore, the boundary conditions of this plate are satisfied by approximating the lateral deflections with the following equation:

$$\zeta = \sum_{M=1}^{\infty} \sum_{N=1}^{\infty} A_{MN} \sin \frac{M\pi x}{a} \sin \frac{N\pi y}{b} \qquad (47)$$

To check the boundary conditions it is first noted that the boundary conditions requiring lateral deflections (ζ) to be equal to zero along all edges (x = 0 and z; y = 0 and b) are satisfied. Similarly, if it is recalled that

bending moments are functions of ζ_{xx} and ζ_{yy} with

$$\zeta_{xx} = -\sum_{M=1}^{\infty}\sum_{N=1}^{\infty} A_{MN}\frac{M^2\pi^2}{a^2}\sin\frac{M\pi x}{a}\sin\frac{N\pi y}{b}$$

$$\zeta_{yy} = -\sum_{M=1}^{\infty}\sum_{N=1}^{\infty} A_{MN}\frac{N^2\pi^2}{b^2}\sin\frac{M\pi x}{a}\sin\frac{N\pi y}{b}$$

it becomes obvious that the requirements for zero bending moments along the edges are also satisfied. When the Ritz method is applied, it is only necessary to satisfy the forced boundary conditions, i.e. $\zeta = 0$ along the edges, but to satisfy the natural boundary conditions, i.e. $\zeta_{xx} = \zeta_{yy} = 0$ along the edges, is desirable since it causes the series representing the deflections to converge more rapidly toward the exact deflections. This rapid convergence is important, because the primary difficulty in this solution is in choosing enough terms from equation (47) to closely approximate the actual shape without having so many that the resulting equations are so lengthy that they become unwieldy. Later in the report, the accuracy of the approximation for lateral deflection is examined by noting the convergence of curves which show critical buckling load plotted versus the number of terms chosen from equation (47) to represent ζ.

To begin the solution, the appropriate derivatives of ζ are substituted into equation (46) giving

$$\int_0^a\int_0^b \Bigg\{ 2P_Y \Bigg[\sum_{M=1}^{\infty}\sum_{N=1}^{\infty} A_{MN}\frac{M\pi}{a}\cos\frac{M\pi x}{a}\sin\frac{N\pi y}{b}\Bigg] \Bigg[\sum_{P=1}^{\infty}\sum_{Q=1}^{\infty} A_{PQ}\frac{Q\pi}{b}\sin\frac{P\pi x}{a}\cos\frac{Q\pi y}{b}\Bigg]$$
$$+ H_x\Bigg[\sum_{M=1}^{\infty}\sum_{N=1}^{\infty} A_{MN}\frac{M^2\pi^2}{a^2}\sin\frac{M\pi x}{a}\sin\frac{N\pi y}{b}\Bigg]^2 \qquad (48)$$
$$+ H_Y\Bigg[\sum_{M=1}^{\infty}\sum_{N=1}^{\infty} A_{MN}\frac{N^2\pi^2}{b^2}\sin\frac{M\pi x}{a}\sin\frac{N\pi y}{b}\Bigg]^2$$
$$+ H_{XY}\Bigg[\sum_{M=1}^{\infty}\sum_{N=1}^{\infty} A_{MN}\frac{MN\pi^2}{ab}\cos\frac{M\pi x}{a}\cos\frac{N\pi y}{b}\Bigg]^2\Bigg\} dy\,dx$$
$$= 0$$

Then performing the indicated integrations leads to the following equation for P_y:

$$P_Y = -\frac{\displaystyle\sum_{M=1}^{\infty}\sum_{N=1}^{\infty}\left\{A_{MN}^2\frac{\pi^4 ab}{32}\left[H_x\frac{M^4}{a^4}+H_Y\frac{N^4}{b^4}+H_{XY}\frac{M^2N^2}{a^2b^2}\right]\right\}}{\displaystyle\sum_{M}\sum_{N}\sum_{P}\sum_{Q} A_{MN}A_{PQ}\frac{MNPQ}{(M^2-P^2)(Q^2-N^2)}} \qquad (49)$$

The letters M, N, P and Q represent integers such that $M \pm P$ and $N \pm Q$ are odd numbers. This equation, it is noted, is quite similar to the equation for the critical buckling load of an ordinary flat plate in shear as developed by Timoshenko and Gere. [3]

It is noted that equation (49) gives the buckling load which would cause the panel to buckle into the shape which is defined by the coefficients Amn. Since an infinite number of choices of Amn are possible, a corresponding infinite number of buckling loads (Py) can be computed. However, if it is realized that the panel will buckle as soon as the applied load is increased to the minimum possible load which corresponds to a deflected equilibrium configuration as defined by equation (49), then it is apparent that the buckling load of interest will be the minimum Py given by equation (49). This minimum value of Py is identified by the symbol P_{cr}, and is determined by considering P_y in the form

$$P_Y = -R/T \tag{50}$$

with

$$R = \sum_{M=1}^{\infty}\sum_{N=1}^{\infty} A_{MN}^2 \frac{\pi^4 ab}{32}\left[H_x\frac{M^4}{a^4} + H_Y\frac{N^4}{b^4} + H_{XY}\frac{M^2N^2}{a^2b^2}\right]$$

$$T = \sum_{M}\sum_{N}\sum_{P}\sum_{Q} A_{MN}A_{PQ}\frac{MNPQ}{(M^2-P^2)(Q^2-N^2)}$$

Then, applying the minimizing condition

$$\partial P_Y/\partial A_{ij} = 0 \tag{51}$$

to equation (50) the result becomes

$$\partial R/\partial A_{ij} + P_Y\left(\partial T/\partial A_{ij}\right) = 0 \qquad (52)$$

Now, substituting the expressions for R and T into equation (52), and performing the indicated differentiations, the following equation defining P_{cr} is obtained:

$$\frac{k_{MN} A_{MN}}{P_{cr}} + \sum_P \sum_Q A_{PQ} \frac{MNPQ}{(M^2-P^2)(Q^2-N^2)} = 0 \qquad (53)$$

in which

$$k_{MN} = \frac{\pi^4 ab}{32}\left[H_X \frac{M^4}{a^4} + H_Y \frac{N^4}{b^4} + H_{XY} \frac{M^2N^2}{a^2b^2}\right]$$

Equation (53) can be expanded into a system of linear homogeneous equations. The nature of the system is observed by first recalling that M + P and N + Q are required to be odd numbers, and therefore M + N + P + Q must be an even number. Thus if M + N is an even number, then P + Q must also be an even number. Similarly if M + N is an odd number, then P + Q must also be an odd number. Consequently, each equation from (53) involves only A_{ij} for which i + j is either even or odd, thereby generating two independent sets of equations. If M + N is an even number, the set of equations describes a

bending pattern defined as symmetric bending in this paper, and if M + N is an odd number the buckled pattern is referred to as antisymmetric buckling. [7] A panel with a symmetric buckled shape has a wave pattern which is symmetric about a line that passes through the center of the panel making an angle $\Theta = \tan^{-1}\alpha$ with the y axis as shown in Figure 18.

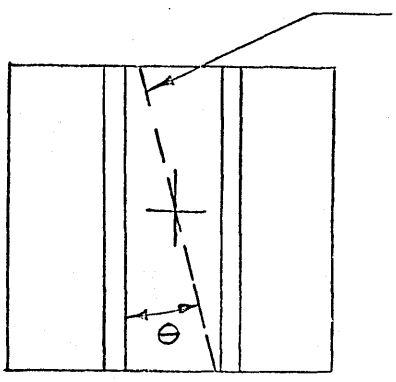

Figure 18

Similarly an antisymmetric buckled pattern has a wave pattern which is antisymmetric about this line. In the analysis of ordinary flat plates in shear similar sets of equations are obtained, and the set of equations corresponding to symmetric bending results in the minimum value of the buckling load with the exception of long narrow plates, i.e. $a/b > 2$ [3], in which case both symmetric and antisymmetric bending must be checked.

The primary purpose of this solution is to serve as a check on the accuracy of the single term approximation

for ζ, consequently the solution need be pursued only so far as to allow this check to be made. Because of this, and based upon the fact that all of the panels tested in shear as a part of this investigation failed with symmetric buckling patterns, only symmetric buckling is considered in this analysis.

To determine the buckling load for symmetric buckling, the set of homogeneous equations for which M + N and P + Q are even numbers is examined. It is known that if a set of homogeneous equations is to have a non-trivial solution, then the determinant of its coefficients must equal zero. Now, imagine k different coefficients (A_{ij}) used in the expansion of expression (53) into a set of k homogeneous equations. Then, setting the determinant of the coefficients of the A_{ij}'s equal to zero results in a k^{th} order polynomial in $(1/P_{cr})$. The inverse of the maximum root of this polynomial corresponds to the minimum value of P_{cr}, i.e. the critical buckling load for the panel.

In preliminary studies the determinant given in Table 1 with k = 25 was examined. This determinant results from considering all of the terms applicable to symmetric buckling when M and N are allowed to vary from one to seven. The computer program listed in part (a) of Appendix B is used to expand and solve any determinant considered. From the preliminary work it became obvious that larger values of M than seven were going to be required to obtain

proper convergence of P_{cr}. Since the dimensions of the program would not permit much more expansion, and the time involved in computing a larger determinant becomes excessive, the set of equations with M and N varying from one to seven was examined to determine which terms were the major contributors to P_{cr}. It was found that the use of a k = 7 determinant which is composed of only the terms corresponding to M equals one through seven and N equals one and two resulted in values of P_{cr} within two percent of the values obtained using the total determinant with k = 25.

On the basis of the preceeding information, the final representation of the double summation in equation (53) is specified to include all terms applicable to symmetric buckling with M varying from one to eighteen and N taking the values one and two. The determinant of the coefficients of the A_{ij}'s corresponding to this set of equations is given in Table 2. When this solution is applied it would certainly be expected that the choice for M be at least as large as the number of buckles in the panel being analyzed. Consequently, the convergence of P_{cr} versus the number of terms chosen to approximate the infinite series should always be checked as explained later in the report in order to guarantee that enough terms have been chosen to closely approximate the infinite series. Notice that the determinant is symmetric and that all terms except

those on the diagonal are constant for any panel. The diagonal terms are equal to k_{mn} which is recalled to be as follows:

$$k_{MN} = \frac{\pi^4 ab}{32}\left[H_X \frac{M^4}{a^4} + H_Y \frac{N^4}{b^4} + H_{XY} \frac{M^2 N^2}{a^2 b^2}\right]$$

Therefore, the diagonal terms are seen to be functions of the panel geometry of the particular panel under consideration. Thus, to obtain P_{cr} for a particular panel involves computing the appropriate diagonal terms corresponding to Table 2, then putting them into the computer program as defined in Appendix B, part (a).

(b) Developing a Solution for the Critical Buckling Load and the Corresponding Deflection Pattern with a Simplified Approximation of Lateral Deflections.

A second small deflection solution is derived since it is desirable to obtain an approximate form for ζ which can be more easily handled than the preceeding infinite series approximation. Again, equation (46) is used as the condition which specifies the critical buckling load. This time the expression

$$\zeta = A \sin\frac{\pi Y}{b} \sin\frac{m\pi}{a}(x - \alpha Y) \qquad (54)$$

is chosen to approximate the lateral deflection of the panel. As noted previously, it is felt that equation (54)

is a good choice for ζ since it gives a single term approximation of the lateral deflections, and observation of actual tests show the buckled pattern to assume a shape similar to the one which equation (54) defines. This approximation is also desirable since once α and n are determined, where α is the tangent of the angle which the buckles make with the y axis and n is the number of waves occurring in the plate, the buckled form is completely described.

One fault of this approximation for lateral deflection is that boundary conditions are not satisfied as well as they were with the infinite series approximation. In fact, the only boundary condition which is satisfied is that of zero lateral deflection along the edges y = 0 and y = b. The other forced boundary condition which should actually be satisfied when the Ritz method is applied is that of zero lateral deflections along the edges x = 0 and x = a. However, in the limit with H_x equal to zero, a zero moment (M_x) is needed in order to bend the edges back coincident with the frame. In reality, H_x is not zero but it is very small in comparison to H_y. Thus, it would take only a very small moment (M_x) to bend the edges of the panll to match the configuration of the frame, and the corresponding change in strain energy of the panel would be small.

To begin the solution, the expression for ζ from equation (54) is substituted into the criteria for netural equilibrium given in equation (46), and the following

equation is obtained:

$$\int_0^a \int_0^b \Bigg\{ 2P_Y \Bigg[A^2 \frac{m\pi^2}{ab} \cos\frac{\pi Y}{b} \sin\frac{\pi Y}{b} \cos\frac{m\pi}{a}(x-\alpha Y) \sin\frac{m\pi}{a}(x-\alpha Y) - A^2 \frac{\alpha m^2 \pi^2}{a^2} \sin^2\frac{\pi Y}{b} \cos^2\frac{m\pi}{a}(x-\alpha Y) \Bigg]$$

$$+ H_Y \Bigg[\left(\frac{A\pi^2}{b^2} + A\frac{\alpha^2 m^2 \pi^2}{a^2} \right)^2 \sin^2\frac{\pi Y}{b} \sin^2\frac{m\pi}{a}(x-\alpha Y) + 4A^2 \frac{\alpha^2 m^2 \pi^4}{a^2 b^2} \cos^2\frac{\pi Y}{b} \cos^2\frac{m\pi}{a}(x-\alpha Y) + 4A^2 \frac{\alpha m \pi^2}{ab} \left(\frac{\pi^2}{b^2} + \frac{\alpha^2 m^2 \pi^2}{a^2} \right) \cos\frac{\pi Y}{b} \sin\frac{\pi Y}{b} \cos\frac{m\pi}{a}(x-\alpha Y) \sin\frac{m\pi}{a}(x-\alpha Y) \Bigg]$$

$$+ H_X A^2 \frac{m^4 \pi^4}{a^4} \sin^2\frac{\pi Y}{b} \sin^2\frac{m\pi}{a}(x-\alpha Y)$$

$$+ H_{XY} \Bigg[\frac{A^2 m^2 \pi^4}{a^2 b^2} \cos^2\frac{\pi Y}{b} \cos^2\frac{m\pi}{a}(x-\alpha Y) + \frac{A^2 \alpha^2 m^4 \pi^4}{a^3 b} \sin^2\frac{\pi Y}{b} \sin^2\frac{m\pi}{a}(x-\alpha Y) + \frac{2A^2 \alpha m^3 \pi^4}{a^3 b} \sin\frac{\pi Y}{b} \cos\frac{\pi Y}{b} \sin\frac{m\pi}{a}(x-\alpha Y) \cos\frac{m\pi}{a}(x-\alpha Y) \Bigg] \Bigg\} dY\, dX \quad (55)$$

$$= 0$$

After integration, equation (55) reduces to

$$-P_Y\frac{\alpha m^2}{2a^2} + H_Y\left[\frac{\pi^2}{4b^4} + \frac{\alpha^2 m^2\pi^2}{2a^2b^2} + \frac{\alpha^4 m^4\pi^4}{4a^4} + \frac{\alpha^2 m^2\pi^2}{a^2b^2}\right] + H_X\left[\frac{m^4\pi^2}{4a^4}\right] + H_{XY}\left[\frac{m^2\pi^2}{4a^2b^2} + \frac{\alpha^2 m^4\pi^2}{4a^4}\right] = 0$$

Now solving for P_y and simplifying the results gives

$$P_Y = H_Y\pi^2\left[\frac{a^2}{2\alpha m^2 b^4} + \frac{3\alpha}{b^2} + \frac{\alpha^3 m^2}{2a^2}\right] + H_X\pi^2\left[\frac{m^2}{2\alpha a^2}\right] + H_{XY}\pi^2\left[\frac{1}{2\alpha b^2} + \frac{\alpha m^2}{2a^2}\right] \qquad (56)$$

Equation (56) gives the buckling load, but until this point in the analysis α and n are undetermined. Again, if it is recalled that the minimum load for which a deflected equilibrium configuration is possible is P_{cr}, it then follows

that the criteria

$$\partial P_Y / \partial m = 0 \tag{57a}$$

$$\partial P_Y / \partial \alpha = 0 \tag{57b}$$

must be satisfied.

Now, substituting P_y given in equation (56) into equation (57a) and simplifying the resulting equation, gives

$$m = \frac{a}{b}\left(\frac{H_Y}{\alpha^4 H_Y + \alpha^2 H_{XY} + H_X}\right)^{1/4} \tag{58}$$

with n restricted to a positive real number. Thus, once α is determined n can be determined from equation (58). In general the solution of equation (58) does not result in a value for n which is an integer, but since an actual buckled pattern must have an even number of waves, the value of n given by equation (58) should be rounded off to the nearest integer when predicting the number of waves to be formed and the corresponding buckling load. If the value of n is approximately half-way between two integers, both integer values of n should be considered when computing P_{cr}.

To solve for α, the expression for P_y given by equation (56) is substituted into equation (57b); n is then

replaced by the expression given in equation (58). Performing the indicated operations and simplifying the results leads to the equation

$$8H_Y^2\alpha^8 + \frac{27}{4}H_XH_{XY}\alpha^6 + \left(11H_XH_Y - \frac{11}{4}H_{XY}^2\right)\alpha^4 + \left(\frac{H_{XY}^3}{4H_Y} - 3H_XH_{XY}\right)\alpha^2 + \left(\frac{H_{XY}^2H_X}{4H_Y} - H_X^2\right) = 0 \qquad (59)$$

One of the manipulations that was necessary in obtaining equation (59) was that of squaring both sides of an equation which eventually reduced to equation (59), consequently introducing extraneous roots into equation (59). It is noted, that the root $\alpha = c$ which is of interest must be a real number. Then, if c is a real root of equation (59), -c is also found to be a real root of equation (59). The proper choice for α is determined by considering the following figure:

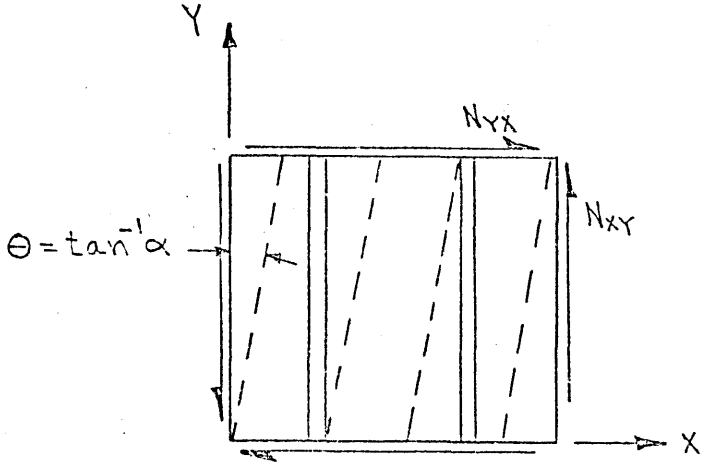

Figure 19

In the preceeding sketch, the dashed lines define the general direction of the waves in the plate after buckling. Thus, the general direction of the buckled pattern is known, and α may always be viewed as a positive number such that

$$\alpha = \tan\theta$$

and θ is the angle measured from the y axis to a line defining the direction of the buckles as shown in the preceeding sketch.

Equation (59) can be simplified further by noting that

$H_x = (0) H_{xy}$ = order of magnitude of H_{xy}

$H_x H_{xy} = (0) H_{xy}^2$

$H_x << H_y$

$H_{xy} << H_y$

Therefore,

$H_x^2 >> H_{xy}^2 (H_x/H_y)$

$H_x H_y >> H_{xy}^2$

$H_x H_{xy} >> H_{xy}^3/H_y$

Consequently equation (59) is further reduced to

$$8H_y^2\alpha^8 + \frac{27}{4} H_x H_{xy}\alpha^6 + 11 H_x H_y \alpha^4$$
$$-3 H_x H_{xy}\alpha^2 - H_x^2 = 0 \qquad (60)$$

Now, proceeding under the assumption that α is positive, the desired value of α is obtained by setting equation (60) equal to $f(\alpha)$ and plotting a curve of $f(\alpha)$ versus α to determine the value of α for which $f(\alpha) = 0$.

With the preceeding tools it is now possible to examine the buckling of an actual corrugated plate in shear in much more detail than has been done in the past. The angle formed by the buckled pattern is seen to no longer be 45^{o} as is the case for a flat plate. It is interesting to note that the maximum possible angle is 45^{o} occurring only for the flat plate, and that if the magnitudes of H_x and H_{xy} go to zero with a non-zero H_y, then the angle α also goes to zero. It is also seen from equation (58) that the corresponding n approaches infinity. This implies that if H_x and H_{xy} equal zero the buckles will occur parallel to the corrugations, but it can be shown that on planes parallel to the corrugation the compressive stress is zero. However this limiting case can still be imagined if it is realized that $H_x = 0$, i.e. no bending stiffness, implies that a zero compressive load would buckle the panel. Obviously this situation is not physically realizable, but it does point out the trend of α and n as the ratio H_x/H_y is diminished, i.e. the corrugations are made deeper and/or the plate made thinner.

(c) Comparison of the Two Small Deflection Solutions

When assuming a function closely approximating the lateral deflections of a plate, it is desirable that this

function be in a simplified form which lends itself well to the manipulations to which the function must be subjected when applying the Ritz method, and that it be of such a nature as to readily describe the deflected shape of the panel. In meeting these qualifications

$$\zeta = A \sin \frac{\pi Y}{b} \sin \frac{m\pi}{a}(x - \alpha Y)$$

appears to be such a function. Here the single term affords relatively easy manipulation, and the nature of the deflected panel is clearly described by the parameters A, n and α. Now the solution resulting from the use of this function can be compared to the results obtained from the use of the infinite series (which as stated before is a more accurate analysis) in order to verify that the use of this single term function leads to an accurate analysis of corrugated plates in shear. If it can be shown that both expressions result in approximately the same predictions of critical buckling loads, then the single term approximation for ζ will be assumed to be a close approximation of the actual deflected pattern.

Again it is noted that the accuracy of the solution derived from the infinite series approximation of ζ depends upon the number of terms chosen to represent ζ. Recalling that the Ritz method specifies, that as the approximation of the lateral deflections is made increasingly more accurate, the predicted value of the corresponding buckling

load approaches the actual buckling load as an asymptote; it then becomes evident that an idea of the accuracy of the final predicted buckling load can be obtained by observing the convergence of P_{cr} as the number of terms chosen to represent ζ is increased. Therefore, the computer program listed in part (a) of Appendix B is organized in such a way that any number of terms may be considered up to the maximum number of terms in the basic determinant.

To compare predicted buckling loads obtained from the infinite series solution and the single term solution, the buckling loads are calculated by both methods for the primary panels used in the experimental portion of this investigation. These panels are the Butlerib and the standard sine-wave corrugated panel. The appropriate section properties and geometry of all cross section are shown in Figures 41 and 42, and the overall dimensions of the panels are given in Table 3. The buckling load is computed for each of these panels using various numbers of terms to approximate the infinite series, and the results are plotted in Figures 32, 33 and 34 and listed in Table 4. From these figures, it is clear that the values of P_{cr} are rapidly converging, and in each case the final values of P_{cr} give an approximation of the buckling load seen to easily be within one percent of the asymptote. It is pointed out that the accuracy of this solution is relative to the exact solution, but the exact solution is a solution to the problem as it has been defined

in the previous theoretical analysis. Therefore, even an exact solution inherently has in it error due to any approximations and any assumptions included in the theoretical background. Thus the degree of accuracy discussed here should not be confused with the degree of accuracy which is found when the theoretical predictions and test data are compared later in this report.

Next, the critical buckling loads are computed for the same panels using equation (56) which was derived from the single term approximation of ς, and the results are shown as horizontal dashed lines in Figures 32, 33, and 34 and are listed in Table 5. It is observed that the infinite series solutions are converging to values within approximately three percent of the values computed by equation (56). Therefore, the verification that the function

$$\varsigma = A \sin \frac{\pi Y}{b} \sin \frac{m\pi}{a}(x - \alpha Y)$$

must closely represent the buckled patterns of the plates is obtained. Hereafter, in this report only this single term approximation is used, since it affords a more complete examination of the buckling problem than does the infinite series approximation of ς, and it has been shown to be reasonably accurate.

This completes the small deflection analysis of corrugated panels under the action of external shear loads. At this point solutions have been developed which define

the critical buckling load and the shape into which the panel buckles. It is desirable to also develop a large deflection analysis, i.e. large w, in order to examine the post buckling behavior of corrugated panels in shear. A large deflection analysis is a tool which permits considerable insight in the examination of a corrugated panel in shear since it again defines the initial buckling behavior given by the small deflection analysis, and in addition results in the derivation of a post buckling load-deflection relation.

CHAPTER VI

DEVELOPING A LARGE DEFLECTION THEORY

The equations developed in the preceeding section predict the buckling load and the corresponding buckled shape of a corrugated panel in shear. It is possible to gain considerably more knowledge than this about the behavior of the panels by conducting a large deflection analysis. This analysis results in a load versus lateral deflection relation which in turn 1) allows an estimate of the post buckling strength of an arbitrary corrugated panel, 2) indicates the possible existence of a "snap-through" type of buckling at loads less than the buckling load predicted by the small deflection theory, i.e. a behavior pattern somewhat similar to the buckling behavior of a thin shell, and 3) presents a means of better correlating theoretical predictions with experimental data from imperfect experimental test specimens.

The large deflection analysis presented here is based upon the assumption that the edges of the panel can move slightly, and hence that the membrane strains remain constant during lateral displacement of the panel. This assumption results in the only manageable method of solution for the problem, and fortunately, it seems to correspond fairly accurately to situations encountered in

actual building construction and in the tests considered in this paper. In these tests and generally in construction, the edges of the panels are fastened to relatively flexible fixtures.

Based upon the preceeding assumption, the changes in the membrane strains are

$$\Delta\epsilon_x = \Delta\epsilon_y = \Delta\gamma_{xy} = 0$$

Then, if the configuration for zero potential energy is designated as the straight loaded form, the general expression for strain energy in terms of strains when the plate is in a deflected configuration becomes

$$U = \int_0^a \int_0^b \left\{ H_x \theta_x^2 + H_y \theta_y^2 + H_{xy} \theta_{xy}^2 \right\} dy\, dx \qquad (61)$$

In order to account for larger deflections than were considered in the small deflection theory, the strain-displacement relations defining Θ_x and Θ_y given in equation (25) are replaced by the following exact expressions:

$$\Theta_x = w_{xx} \Big/ (1 + w_x^2)^{3/2}$$
$$\Theta_y = w_{yy} \Big/ (1 + w_y^2)^{3/2} \qquad (62)$$

The expression for Θ_{xy} given by

$$\theta_{xy} = w_{xy}$$

is left unchanged even though it is also an approximation. The reason for this can be observed later in the report by noting that the contribution of the term containing Θ_{xy} to the values of P_{cr}, α, and n is very small compared to the contribution resulting from the bending moments. Consequently, it seems unnecessary to improve the accuracy of this term.

From equation (61) it can be seen that, actually, θ_x^2 and θ_y^2 are of interest rather than θ_x and θ_y. Hence the expressions

$$\Theta_x^2 = W_{xx}^2/(1+W_x^2)^3$$
$$\Theta_y^2 = W_{yy}^2/(1+W_y^2)^3 \qquad (63)$$

must eventually be integrated over the area of the plate. To put these expressions in a form which can be more easily integrated, the quantities $1/(1+W_x^2)^3$ and $1/(1+W_x^2)^3$ are expanded in the form of a Maclaurin series and the results obtained are[8]

$$\Theta_x^2 = W_{xx}^2\left(1-3W_x^2+6W_x^4---\right)$$
$$\Theta_y^2 = W_{yy}^2\left(1-3W_y^2+6W_y^4----\right) \qquad (64)$$

The preceeding expressions are infinite series, but θ_x^2 and θ_y^2 can be accurately approximated for fairly large deflections by retaining the first three terms of the approximate series from (64). The accuracy of the approximation diminishes of course, as lateral deflections, and

correspondingly, w_x and w_y increase. The equation for the change in strain energy then becomes

$$U = \frac{1}{2}\int_0^a\int_0^b \left\{ H_x W_{xx}^2 (1-3W_x^2+6W_x^4) + H_y W_{yy}^2 (1-3W_y^2+6W_y^4) + H_{xy} W_{xy}^2 \right\} dy\,dx \tag{65}$$

In addition to the strain energy given by equation (65), it is necessary to develop a compatible form of the change in external potential energy. To do this, it is recalled that

$$\Omega = -\int_0^a\int_0^b P_y u_y \, dy\,dx$$

Since

$$\gamma_{xy} = u_y + v_x + w_x w_y$$

and for the panels investigated herein it is assumed that

$$v_x = 0$$

it is seen that

$$u_y = -w_x w_y$$

Thus, the change in the external potential energy takes the form[3]

$$\Omega = \int_0^a\int_0^b P_y w_x w_y \, dy\,dx \tag{66}$$

Combining equations (65) and (66), the total change in potential energy is

$$V = \frac{1}{2}\int_0^a\int_0^b \Big\{ H_x W_{xx}^2 (1 - 3W_x^2 + 6W_x^4) + H_Y W_{YY}^2 (1 - 3W_Y^2 + 6W_Y^4) + H_{xY} W_{xY}^2 + 2P_Y W_x W_Y \Big\} dY\, dx \tag{67}$$

To complete the solution, it is next necessary to assume an expression for the lateral deflections. Based on the small deflection analysis, w is again assumed in the form

$$W = A \sin\frac{\pi Y}{b} \sin\frac{m\pi}{a}(x - \alpha Y)$$

and n are assumed to be known from the small deflection analysis, while A presents the unknown amplitude of the lateral deflection and is to be determined as a function of the external load.

Substituting this expression for w into equation (67) gives

$$V = \frac{1}{2}\int_0^a\int_0^b \Big\{ H_x \Big[A^2\frac{m^4\pi^4}{a^4} \sin^2\frac{\pi Y}{b} \sin^2\frac{m\pi}{a}(x - \alpha Y)\Big] \Big[1 - 3A^2\frac{m^2\pi^2}{a^2} \sin^2\frac{\pi Y}{b} \cos^2\frac{m\pi}{a}(x - \alpha Y) + 6A^4\frac{m^4\pi^4}{a^4} \sin^4\frac{\pi Y}{b} \cos^4\frac{m\pi}{a}(x - \alpha Y)\Big] + H_Y \Big[A\Big(\frac{\pi^2}{b^2} + \frac{\alpha^2 m^2\pi^2}{a^2}\Big) \sin\frac{\pi Y}{b} \sin\frac{m\pi}{a}(x - \alpha Y) + A\frac{2\alpha m\pi^2}{ab} \cos\frac{\pi Y}{b} \cos\frac{m\pi}{a}(x - \alpha Y)\Big]^2 \Big[1 - 3\Big(\frac{A\pi}{b}\cos\frac{\pi Y}{b} \sin\frac{m\pi}{a}(x - \alpha Y) - A\frac{\alpha m\pi}{a} \sin\frac{\pi Y}{b} \cos\frac{m\pi}{a}(x - \alpha Y)\Big)^2 \tag{68}$$

(cont. on following page)

(cont. for preceeding page)

$$+6\left(\frac{A\pi}{b}\cos\frac{\pi Y}{b}\sin\frac{m\pi}{a}(x-\alpha Y)-A\frac{\alpha m\pi}{a}\sin\frac{\pi Y}{b}\cos\frac{m\pi}{a}(x-\alpha Y)\right)^4\Bigg]$$

$$+H_{XY}A^2\left[\frac{m\pi^2}{ab}\cos\frac{\pi Y}{b}\cos\frac{m\pi}{a}(x-\alpha Y)\right. \tag{68}$$

$$\left.+\frac{\alpha m^2\pi^2}{a^2}\sin\frac{\pi Y}{b}\sin\frac{m\pi}{a}(x-\alpha Y)\right]^2$$

$$+P_Y A\frac{m\pi}{a}\sin\frac{\pi Y}{b}\cos\frac{m\pi}{a}(x-\alpha Y)\left[\frac{A\pi}{b}\cos\frac{\pi Y}{b}\sin\frac{m\pi}{a}(x-\alpha Y)\right.$$

$$\left.-A\frac{\alpha m\pi}{a}\sin\frac{\pi Y}{b}\cos\frac{m\pi}{a}(x-\alpha Y)\right]\Bigg\}\,dy\,dx$$

and then integration of equation (68) results in

$$V = A^2L - A^4J + A^6K \tag{69}$$

with

$$L = -P_Y\frac{\alpha m^2\pi^2 b}{4a} + H_X\frac{m^4\pi^4 b}{8a^3}$$

$$+H_Y\left[\frac{\pi^4 a}{8b^3}+\frac{3\alpha^2m^2\pi^4}{4ab}+\frac{\alpha^4m^4\pi^4 b}{8a^3}\right]$$

$$+H_{XY}\left[\frac{m^2\pi^4}{8ab}+\frac{\alpha^2m^4\pi^4 b}{8a^3}\right]$$

$$J = + H_x \frac{9m^6\pi^6 b}{128\, a^5} - H_Y\left[\frac{3\alpha^2 m^2 \pi^4}{16ab}\beta\right.$$

$$+ \left(\frac{9\pi^2 a}{128\, b} + \frac{9\alpha^2 m^2 \pi^2 b}{128 a}\right)\beta$$

$$\left. - \frac{9\alpha^2 m^2 \pi^6}{32\, a b^3} - \frac{9\alpha^4 m^4 \pi^6}{32\, a^3 b}\right]$$

$$K = + H_x \frac{15 m^8 \pi^8 b}{256\, a^7} + H_Y\left[\left(\frac{15 a \pi^4}{256\, b^3} + \frac{15\alpha^4 m^4 \pi^4 b}{256\, a^3}\right.\right.$$

$$\left. + \frac{9\alpha^2 m^2 \pi^4}{128 ab}\right)\beta^2 - \left(\frac{3\alpha^2 m^2 \pi^6}{16\, a\, b^3} + \frac{3\alpha^4 m^4 \pi^6}{16 a^3 b}\right)\beta$$

$$\left. + \frac{15\alpha^2 m^2 \pi^8}{64 a b^5} + \frac{15\alpha^6 m^6 \pi^8}{64 a^5 b} + \frac{9\alpha^4 m^4 \pi^8}{32 a^3 b^3}\right]$$

and

$$\beta = \left(\frac{\pi^2}{b^2} + \frac{\alpha^2 m^2 \pi^2}{a^2}\right)$$

Since in this case V is the potential energy corresponding to a laterally deflected configuration, it is necessary to examine $\delta V = 0$ in order to determine the amplitude of the deflected equilibrium configurations, and

thereby obtain an expression which relates loads and deflections. Since V is considered to be a function of the single variable A, $\delta V = 0$ results in

$$\delta V = (2AL - 4A^3J + 6A^5K)\delta A = 0$$

Thus for an arbitrary variation δA, the equation

$$A(2L - 4A^2J + 6A^4K) = 0 \tag{70}$$

must be satisfied if the deflected configuration is an equilibrium configuration.

Obviously, A = 0 satisfies the equilibrium condition, therefore varifying that the straight form is an equilibrium configuration. For any laterally deflected form to be an equilibrium configuration, the equation

$$L - 2A^2J + 3A^4K = 0 \tag{71}$$

must be satisfied. This in turn implies that for a laterally deflected equilibrium configuration to exist

$$A^2 = \frac{J \pm (J^2 - 3KL)^{1/2}}{3K} \tag{72}$$

If equation (72) is examined so that the relations between load and deflection can be more clearly defined, it is noted that, because A must always be real, the following inequalities must be satisfied

$$J \pm (J^2 - 3KL) \geq 0 \tag{73}$$

and

$$J^2 - 3KL \geq 0 \tag{74}$$

It should be pointed out that J and K are positive constants for each particular panel, and that L is a function of the external load P_y in the form

$$L = -C_1 P_y + C_2 \tag{75}$$

in which C_1 and C_2 are also positive constants for each particular panel.

Consequently, the inequality given in expression (74) is seen to be a function of P_y, and hence, this minimum value which P_y can obtain if real non-zero values of A are to exist is defined by

$$J^2 - 3KL = 0 \tag{76}$$

If the magnitude of P_y is below that which is defined by equation (76), the only real value of A which satisfies the condition defining possible equilibrium configurations, i.e. equation (70), is again zero, i.e. the straight form of the plate.

It is interesting to note that at this point of minimum P_y, A is not equal to zero but instead

$$A = \pm \left(J/3K\right)^{1/2} \tag{77}$$

Therefore, it is apparent that in the deflected configuration corresponding to $A = \pm \left(J/3K\right)^{1/2}$ the allowable external load is less than the critical buckling load as illustrated by Figure 20.

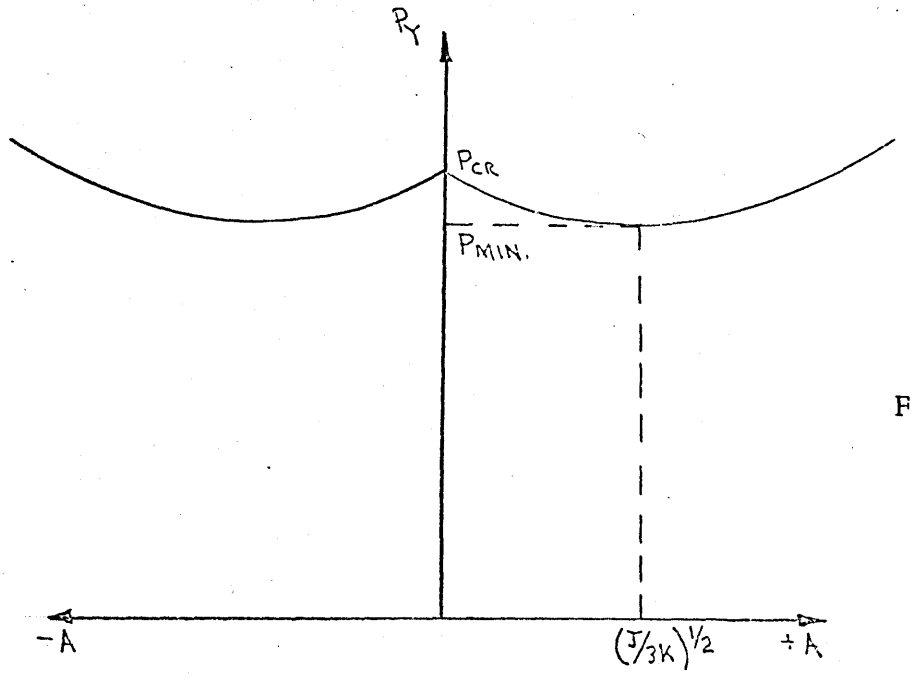

Figure 20

To determine the critical buckling load, equation (72) reduces to the condition

$$L = -P_Y \frac{\alpha m^2 \pi^2 b}{4a} + H_X \frac{m^4 \pi^4 b}{8a^3}$$

$$+ H_Y \left[\frac{\pi^4 a}{8b^3} + \frac{3\alpha^2 m^2 \pi^4}{4ab} + \frac{\alpha^4 m^4 \pi^4 b}{8a^3} \right] \qquad (78)$$

$$+ H_{XY} \left[\frac{m^2 \pi^4}{8ab} + \frac{\alpha^2 m^4 \pi^4 b}{8a^3} \right] = 0$$

Notice that equation (78) is exactly equation (56) which is the expression for the critical buckling load developed in the theory of small deflections.

It is also observed that for values of $(J^2-3KL)^{1/2}$ in the interval

$$0 < \left| (J^2-3KL)^{1/2} \right| \leq |J|$$

there are two possible laterally deflected equilibrium configurations for the same load P_y.

It is pointed out that as A increases, the accuracy of this theory is reduced. No exact range of accuracy is defined. However, a better indication of the accuracy of the theoretical analysis is presented later in the report when theoretical predictions are compared with actual test data.

The primary information to be gained from this large deflection theory is that in the region of the bifurcation

point (i.e. $P_y = P_{cr}$, $A = 0$) a corrugated panel will deflect considerably with a small increase in load. The panel may even buckle before it reaches P_{cr} and jump across to the P_{min} buckled configuration as frequently occurs in the buckling of shells.

This completes the theoretical analysis of the buckling of an arbitrary corrugated panel under the action of shear loads. In the following chapters, tests of several corrugated panels loaded in shear are discussed and the test results are correlated with the theoretical analysis.

CHAPTER VII

TESTING OF CORRUGATED PANELS IN SHEAR

a) Description of Testing Frame and Equipment

The theoretical analysis which has been developed in preceeding chapters describes the buckling of an arbitrary corrugated plate. It is now possible to gain a better understanding of this problem by conducting an experimental investigation which verifies and supplements the theoretical study. Before discussing the testing procedures carried out as a part of this investigation, it is necessary to describe the apparatus which was designed to test corrugated panels in shear.

All of the equipment used in this experimental work, aside from the basic test frame, is identified in Table 6. The basic frame is shown in Figures 35 and 36. Primary members of the frame are constructed from five-inch-square steel box beams, and hereafter each of these members will be identified in the manner defined by Figure 36.

The frame is constructed by welding yoke plates to both ends of member ①, to member ② at C and to member ④ at D; these in turn fit around the adjacent member. Thin shims are placed under the yoke plates before welding so that the yoke plates will slide over the adjacent member. At corners A, B, and C, .995 inch diameter Tobin

bronze pins are placed into one inch diameter holes which are drilled through the yoke plates and the member around which the yoke plates fit, as shown in Figure 36. At the remaining corner D, a steel sleeve is welded into member ③. A two inch diameter Tobin bronze pin is then used to pin members ③ and ④ together and in doing so passes through the sleeve as shown in Figure 36. It should be noticed that the pin also passes through two 3/4 inch thick yoke plates. These plates are welded to the 8 WF 35 beam which is part of the structure that carries the frame reaction to the floor.

In order that panels of more than one size can be tested, the frame is constructed in such a manner as to make it adjustable in both the x and y directions. Adjustment in the x direction is made possible by drilling one inch diameter holes at various locations in members ② and ④. The pins at A and B can be removed, allowing member ① to be moved to a new position at which point it is fastened in place by reinserting the pins as shown in the following sketch:

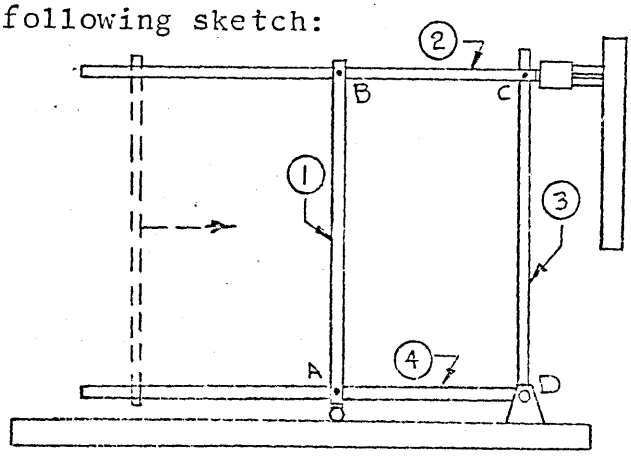

Figure 21

Adjustment in the y direction is obtained by drilling one inch diameter holes at various locations in member ③. By removing member ① and the pin at C, member ② can be repositioned along member ③. A new member ① of the proper length is then added to the frame and pinned at A and B as shown in the following figure:

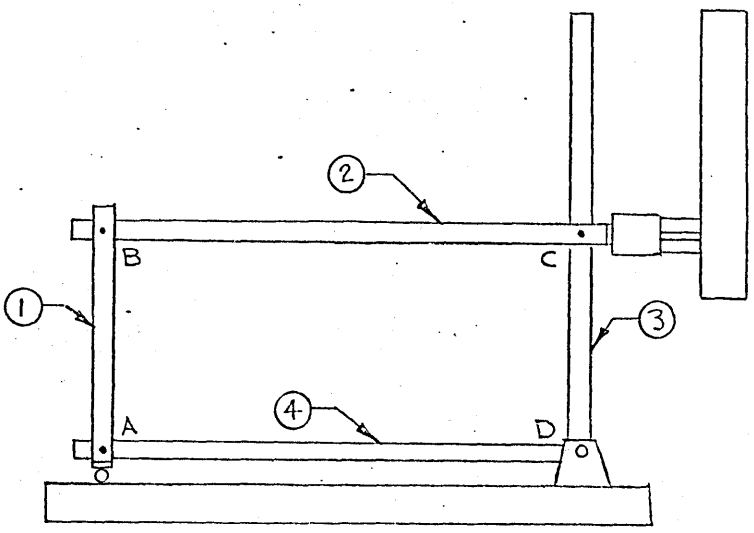

Figure 22

Obviously, this requires that a member ① be available in all of the lengths to which the frame must be adjusted in the y direction.

The entire frame is positioned 30 inches off of the floor thereby allowing an access space to aid in the installation of the panels and in the checking of failures. Frame member ② rests on two one inch diameter bars which serve as rollers, and which in turn rest on steel supports as shown in Figure 35. Each of these steel

supports has four 1/2 inch diameter bolts attached to the base in such a way that they may be screwed in or out, and thereby adjust the height of the steel support as shown in the following figure. These adjustments aid in keeping the total frame level.

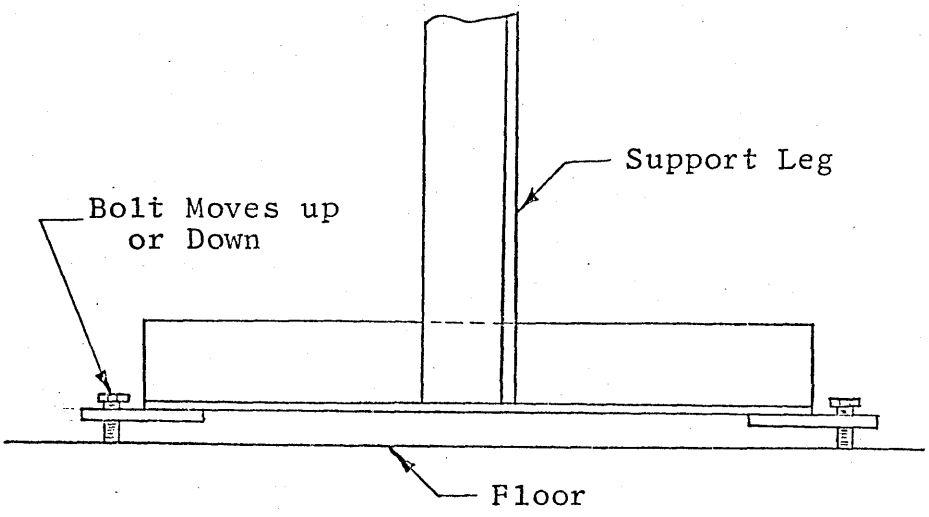

Figure 23

The frame also rests on a fixed support at approximately the center of member ④ as shown in Figure 36.

After the frame is adjusted to the proper size and leveled, a panel is fastened to all four sides of the frame, and the load is applied into member ② as a compression load at C by means of two 40,000 pound capacity hydraulic jacks; see Figure 37. The jacks also bear against the 8 WF 35 beam as shown, and the load is then transferred to the floor. Hydraulic fluid is supplied to the jacks from the pressure cylinder shown in Figure 37.

The large cylinder positioned between the jacks and the frame is a 100,000 pound capacity load cell which measures the load applied to it, and hence to the frame. The load cell rests on a wooden platform, which in turn rests on castors, thereby allowing the load cell to move forward as the jacks are extended. It should be noted that a bearing plate is welded onto the ends of the yoke plates in order to transmit the load from the load cell to the yoke plates and on into the basic frame. This load is then indicated on the recorder which is also shown in Figure 37.

The calibration of the load cell is checked by placing the load cell into a Baldwin Universal 120,000 pound hydraulic testing machine and applying compression loads in increments up to a total of 80,000 pounds. The load readings taken from the Baldwin Universal testing machine and the recorder attached to the load cell upon comparison are found to differ by less than one-half of one percent. Therefore, the load cell recordings are used throughout the experimental analysis of this problem withour correction.

The reactions to the load applied to the frame at C occur through a 2 and 3/8 inch diameter steel roller at A as shown in Figure 38 , and through the 2 inch diameter bronze pin at D as shown in Figure 39 . In each frame configuration, the load necessary to deflect the frame without

a panel installed in it is determined before any panels are installed, and in this investigation the necessary load was always found to be less than five pounds. Since the smallest buckling load measured was approximately 1500 pounds, the load necessary to deflect the frame alone is considered negligible, and thus the entire applied load is assumed to contribute to the deflection of the actual panel.

After each panel is installed, dial indicators are positioned to measure the deflections indicated by the arrows in the following figure.

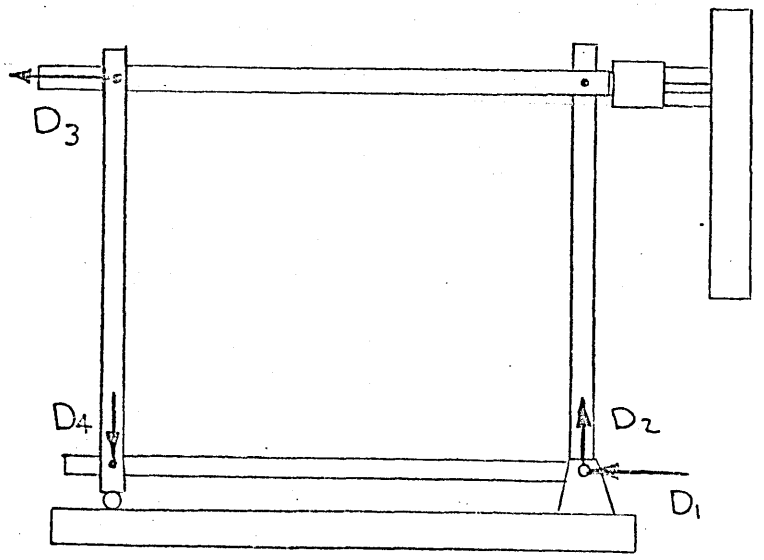

Figure 24

D_1, D_2, D_3 and D_4 identify the particular gages as listed in Table 6. Gage D_4 is shown in Figure 38, the gages D_1 and D_2 are seen in Figure 39 and gage D_3 is pictured in

Figure 40. The gages D_1, D_2 and D_4 measure the deflection of the support structure, and the gage D_3 measures the shear deflection plus additional deflection resulting from the support structure deflections measured by D_1, D_2 and D_4. Therefore, using readings from these four gages, the actual shear deflection can be determined. For many of the tests, an additional gage, D_5, is added to measure lateral displacements in the center of the panel as indicated by the following figure:

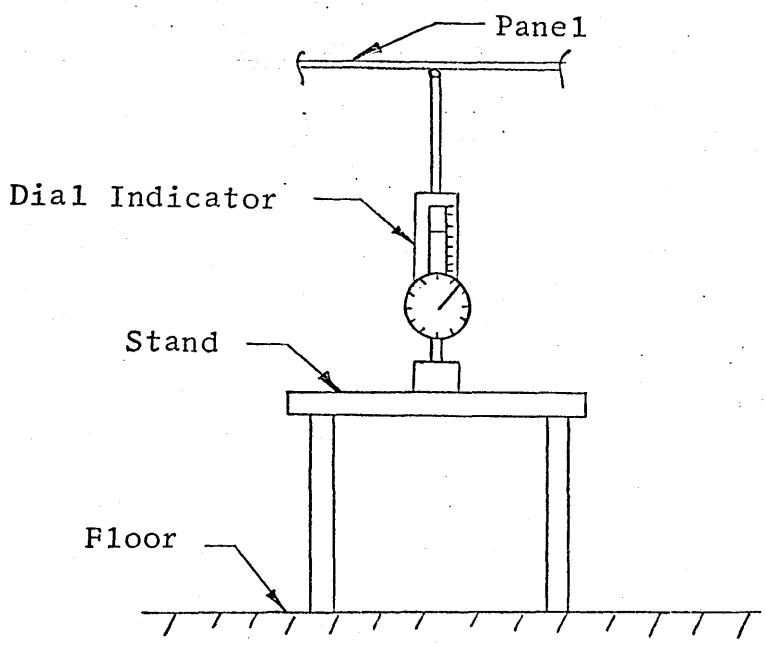

Figure 25

Several problems were encountered in the measurement of lateral deflections. First, it is obvious that as the load is applied the panel moves in the xy plane as illustrated in the following figure:

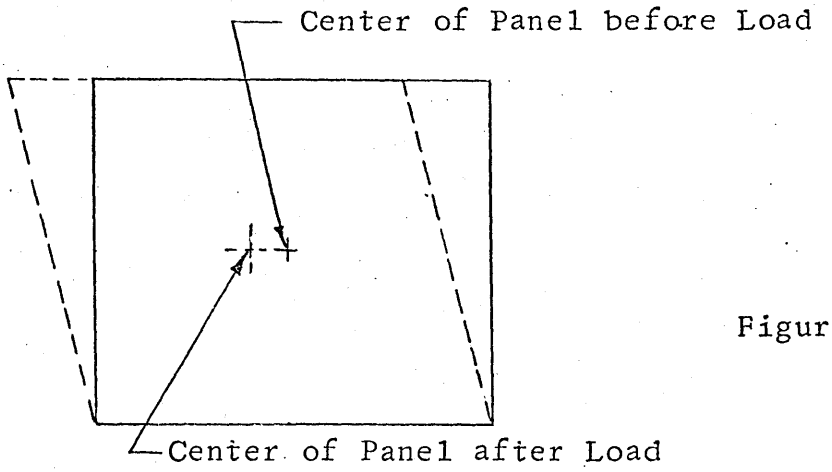

Figure 26

Consequently, the panel moves with respect to the stationery gage. Thus the gage readings obtained at each load level correspond to a slightly different point on the panel. Secondly, a corrugaged panel in general does not have a large flat spot on which to place the gage. Therefore, as the panel shifts under the applied load, the gage placed against the panel can indicate considerable lateral deflection by sliding up and down the corrugations without the actual occurrence of any lateral displacement. The technique used to avoid this problem is illustrated in Figure 27

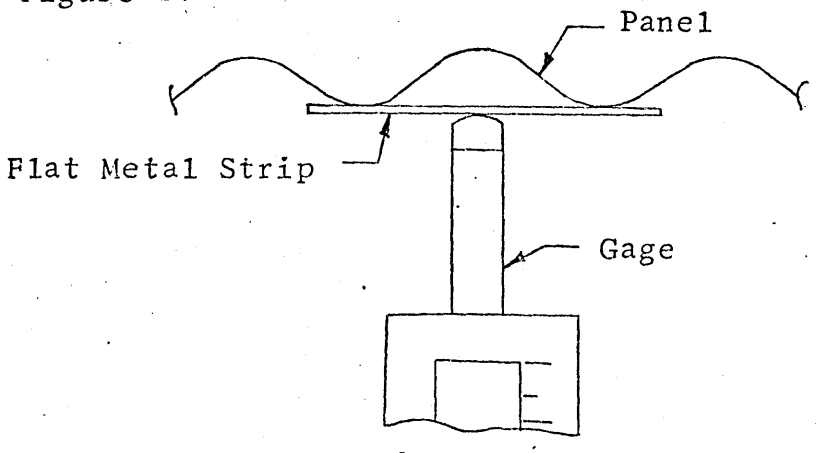

Figure 27

The flat metal strip is positioned in such a way that as the panel moves the gage pointer will slide on the strip and not up and down the corrugations. This certainly minimizes the error in the lateral deflection readings, but does not entirely eliminate it, because as the panel bends and twists the metal strip does not remain horizontal. Consequently, as the panel moves, the gage indicates lateral deflections which to some degree are a function of the slope of the metal strip. Thus, it is obvious that the measured lateral deflections are somewhat in error. From observation of the tests conducted as a part of this investigation, it seems reasonable to estimate this error to be less than ten percent. The value of the post buckling study is most closely connected to the understanding of the general trends exhibited by the variation of load versus lateral deflection, and not the precise magnitude of the lateral deflections. Therefore, the lateral deflections recorded herein are quite adequate for this post buckling investigation.

b) Experimental Procedures and Test Results

At this point it would be well to briefly mention the sequence in which the experimental and theoretical investigations of this problem of buckling were performed. The Butler Manufacturing Company instigated this study of corrugated panels under the action of shear loads by sponsoring a testing program to determine the shear strength of several of the panels manufactured by their company.

The experiments were begun before the theoretical study and, as a result, there are a few instances in which it will be noted that different test data or procedures would have been of interest, but were not obtained since the theory which indicated this interest had not yet been developed. However, the changes in the experimental work which might have occurred had the theory been developed first are fairly insignificant, and the final experimental and theoretical analyses are felt to blend together very well.

Three different types of corrugated panels were tested to determine the buckling behavior of each. The Butlerib panels and the standard sine-wave corrugated panels were used to substantiate and supplement the preceeding theoretical analysis, and the M36 panels were tested in order to illustrate some of the limits of that theory. The cross-sectional geometry and section properties of the Butlerib, sine-wave, and M36 panels are given in Figures 41, 42, and 43 respectively, and all of the tests conducted are identified in Table 3.

The installation of the panels into the frame proved very time consuming and in many cases quite difficult. Since these panels are all manufactured as small panels approximately three feet wide, it was necessary to splice several of the narrow panels together to form the larger panels to be tested. In doing this, the narrow panels

were first fastened into the frame around the outer edges in order that these edges be aligned properly with the fixtures which connected the panels to the frame. It was then necessary to crawl carefully onto the panel to drill all of the splice holes. Steel bolts 1/4 inch in diameter were used in splicing the panels and in attaching them to the end and side fixtures. All side seams contained four inch bolt spacings, and two steel washers were used on each bolt. See Figure 28.

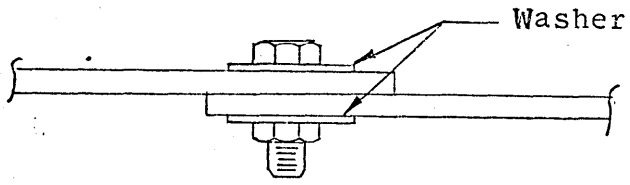

Figure 28

Practice and extreme care were necessary in forming the splices without causing the panels to assume a severely bowed shape. Still, with all the precautions which were taken, the panels assumed a slightly bowed shape in the test frame and in a few cases the bowing was quite pronounced. It was noted that slight lateral deflections started earlier with these severely bowed panels, but the panels failed at essentially the same load as did similar panels without the obvious initial bow. Therefore, while attempts to keep the panel horizontal continued to

be made, it was not felt to be a serious problem when slight bowing did occur.

After the installation of a panel into the frame, the actual testing of the panel was quite simple. All of the gages were positioned and the zero readings taken before any load was applied. Then load was applied in increments of $\triangle P$ pounds, the size of the increments being determined before beginning each test, until the panel could carry no more load and consequently would collapse. After each load increment was applied the load was held constant, and the deflections indicated by each gage were recorded.

Holes and fasteners were examined following each test, and in every case were found to be undamaged thereby guaranteeing that fastener failure in no way affected the panel behavior.

It was observed that these panels were not manufactured to close tolerances, and therefore, thickness and shape were found to vary slightly with each individual narrow pannel. It was also noted, that a few panels would curl slightly when resting on a flat surface indicating the existance of certain amounts of prestress. These inconsistencies must be tolerated, however, since to eliminate them in panels as large as the ones used in these tests would be practically impossible.

In the following discussion, length will be considered to be the dimension in the y direction (parallel to corrugation) and width the dimension in the x direction (perpendicular to the corrugation).

The first series of panels tested were the Butlerib panels. In this case, the small panels used in forming the large panels to be tested were three feet wide and extended the full length of the composite panel. Composite panels were tested with overall dimensions of 9 feet by 9.58 feet (width = 9 feet, length = 9.58 feet), 15 feet by 9.58 feet, 9 feet by 13.58 feet and 15 feet by 13.58 feet. The results of these tests indicate the effects of changes in length and width on the buckling behavior of a corrugated panel in shear.

These panels were bolted along each side to a light steel clip and along the base and top to a 1/8 inch thick steel angle, and these in turn were bolted to the frame as shown in Figures 44 and 46. The small panels were spliced together along the top of a major corrugation; also shown in Figure 44. It is realized that small moments are introduced into the panel in addition to the shear force since the load is not transferred to the panel at the center of the box section, but these moments are completely negligible. A Butlerib panel with a width of 15 feet and length of 13.58 feet is shown installed in the testing frame before a test in Figure 45.

Three tests were conducted on each panel size with the exception of the 15 x 13.58 panel for which only one test was conducted due to a shortage of panels. It was initially felt that a large deflection analysis would not be included in this investigation. Thus, lateral deflections were not recorded during the first five tests. However, at that point it was decided to examine the post buckling behavior of corrugated plates in shear, and therefore lateral deflections were read from gage D_5 during the remaining Butlerib tests, i.e. R22, R30, R31, R32 and R40. Deflections were also read from gages D_1, D_2, D_3 and D_4, i.e. shear deflections, and the data was then recorded in Tables 7 through 16. Photographs showing typical buckled panels are given in Figures 47, 48, 49 and 50. The final shear deflections listed in the tables were calculated with the computer program which is listed in part (c) of Appendix B. The shear deflections corresponding to the 9 feet by 13.58 feet panels for which no lateral deflections were measured are plotted versus external load in Figure 51, and the available lateral deflections corresponding to the other panels are plotted versus applied load in Figures 52, 53 and 54.

When the panels collapsed creases were formed across the ridges of many of the major corrugations, demonstrating the final failure to be a plastic failure.

The crippling of the major corrugations occurred due to large bending moments, and hence corresponding high stresses in the outer fibers of these relatively deep corrugations. The bending strength of the Butlerib panels is almost totally contained in the major corrugations, and therefore, when these corrugations fail, the total panel essentially collapses, even though the other parts of the panel have not experienced any plastic flow. This suggests the buckling failure of a Butlerib panel in actual service would be of a catastrophic nature.

The most significant behavior pattern which can be observed from this data is that large deflections occur corresponding to loads just slightly higher than the buckling loads. It is also interesting to note that the data shows that the buckling loads of the panels tested are not very sensitive to width changes, i.e. for panels of both lengths, the panels 9 feet and 15 feet wide failed at approximately the same load per foot. However, it can be seen that the buckling load was extremely sensitive to changes in panel length with the shorter panels exhibiting the most strength.

After each test was completed, estimates were made of the angle ($\ominus$) between the y axis and the direction of the buckles. From observation of the buckled pattern, it appeared that this angle was clearly defined. However, upon making the measurements, it soon became evident that

a band of angles would have to be estimated since the large width of an individual buckle and the effect of the edge conditions made it very difficult to precisely define the angle. As a result, the angle Θ was estimated as between 6.5 and 13 degrees for the Butlerib panels. The edge fixity caused the direction of the buckles to curve near the edge of the panels as illustrated in the following figure:

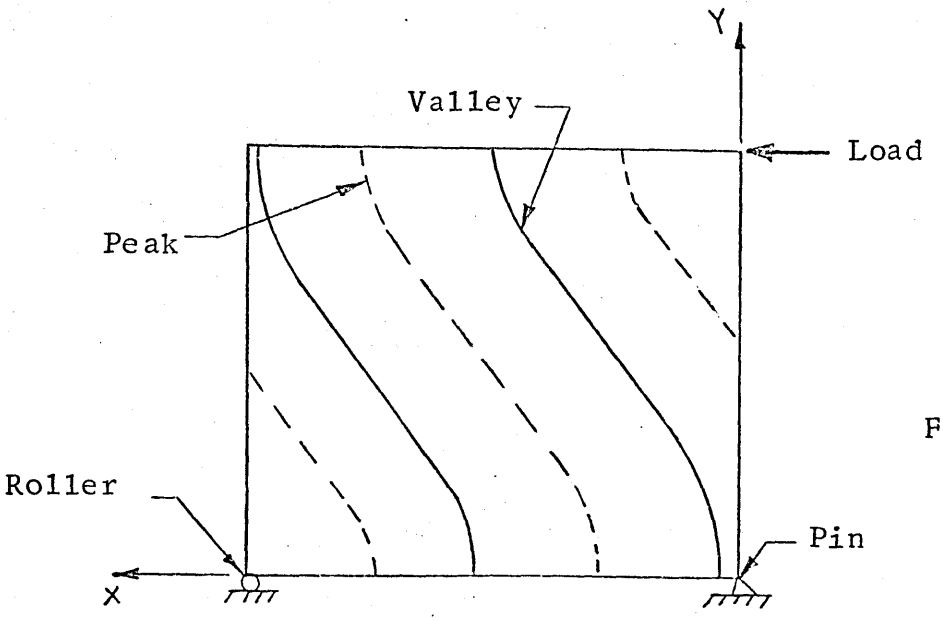

Figure 29

The lateral deflections were further identified after each test by counting the number of half-waves (n). These observations are recorded in Table 17. The plus sign given with the value n for the tests R30, R31, R32 and R40 indicates that the panel attempted to form a shape which didn't contain an even number of waves. Recall that the distance between major corrugations is one foot; then, looking at Figure 49, it can be seen that the

first two complete waves from the right are approximately two feet in length. It is interesting to note that the theory developed and discussed later in this report indicates this might happen by prediction of a value for n which is half-way between two integer values.

The second series of panels tested were corrugated panels with approximately sine-wave cross-sections. Each composite panel had a width of 8 feet, a length of 9.58 feet and was constructed from three smaller panels each with a 32 inch width. Four tests were constructed using 20 gage material for the first two tests and 24 gage material for the second two tests. By doing this, the effects of thickness could be studied, and two more points with which to check the theoretical analysis were made available.

A typical sine-wave panel is shown just before being bolted to the testing frame in Figure 60. The sine-wave panels were attached to the frame in the manner illustrated by Figure 55. Throughout this set of tests, deflection readings were taken from all five gages and the results are listed in Tables 18 through 21. The corresponding lateral deflections are plotted versus the applied load in Figures 56 and 57. Since lateral deflections were recorded and plotted for all of these tests, it is not necessary to plot the shear deflections. A photograph of a typical panel after failure is shown in Figure 58.

Examination of the curves presenting lateral deflections plotted versus applied load reveals that once the buckling load is reached, large lateral deflections occur corresponding to relatively small increases in the applied load as happened with the Butlerib panels.

It is particularly interesting to note that the buckled pattern for test R51 occurred spontaneously. The load was being held constant and no lateral deflection had occurred when suddenly the panel "popped" into a buckled configuration. During this time the load remained relatively constant. In general, the panels had some sag due to their own dead weight; therefore, they were eccentrically loaded, and deflected somewhat gradually into the buckled pattern as the load was increased. However, it is felt that this panel was perhaps held level by a slight support from gage D_5. In other tests, this gage was placed under the panel with the pointer arm extended half-way so that it only lightly touched the panel, but in this test the gage was wedged under the panel so that it created a light support which may have helped relieve the dead weight of the panel. Most probably the panel had also been installed with less initial bow than was generally the case. Certainly definite conclusions can not be drawn from one test, but it is noted that the buckling behavior encountered in test R51 indicates the existence of a second equilibrium configuration at the same load, such as is encountered in

the buckling of thin shells, and as the large-deflection theory developed here predicts.

Again, if the lateral deflection versus load curves are examined, it is seen that, unlike the Butlerib, after a considerable amount of lateral deflection these panels begin to carry additional load with reduced increases in deflections. However, it is felt that the deflections are already so severe by the time the post buckling strength has any effect, that for most cases the buckling load would still be considered the failure point. The final failure is again a plastic failure, because the panels make almost no attempt to return to the unloaded configuration when the load is relieved.

It should be noted that the sine-wave panel does not depend upon a few deep corrugations for its strength, but instead has many equal corrugations that all serve to resist the internal bending moments. The distances from the neutral axis to the outer fibers are not as great as in the case of the Butlerib, and hence, supposing that the moment of inertia, I_x, was made to be the same for both types of panels, it is apparent that equal moments in both panels would produce smaller outer fiber stresses in the sine-wave panel. Consequently, with bending moments directly related to radius of curvature, much deeper buckles can form in the sine-wave panel before plastic failure occurs. In addition, if one corrugation fails in a portion

of the sine-wave panel in which the radius of curvature has become very small, then the load can be redistributed into the many other corrugations and the panel will not collapse.

Hence, it can be said that, in general, panels which depend upon just a few corrugations to withstand most of the bending loads will exhibit a minimum amount of post buckling strength due to the possibility of local crippling of the major corrugations, and the subsequent failure of the entire panel. Whereas a panel that has its bending strength distributed among many corrugations can probably be expected to possess considerable post buckling strength.

After each test, the angle ($\ominus$) between the y axis and the direction of the buckles was estimated. It was found to be from 28^{o} to 32^{o} for the 20 gage panels and from 23^{o} to 28^{o} for the 24 gage panels. The wave parameter n was also observed for each test and is recorded in Table 17.

The final panels tested were M36 panels. These panels were not tested with expectation of matching the results of the theoretical analysis, but rather to illustrate some of the limitations of the theory developed herein.

The first two tests were conducted with panels 8 feet long and 3 feet wide. The third test panel was 6 feet wide and 12 feet long and the last panel was 9 feet wide and 12 feet long. Each of these last two panels was constructed from panels 3 feet wide and 12 feet long. The sides and splices were attached with steel bolts as shown

in Figure 59 and the top and bottom of each panel were attached to a special base angle which is shown in Figure 61. The base angle was then bolted into the side of the frame.

During these tests, deflections were read from gages D_1 through D_4 and these data are recorded in Tables 22, 23 24 and 25. In each case the failure occurred suddenly and no lateral deflections were visable before the failure occurred. The failures were of a local nature with the buckle extending over one major corrugation only, as shown in Figure 62. The buckles appeared to start in the slanted side walls illustrated in the following figure.

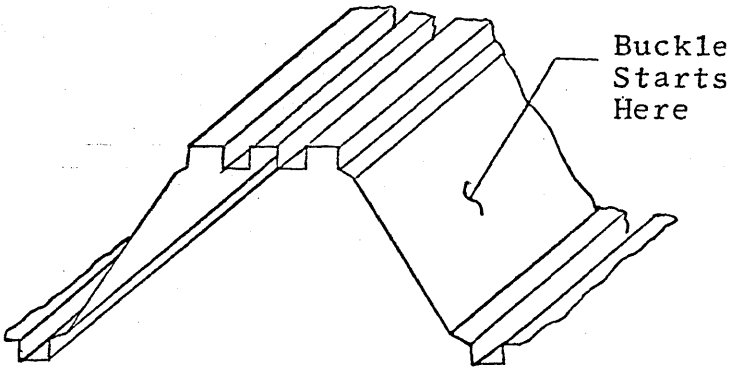

Figure 30

The local failure of these panels indicates that their failures would not be accurately defined by considering the average properties of the panel. Because of this it would be

expected that the panel would fail under less load than an orthotropic panel which has material properties equal to the average material properties of the M36 panel. The implications of these test results are discussed more thoroughly later in this paper when the theoretical and experimental investigations are compared.

This completes the description of the experimental portion of this investigation. Next, a further discussion of the data acquired and a comparison of these data with the theoretical analysis is presented.

CHAPTER VIII

CORRELATION OF TEST DATA WITH THE THEORETICAL ANALYSIS

The test results obtained from the Butlerib and sine-wave panels are now compared to the corresponding results predicted by the theoretical analysis in order to determine how closely the behavior of a corrugated panel loaded in shear is described by the theoretical analysis developed in this paper. The panels which were tested were galvinized, but this coating is assumed to have had no effect on the strength of the panels. Since the exact base metal thickness of the galvanized panels can not be determined, the theoretical predictions are derived corresponding to the upper and lower manufacturing tolerances on the panel thicknesses. As an example, upper and lower limits are predicted for the buckling load rather than one value. The upper and lower limits of the thicknesses of each type of panel are listed in Table 26. Also listed in this table are the corresponding constants H_x, H_y and H_{xy} which have been computed using equations (11), (14), and (18). Using these constants and the appropriate dimensions for a and b corresponding to each test, the predicted values for $\Theta = \tan^{-1}\alpha$ and n are computed using equations (58) and (60); and are listed in Table 17 along with the values of Θ and n obtained from the actual tests.

It is noted that in each case, the predicted and actual values of n are precisely the same. During the testing of the Butlerib panels with dimensions 9 feet by 9.58 feet and 15 feet by 9.58 feet one of the n half-waves was found to be larger than the other half-waves. The theory developed in this paper indicates the possibility of this occurrence since n half-waves are predicted corresponding to the upper limit of the thickness and n + 1 half-waves are predicted corresponding to the lower limit of the thickness. Apparently, the material thickness of the panels was approximately half-way between these two limits. Consequently, the panel attempted to buckle into a shape with n + $\frac{1}{2}$ half-waves, and hence the one long half-wave was developed. It is apparent that the theoretical analysis quite clearly defines the number of half-waves to be formed in a corrugated plate.

The corresponding predicted values for α do not match the actual values of α measured during the tests. It is pointed out, however, that the theory clearly shows the same trend in the change of α as do the tests, i.e. as H_x/H_y becomes smaller, the angle $\theta = \tan^{-1}\alpha$ becomes smaller. There are two factors which may account for the differences between the values of α obtained from the theory and the tests. First, as was pointed out previously, it was extremely difficult to measure the exact angle made by the buckle with the y axis, and even though a range of

angles was measured in an attempt to resolve this problem, it is highly possible that the correct angle was not measured. It is also possible that the theoretical analysis predicts an α somewhat in error due to the fact that boundary conditions are not exactly duplicated by the approximation of later deflections.

It seems, that due to the flexibility of the panel in the x direction, the strain energy level will be changed only slightly if lateral deflections are set equal to zero along the edges x = 0 and a. This permits an accurate value of the buckling load to be obtained without satisfying these boundary conditions. However, it is also conceivable that α might be more sensitive to this boundary condition than is the buckling load. To determine the amount to which this affects α would require extensive additional investigations. It should also be pointed out that the approximation for w defines a buckle which is straight from one edge of the panel to the other, and observation of the tests showed the buckles to curve slightly close to the edges as illustrated by Figure 29. This might also affect the prediction of α. Certainly this is an area for future study.

At first it might be felt that if α were brought into agreement with the theory then the resulting values of n given by equation (58) would no longer agree with the test results. This is not necessarily true, because when

computing n, it was found that for the panels considered herein equation (58) can be closely approximated by the following equation

$$m = \frac{a}{b}\left(H_Y/H_X\right)^{1/4}$$

which does not contain the parameter α.

Since the buckling load predicted by the small deflection theory exactly matches the buckling load that is indicated by the large deflection theory, it will be sufficient to compare the large deflection curve of load versus lateral deflection to the lateral deflections measured during the tests in order to see how closely the buckling load and subsequent lateral deflections are predicted. As mentioned previously, the parameters α and n are treated as constants for each particular panel in the large deflection analysis. Therefore, the values of α and n obtained from the small deflection analysis are used to determine the desired load versus lateral deflection relations.

Lateral deflections were not recorded for any of the 9 feet by 13.58 feet Butlerib panels. Therefore, for this one set of panels, only the theoretical buckling load may be compared to the test data. The buckling load may be easily seen from the shear deflection versus load curves since the panel buckled and then collapsed almost simultaneously causing large changes in the shear

deflections as well as the lateral deflections. Consequently, the predicted upper and lower limits of the buckling load are shown as dashed lines on the plot of shear deflection versus load given in Figure 51. Notice that the actual buckling load is very closely approximated by the theoretical predictions.

For the other configurations of the Butlerib and the two configurations of the sine-wave panel, the computer program listed in part (b) of Appendix B was utilized to compute the coefficients L, J and K of equation (71). These coefficients which define the load versus lateral deflection curve for each panel were computed for both the upper and lower base metal thickness limits, and are listed in Table 27. The resulting predicted curves are shown as dashed lines in Figures 52, 53, 54, 56 and 57. It is observed that, except for the Butlerib panels with b = 9.58 feet, the experimental buckling loads are higher than the predicted values. This might appear incorrect since use of the Ritz Method results in a buckling load higher than the exact theoretical buckling load. However, if the theoretical model is of such a nature that it can not resist as much shear load as can be resisted by the actual physical system, then the Ritz Method applied to this model can result in the prediction of lower buckling loads than occur in actual tests.

It is observed that the predicted buckling loads for the test panels are within 30 percent or less of the

measured buckling loads, and for the majority of the panels this difference is considerably less than 30 percent. This is considered to be an extremely good correlation considering that the boundary conditions have not been precisely matched. It would be extremely difficult to exactly duplicate the boundary conditions of the test panels at y = 0 and b since the panels are neither fixed nor simply supported along these edges. The accuracy of the predicted buckling loads seem even better when one recalls that the buckling load of a column is changed by a factor of four if the boundary conditions are varied from pinned ends to fixed ends. It would be of interest to conduct future studies investigating the effects of various boundary conditions on the buckling load and corresponding shape of the buckled panel.

The test data which are slightly puzzling are obtained from the tests of the Butlerib panels 9.58 feet in length. The buckling loads are noted from Figures 53 and 54 to be very close to the lower limit of the predicted buckling loads so that the concern is certainly not one of accuracy. However, for all other Butlerib panels and the sine-wave panels failure occurred at loads higher than the predicted buckling load, whereas in these two panel configurations the failure occurred just below the lower limit. This set of data consisted of four tests and all of these data were fairly consistant, so that it would appear that the test

data are not in error. The discrepancy may be explained by noting that the manufacturing tolerance on the thickness of the bare steel of these panels is from .0191 to .0217 inches, and the average measured thickness of these particular panels including the thickness of the galvanizing was .0209 inches. Hence, these panels must have been manufactured close to or below the lower thickness limit. Although this discussion can not definitely account for this slight inconsistancy, it is not felt to be a serious development since the predicted and actual failing loads are, as pointed out, still quite close. However, it would be very interesting to conduct an experimental investigation in which panels of many different lengths are considered to determine whether this theory actually accounts for changes in lengths properly, and if not, to determine just what a change in length does to the buckling strength of these panels. It should be noted that both the theory and the experimental results indicate that the buckling load per foot of the panels considered in this report are relatively independent of the width of the panel. It is also noted that in all cases discussed in this paper, the magnitude of the buckling load is primarily determined by the magnitude of the bending stiffness H_y. The bending stiffness H_x has a secondary effect on the buckling load and the twisting stiffness H_{xy} has almost no effect on the buckling load whatsoever. In

addition, it is noted that the twisting stiffness also has a negligible effect on the determination of α and n.

It is seen from Figures 52, 53, 54, 56 and 57 that the post buckling behavior in the region of the bifurcation point is clearly defined by the theoretical analysis. The theoretical analysis indicates that initially a slight drop in load from the buckling load occurs with increased lateral deflections, and correspondingly it points to large lateral deflections when the applied load is increased slightly above the buckling load. This tendency for the panel to deflect considerably after buckling, with small increases in load, is substantiated by the test data. Even the possibility of the panels jumping to a deflected equilibrium configuration before the buckling load is reached is demonstrated by the sine-wave panel test R51; see Figure 56. It is felt that in actual application, the buckling load would most probably be called the failure load even for the sine-wave panels in which the final failure occurred at a load approximately three times as large as the buckling load since it would be difficult to sell a customer a panel which might be required to operate under a configuration which looks as seriously buckled as do the panels at any time beyond the buckling load.

From the appearance of the test data it seems that the large deflection analysis predicts accurately the load versus lateral deflection relation for a panel until

the maximum deflection reaches from .5 to 1.5 inches depending upon the particular panel. It is then apparent that if total plastic failure has not yet occurred, the rate of increase in lateral deflection with applied load will reduce, and the panel will carry more load until the final plastic failure is reached. The eventual post buckling strength is attributed to large increases in the membrane stresses and hence the assumption made herein that these changes are negligible becomes invalid. Thus this theory no longer applies. The fact that the changes in membrane stresses become large when the panel eventually picks up its post buckling strength was made evident when it was observed that the end and side attachement members attempt to pull away from the frame and are consequently considerably deformed during this portion of the test.

The remaining panels tested with results which can be compared to the theoretical analysis are the M36 panels. The upper and lower limits of the predicted buckling loads for the M36 panel are listed in Table 28 along with the actual loads measured during the testing. As expected, the panels failed considerably before the predicted buckling load was reached. The corrugation in these panels are so deep that the effects of a load on one corrugation is rapidly damped out, and hence only slightly affects the behavior of an adjoining corrugation. Consequently the

panel does not behave similar to an orthotropic panel which has material constants equal to the average material constants of the M36 panel. Instead, each individual component of the cross-section, particularly the flat slanted section referred to in Figure 30, behaves somewhat as a separate system, and as a result the panel experiences local failures which occur before the predicted buckling load is reached. From this information, it is obvious that the theory developed herein does not apply to panels similar to the M36 panel.

However, the majority of the corrugated panels used in building construction are of the type represented by the sine-wave and Butlerib panels rather than by the M36 panel. Consequently, the theory developed herein will apply to the majority of corrugated panels.

CHAPTER IX

SUMMARY

In this thesis, theoretical techniques are developed which predict the buckling load, describe the buckled pattern and define the post buckling behavior of a thin corrugated plate (or panel) of arbitrary cross-section under the action of external in-plane shear loads. In conjunction with the theoretical analysis, an experimental investigation has been conducted on such corrugated panels in order to verify and supplement the theoretical analysis. In general, the theoretical analysis is found to clearly describe the buckling behavior of the test panels.

The theoretical analysis is conducted by first developing a model which represents the corrugated panel in shear and lends itself to a mathematical analysis. The model, which is chosen to represent the corrugated panel, is an infinitesimal element of an orthotropic plate which has material constants equal to the average material constants of the corrugated panel. These material constants are determined from an analysis of a square element from the corrugated panel with outside dimensions equal to the distance across one repeating cross-section of the corrugated panel (See Figure 2). The internal

loads which are considered to be acting upon the orthotropic model are bending moments, twisting moments and membrane forces.

Equations defining the buckling load and resulting deflected shape are determined by examining the second variation of the potential energy of the system from a loaded straight configuration, i.e. one with no lateral deflections, of the orthotropic plate. Then the post buckling behavior of this plate is defined by minimizing the potential energy of the system in a loaded and laterally deflected configuration to determine the deflected equilibrium configurations in terms of the external loading. In each case the final solutions are determined by the Ritz Method with the lateral deflections assumed in the form

$$W = A \sin \frac{\pi Y}{b} \sin \frac{m\pi}{a}(x - \alpha Y)$$

In order to show that this approximation for w accurately represents the lateral deflection, it is shown that its use results in the determination of a buckling load within three percent of the buckling load obtained using the potentially very accurate approximation

$$W = \sum_{M=1}^{\infty} \sum_{N=1}^{\infty} A_{MN} \sin \frac{M\pi x}{a} \sin \frac{N\pi Y}{b}$$

When the infinite series is used in the computation of the buckling load it is realized that the accuracy of this

solution is dependent upon the numbers of terms chosen to represent the series. Hence, enough terms are chosen to approximate the infinite series in order to guarantee the resulting values of the buckling load are rapidly converging to the exact solution. Therefore, the buckling load determined by using the infinite series approach is considered quite accurate, and since the use of the two approximations for w result in similar values of the buckling load, the single term approximation must be a good representation of the lateral deflections. Therefore, the single term approximation of w is used throughout the analysis.

The completion of this solution results in equation (56) which is shown to predict loads at which the test panels buckle within thirty percent of the actual buckling load. (For the majority of the panels, the predicted and actual buckling loads differ by less than fifteen percent.) This is felt to be a particularly good correlation, recalling that the degree of edge fixity for the panels is not precisely known and therefore can not be exactly represented in the theoretical analysis. It is probable that this edge fixity is of considerable importance in this problem. It obviously plays an important role in determining the buckling load of a column in which case the buckling load is changed by 400 percent by altering the end fixity from pinned ends to rigidly fixed ends,

and it can reasonably be assumed that it would have a noticeable effect upon orthotropic plates in shear. The theoretical analysis shows the magnitude of the buckling load as primarily a function of the bending stiffness H_y, with the bending stiffness H_x contributing a small amount to the buckling load. The twisting stiffness H_{xy} is found to have negligible effect upon the buckling load for the panels considered in this investigation. Within the limits of the size of the panels tested, the buckling load per foot is found to diminish rapidly as the panels are lengthened, and hold relatively constant as the width of the panels are increased.

When the buckled pattern is defined, it is noted that the number of half-waves n is exactly predicted by equation (58) for all of the cases considered. Equation (58) is a function of α, although it is pointed out that n can be closely approximated by the equation

$$m = \frac{a}{b}\left(H_y/H_x\right)^{1/2}$$

which indicates that n is only slightly dependent upon α. The angle $\Theta = \tan^{-1}\alpha$ as defined by equation (59) is shown to be a constant for a panel with a particular repeating cross-section regardless of the overall dimensions of the panel. The actual magnitudes of the theoretical and experimental values of α do not match closely; however, both theoretical and experimental investigations do clearly

show the trend of α decreasing as the ratio H_x/H_y decreases. It is pointed out that the discrepancy in the magnitudes of α most probably can be attributed to the difficulty in measuring the proper angle from the tests and the possibility of incorrect prediction of α due to the failure of the approximation for lateral deflections to exactly satisfy the boundary conditions in the theoretical analysis.

The final topic discussed in this paper is the post-buckling behavior of an arbitrary corrugated plate in shear. Again, the theoretical analysis is found to quite clearly define the actual panel behavior. It is observed that both the test data and the theoretical load-deflection relation given by equation (74) demonstrate large deflections of a corrugated panel in shear occurring when the applied load is increased only slightly above the buckling load. The theoretical load deflection curve actually shows that P_y drops as lateral deflection increase after the buckling load has been reached. The theory also shows that, after considerable lateral deflection the panel will again carry increased loads.

This behavior permits the existence of more than one equilibrium configuration at one value of applied load. The sine-wave panel test designated by R51 seems to substantiate this prediction, because, while the load was being held constant at a value near the buckling load, the panel suddenly moved into a deflected equilibrium

configuration. During this change from an undeflected to a deflected equilibrium configuration the load remained constant. It is felt that this behavior pattern was not followed by any of the other tests since in general the panels were installed with an initial bow, and hence slight lateral deflections began with the first load as illustrated in the following figure:

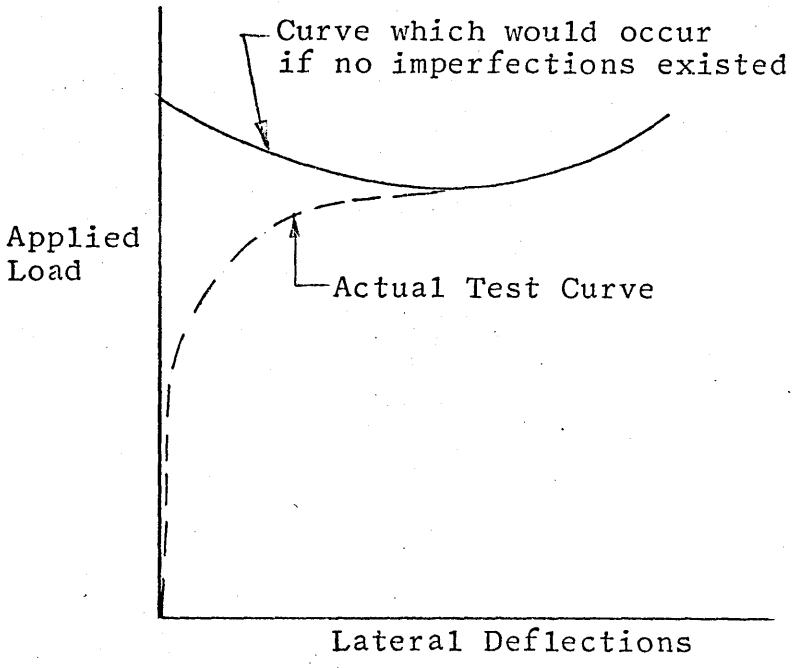

Figure 31

For both the Butlerib and sine-wave panels which were tested, large deflections occur after buckling with small increases in load, but the final post buckling strength is found to be peculiar to each particular type of panel. If the bending strength of a panel is divided among a large number of corrugations, as in the case of

the sine-wave panels, then the plastic failure of the outer fibers of a few corrugations causes a redistribution of the load into some of the other corrugations. Consequently, the panel is able to withstand considerable lateral deflection without experiencing a total collapse. As this type of panel continues to deflect laterally, the membrane forces become quite large, and the panel may exhibit a large amount of buckling strength before it collapses. As an example, the final failure of the sine-wave panels occurred at a load approximately three times the buckling load. On the other hand, if the bending strength of a panel is contained by a few relatively deep corrugations, as in the case of the Butlerib panels, the outer fibers of the major corrugations experience high stresses for relatively small lateral deflections and consequently the major corrugation collapses resulting in an overall panel collapse. Thus, this type of panel exhibits very little post buckling strength.

In conclusion, it can now be stated that the general problem of buckling of an arbitrary corrugated panel under shear loads is now much more clearly defined than before. With the new techniques presented in this report it is possible to examine specific corrugated panels and determine their behavior when loaded in shear. It is the author's belief that the discrepancies between the theoretical and experimental results presented in this thesis are due largely to the imperfect experimental

specimens used. If experiments could be performed on more perfect experimental specimens, i.e. ones which are carefully formed with no pre-stress and fastened at their edges so that the boundary conditions assumed in the theoretical analysis are satisfied, there would most probably be much closer correlation between theory and experiment.

REFERENCES

REFERENCES

1. Bergmann, S. and Reissner, H., Z. Flugtech, u. Motorluftsch., vol. 20, p. 475, 1929.

2. Seydel, E., Z. Flugtech. u. Motorluftsch., vol. 24, p. 78, 1933.

3. Timoshenko, Stephen P. and Gere, James M., Theory of Elastic Stability. New York: McGraw-Hill, 1961.

4. Panlilio, F., Elementary Theory of Structural Strength. New York: John Wiley and Sons, Inc., 1963.

5. Boresi, A. P., Elements of the Mechanics of Deformable Bodies, TAM 451, Dept. of Theoretical and Applied Mechanics, University of Illinois.

6. Timoshenko, Stephen P. and Woinowsky-Krieger, S., Theory of Plates and Shells. New York: McGraw-Hill, 1959.

7. Stein, M. and Neff, J., NACA Tech. Note 1222, 1947.

8. Peterson, Thurman S., Elements of Calculus. New York: Harper and Brothers, 1950.

FIGURES

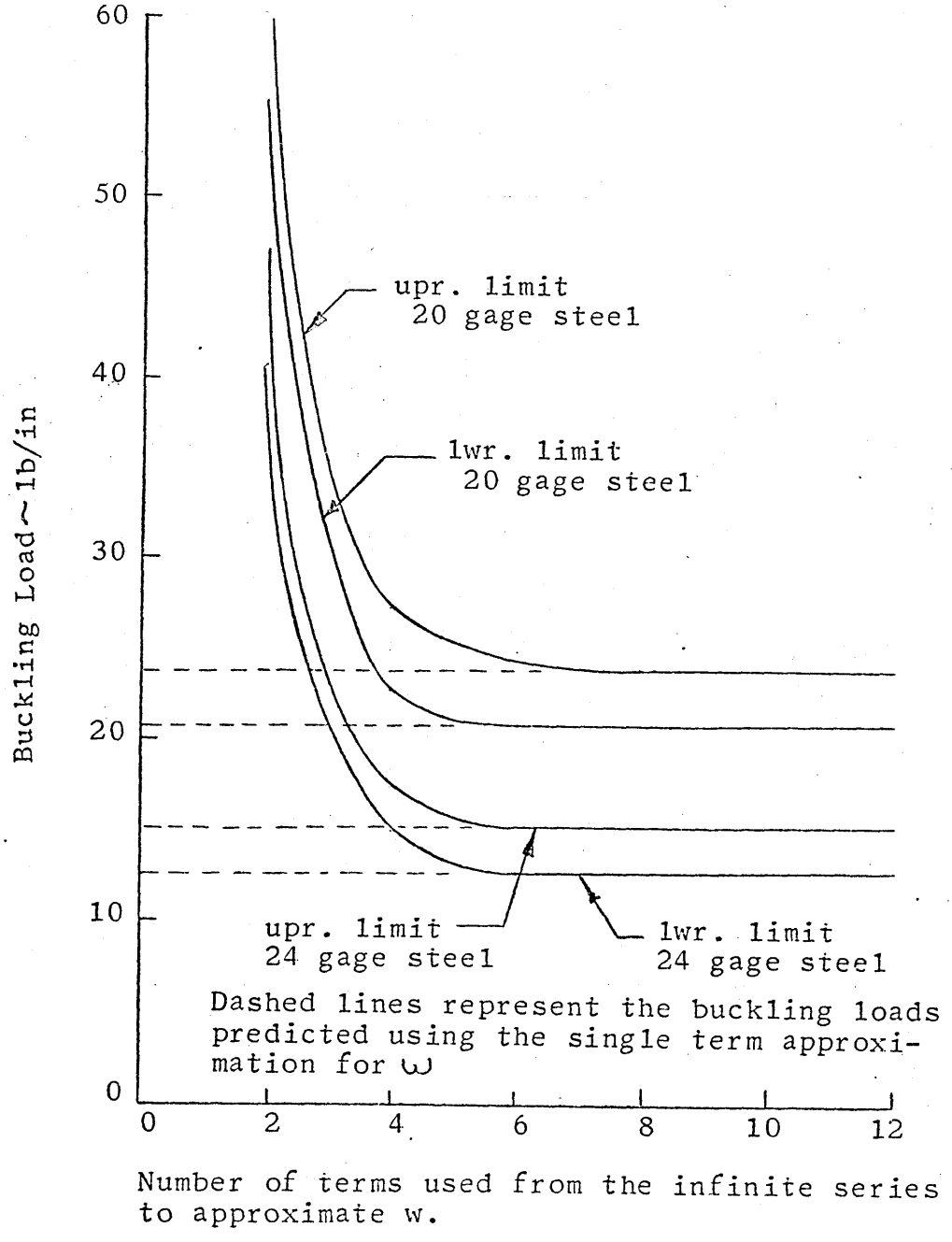

Figure 32. Buckling load versus the number of terms used to approximate w, Sine-wave Panels, a = 8 feet, b = 9.58 feet.

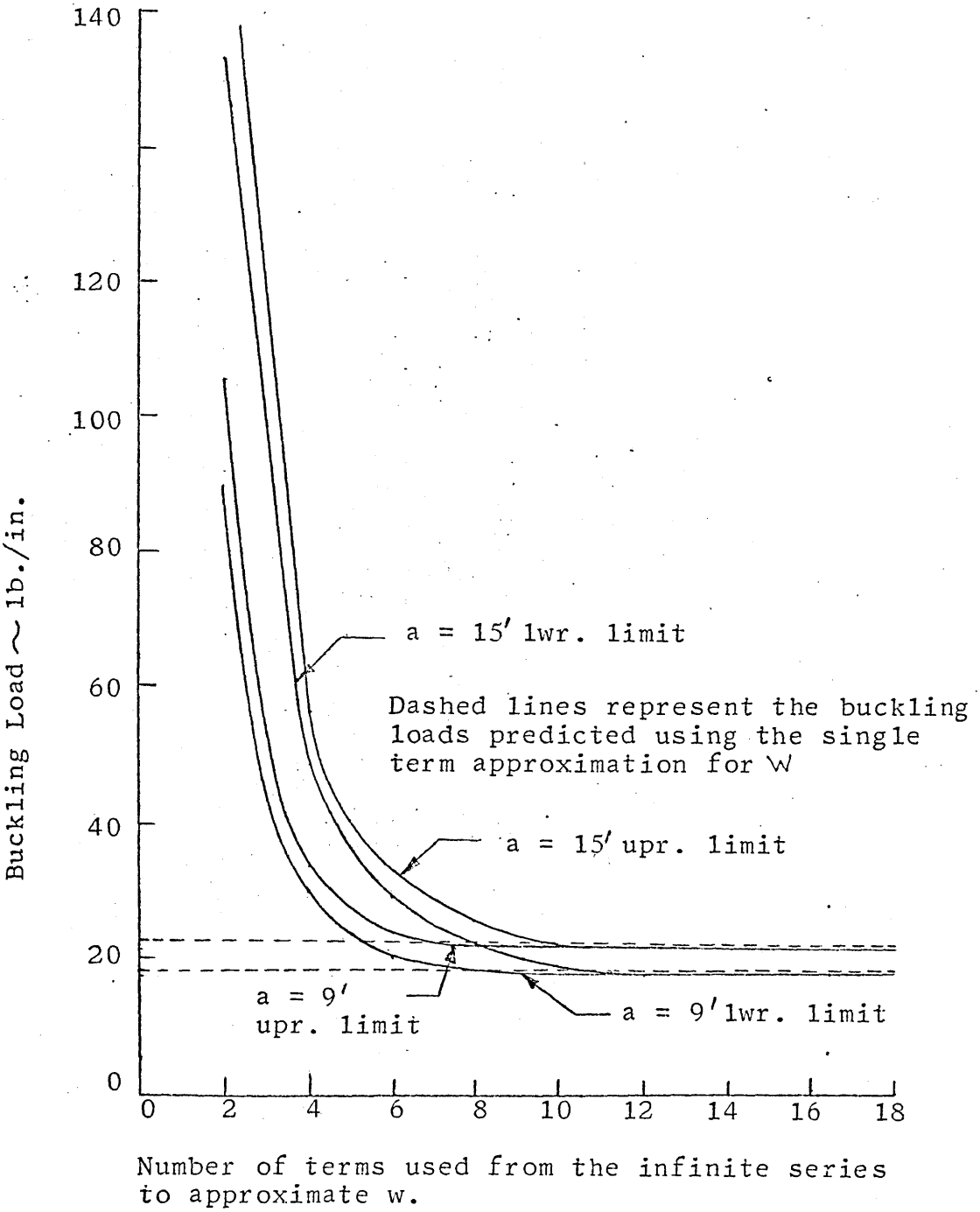

Figure 33. Buckling load versus number of terms used to approximate w, Butlerib Panel, b = 13.58 feet.

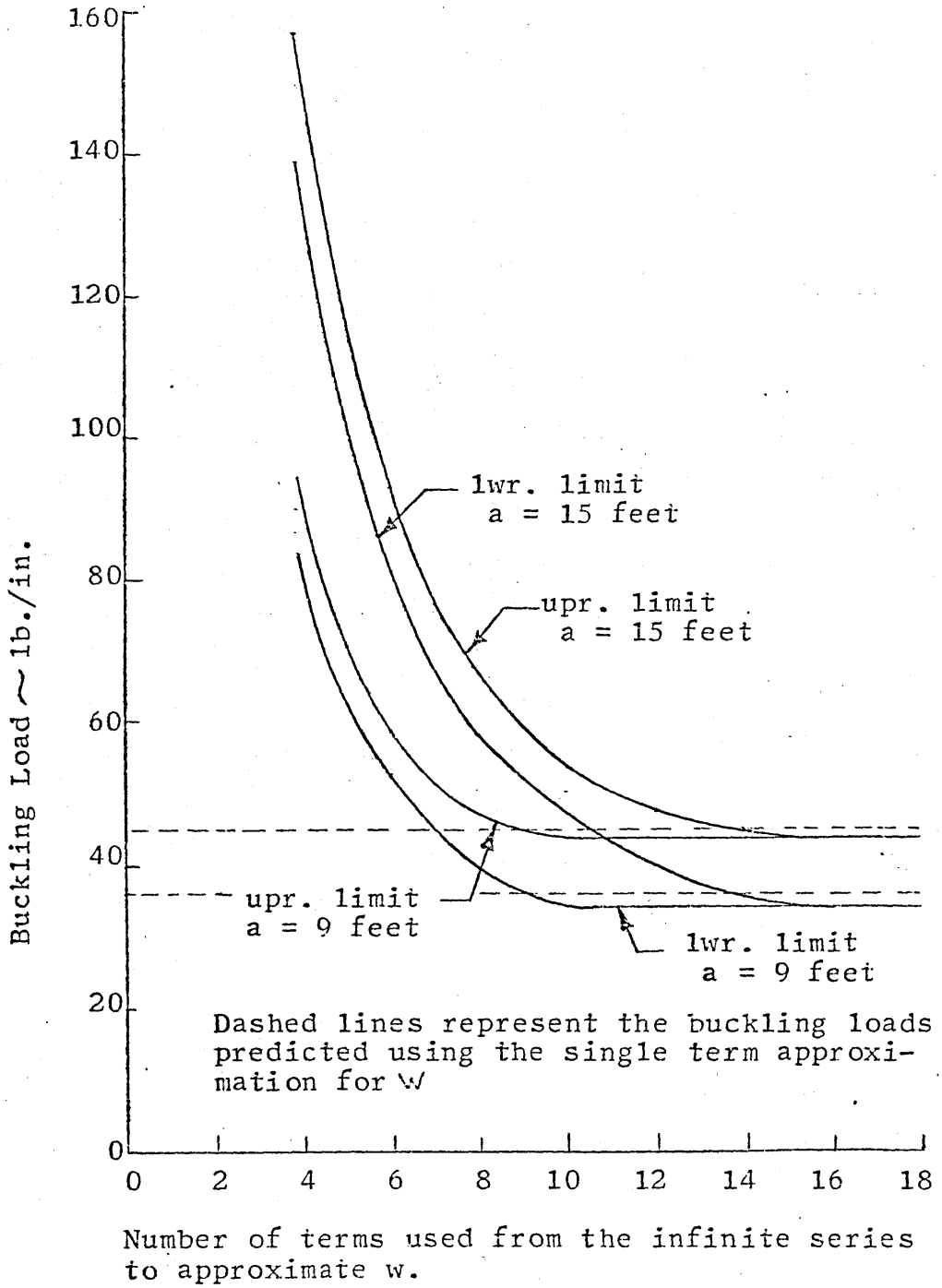

Figure 34. Buckling load versus the number of terms used to approximate w, Butlerib Panels, b = 9.58 feet.

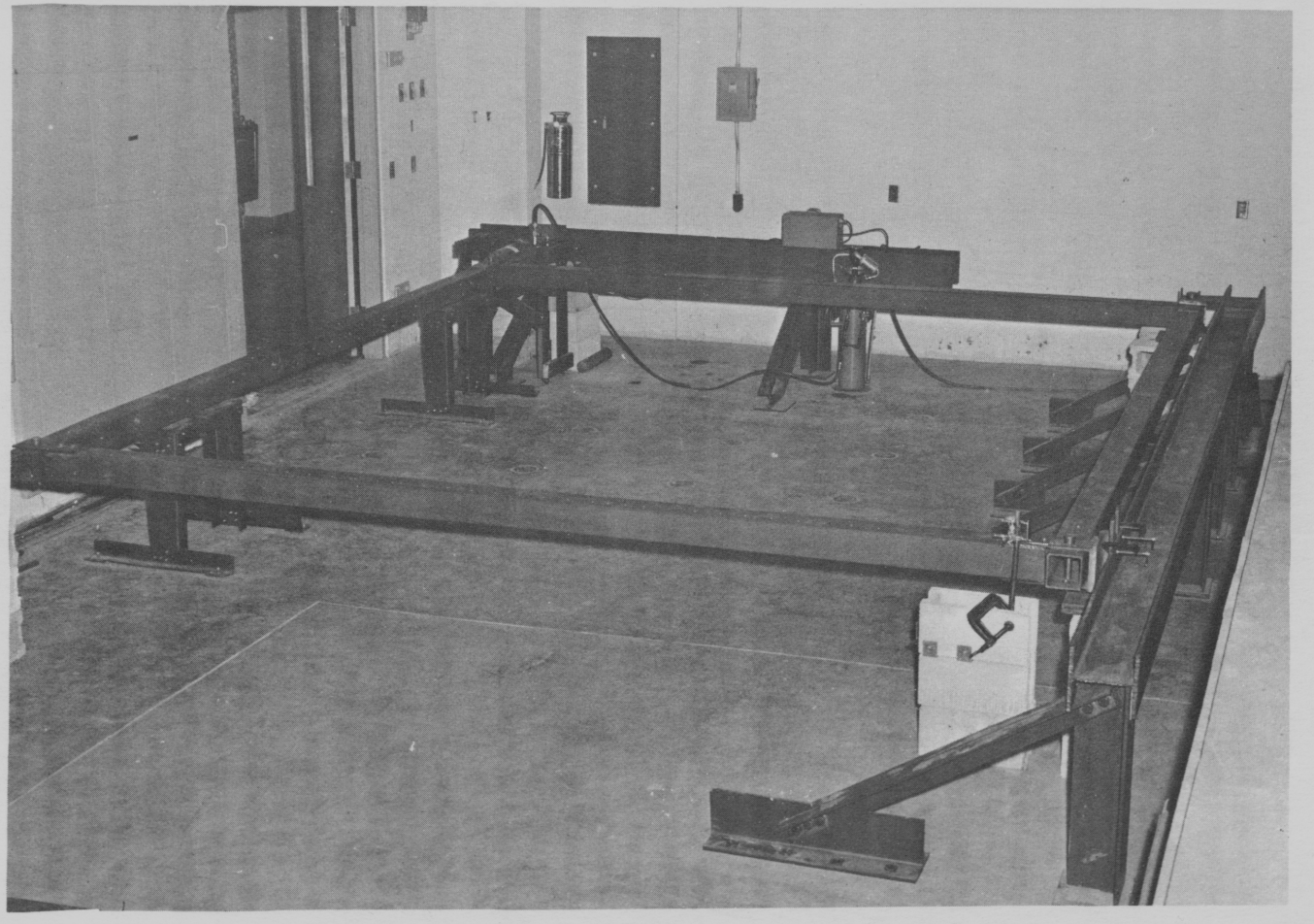

Figure 35. Test Frame.

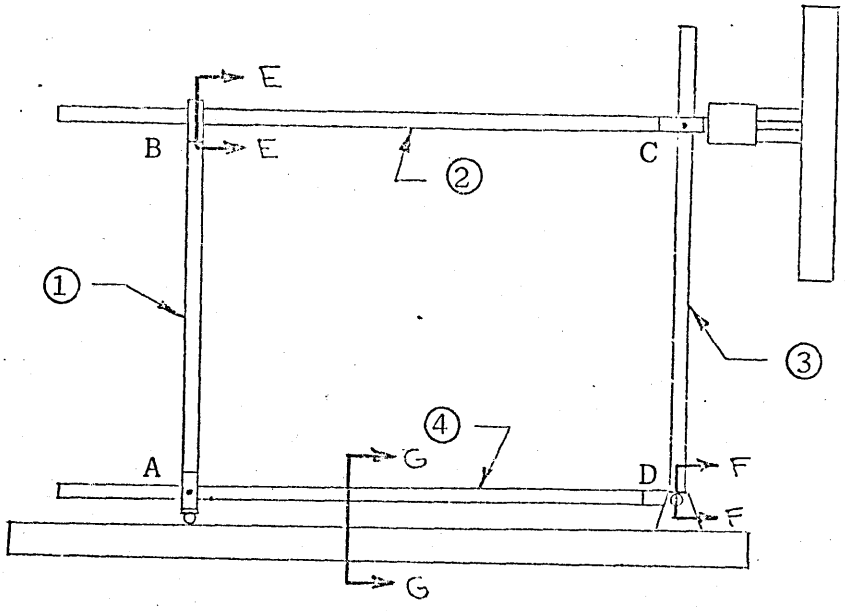

Plan View of Testing Frame

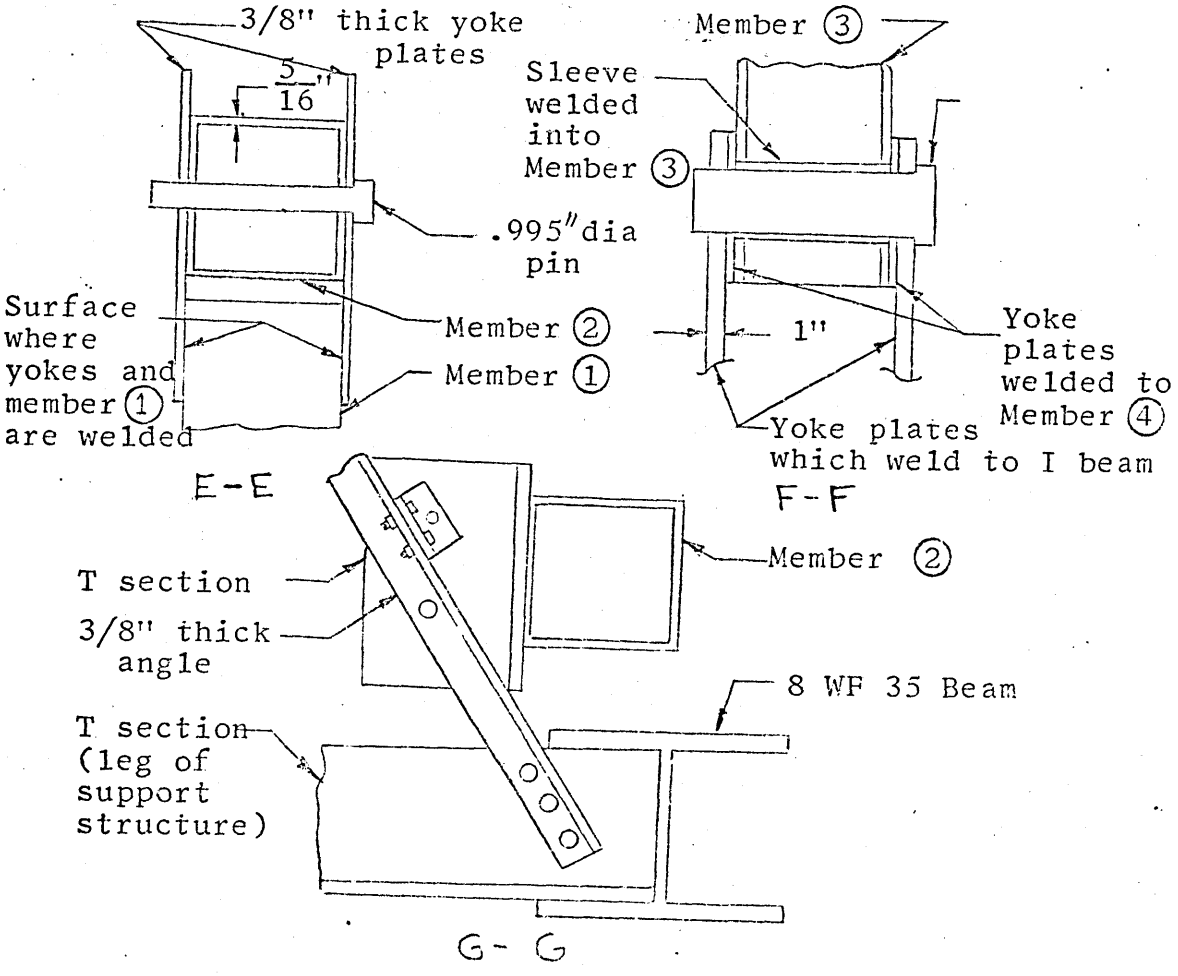

Figure 36. Drawing of basic frame.

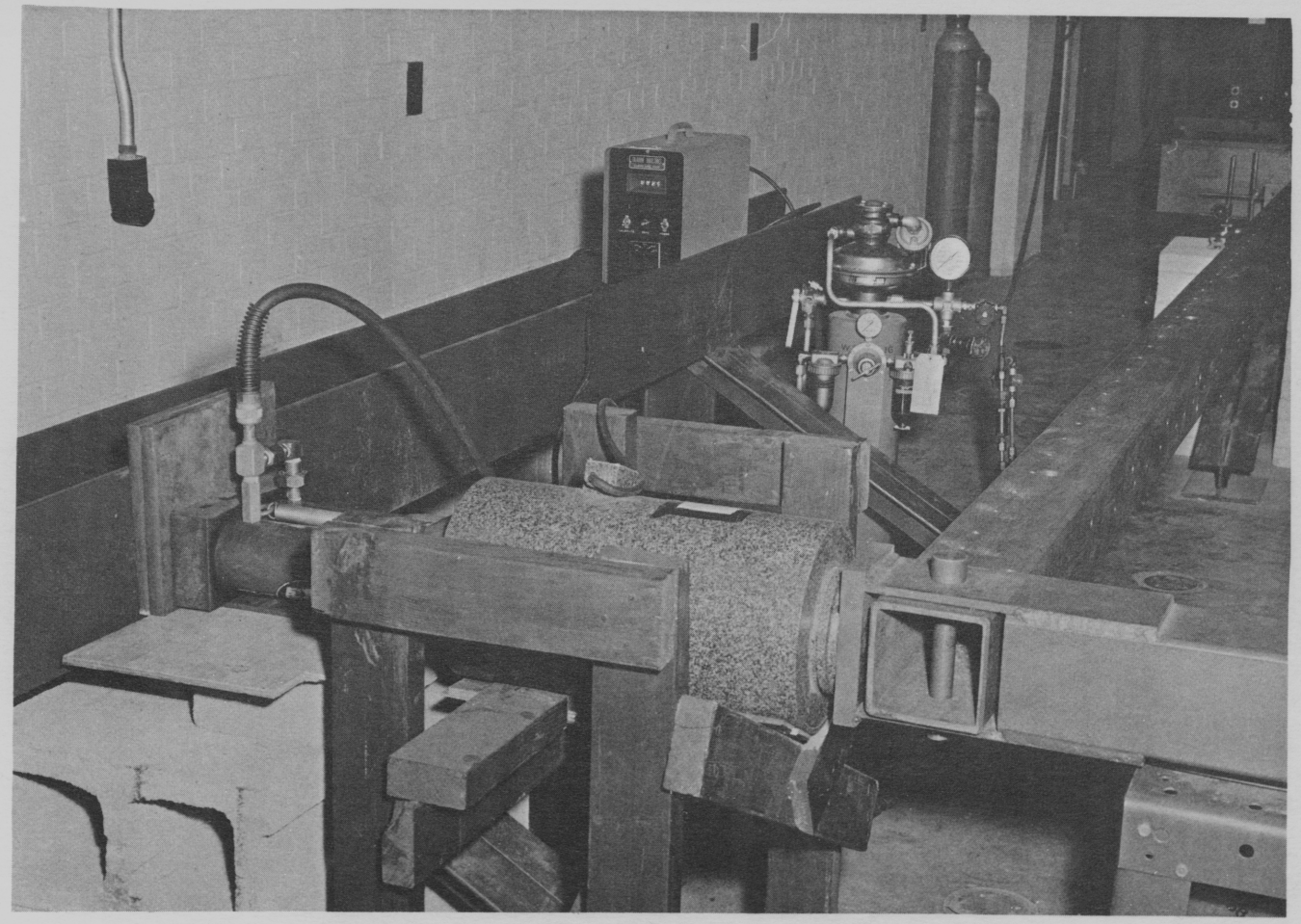

Figure 37. Corner C of Test Frame, Load Cell and Recorder, Hydraulic Jacks and Pressure Cylinder.

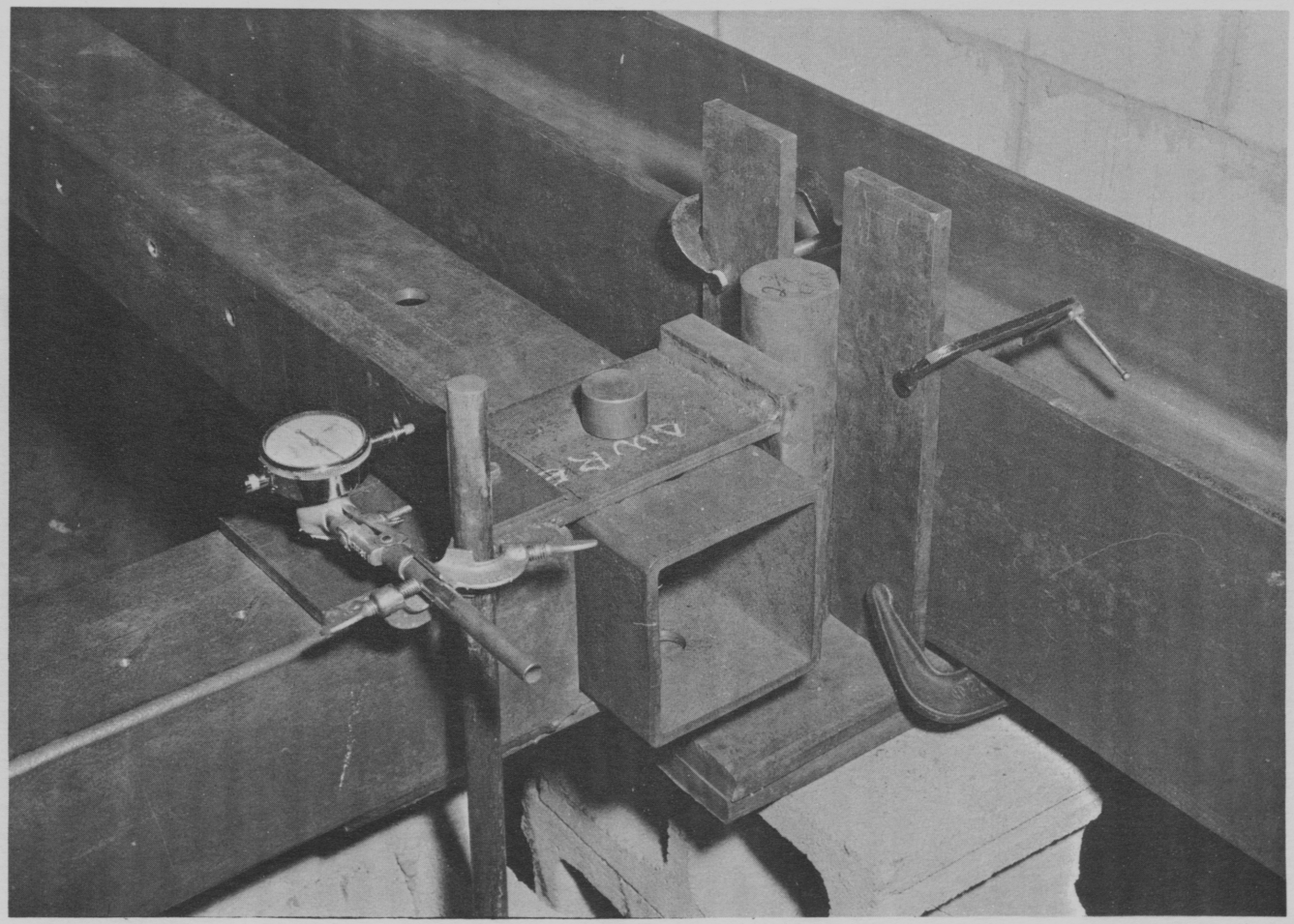

Figure 38. Corner A of Test Frame and Gage D_4.

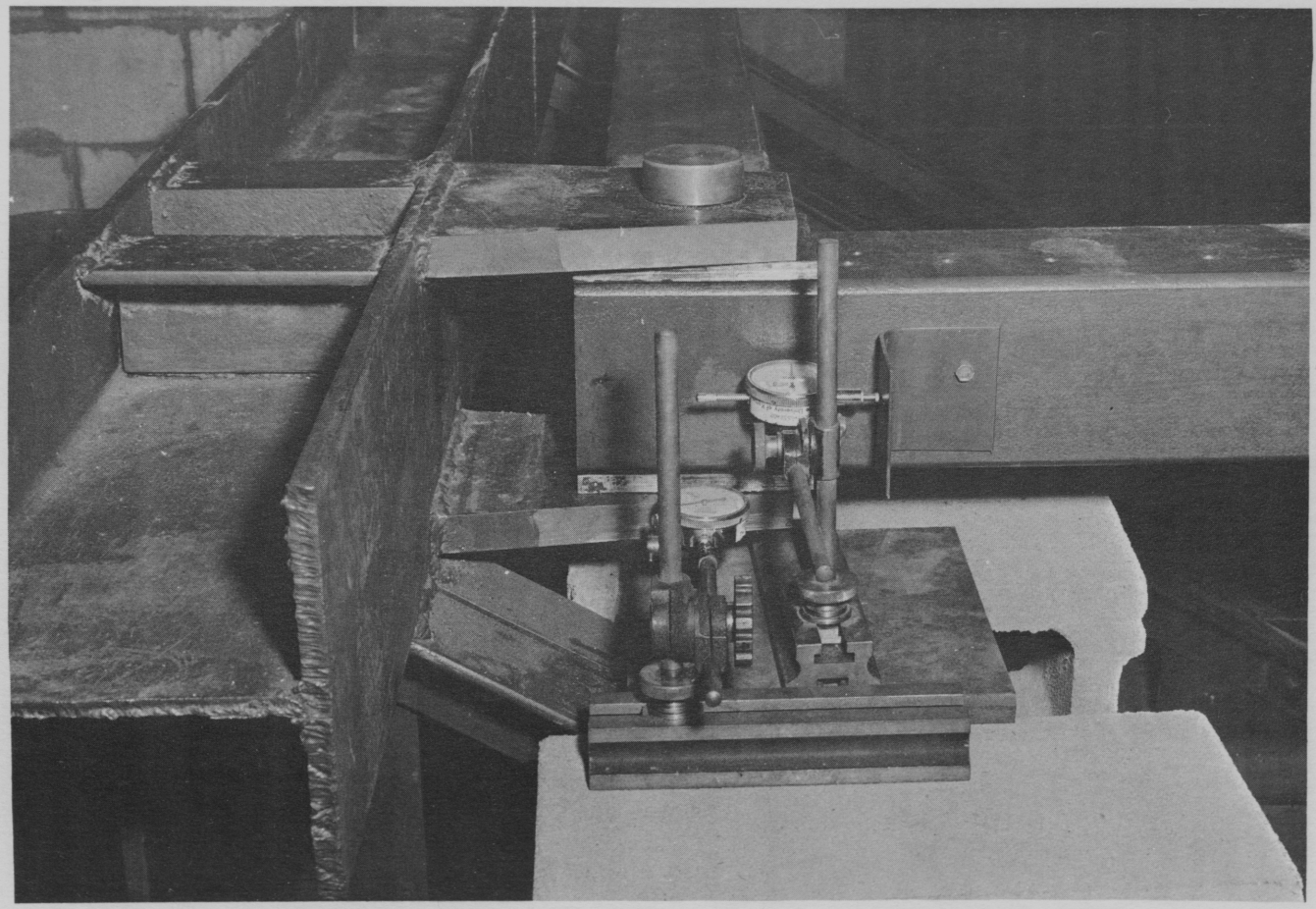

Figure 39. Corner D of Test Frame (Main Pin) and Gages D_1 and D_2.

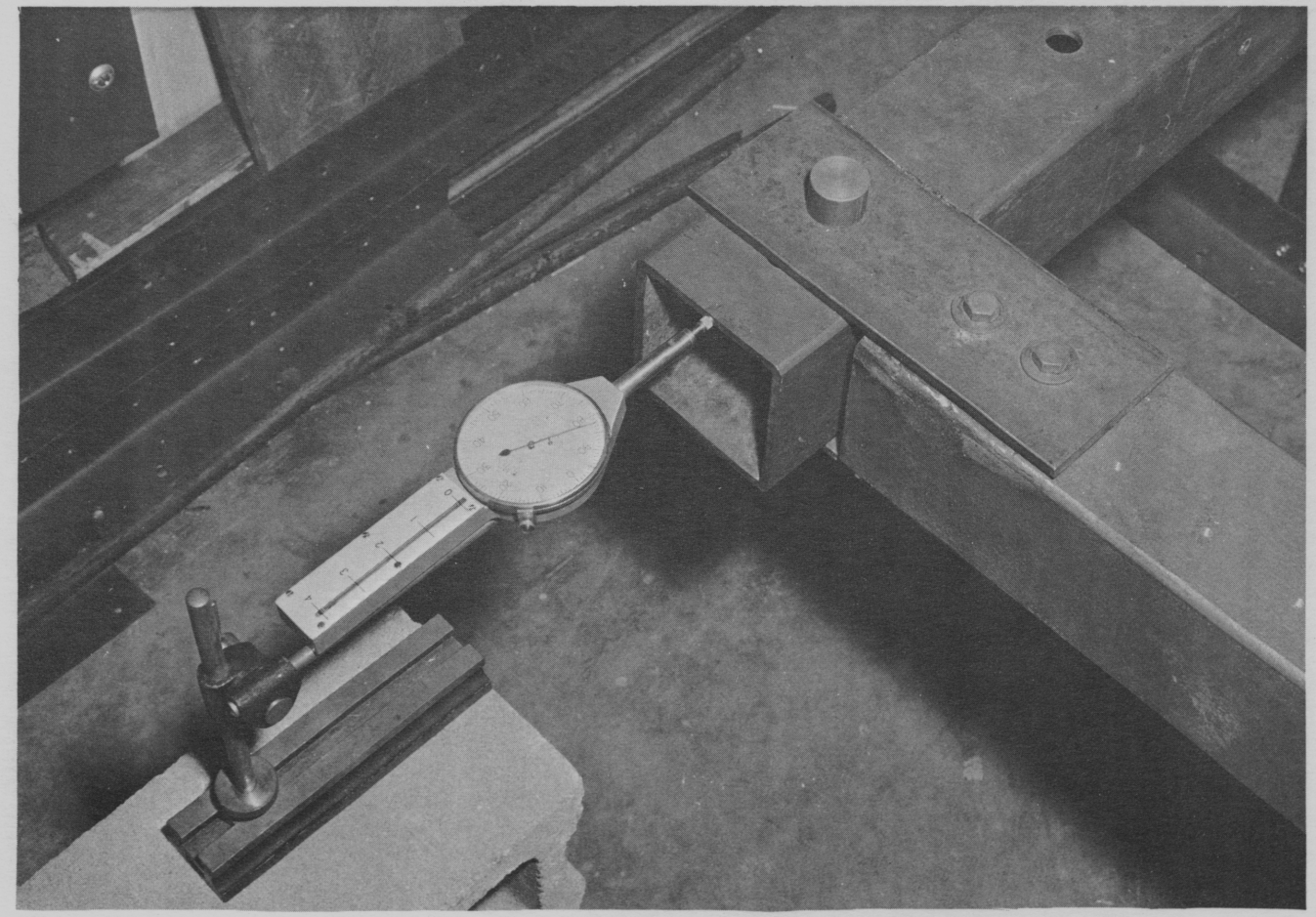

Figure 40. Corner B of Test Frame and Gage D_3.

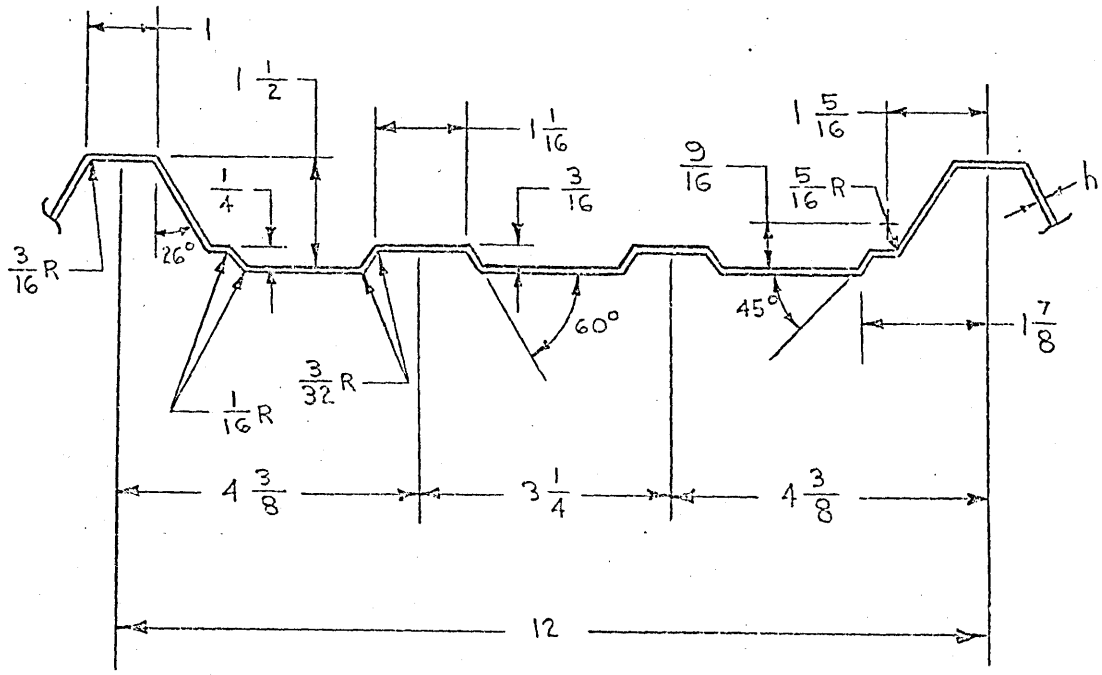

(Repeating Section)

All radii are inside dimensions and all dimensions are given in inches.

Panel Properties

$I = 2.82 \times h \text{ in}^4$

$s = 14.06$ in.

$q = 12.0$ in.

$E = 30 \times 10^6$ psi

$G = 11.5 \times 10^6$ psi

Figure 41. Drawing of the cross-section of the Butlerib Panel.

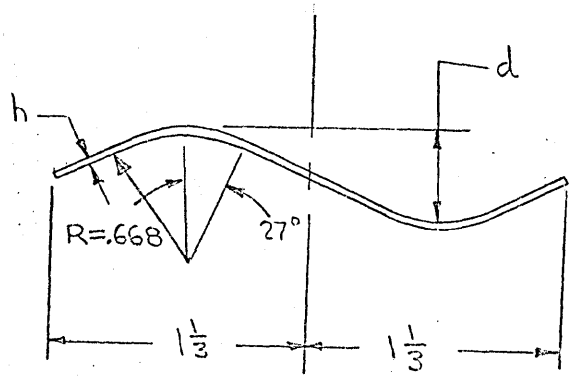

(repeating cross-section)

dimensions given in inches

Panel Properties

s = 12.9 in.

q = 12.0 in.

I = .343 in^4/ft (20 gage steel)

I = .385 in^4/ft (24 gage steel)

d = .470 in (20 gage steel)

d = .496 in. (24 gage steel)

E = 30 x 10^6 psi

G = 11.5 x 10^6 psi

Figure 42. Drawing of the cross-section of the sine-wave panel.

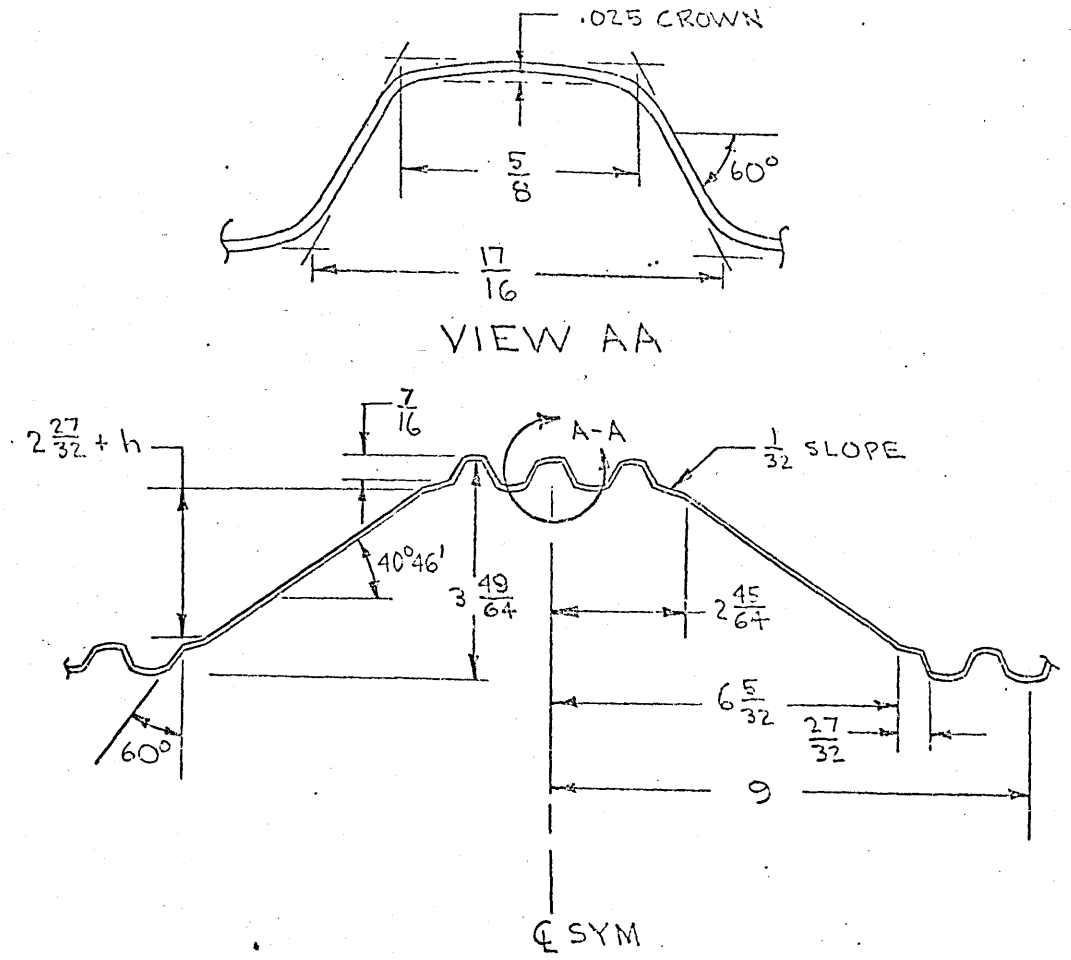

(Repeating Section)

All dimensions are given in inches

Panel Properties

$I = 59.2 \times h \text{ in}^4$

$s = 22.13$ in.

$q = 18.0$ in.

$E = 30 \times 10^6$ psi

$G = 11.5 \times 10^6$ psi

Figure 43. Drawing of the Cross-Section of the M36 Panel.

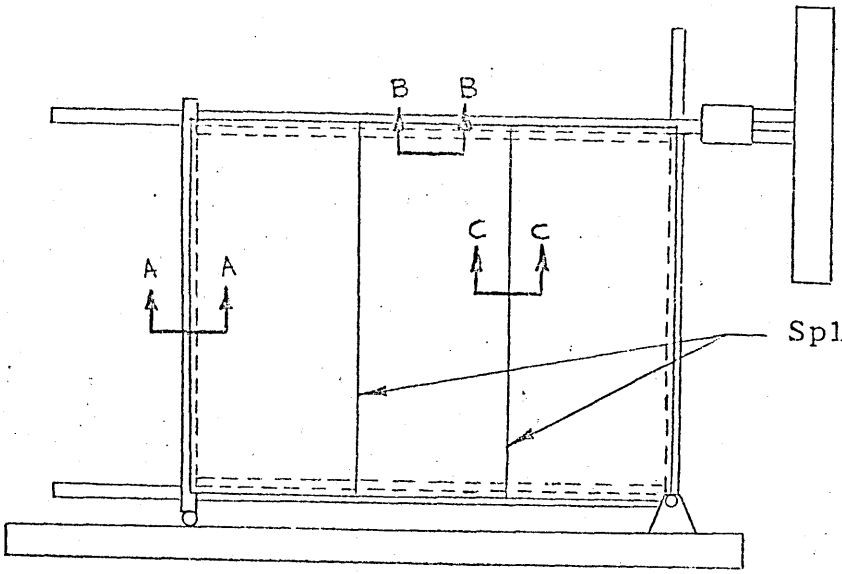

Plan View of testing frame

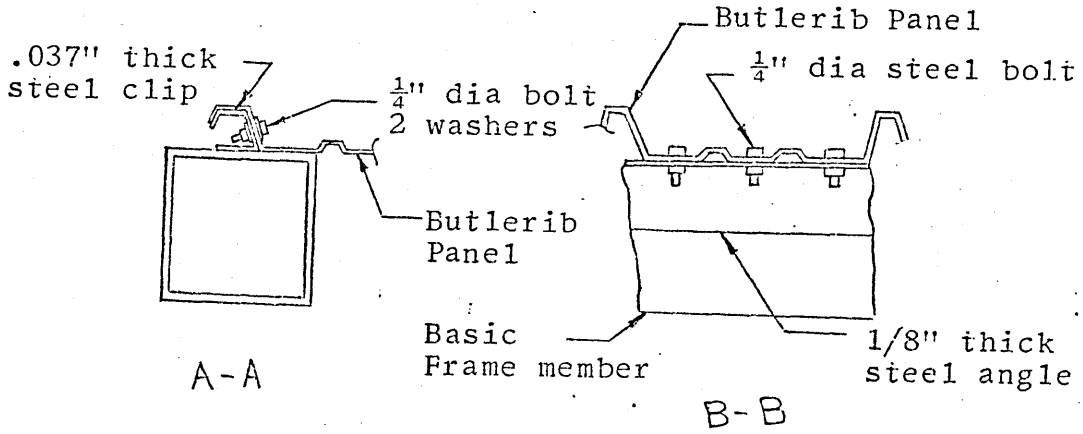

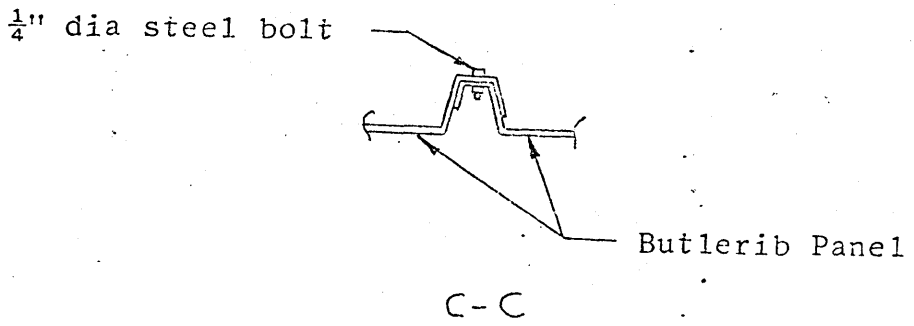

Figure 44. Butlerib Panel edge and splice attachments.

Figure 45. Butlerib Panel Installed in the Test Frame.

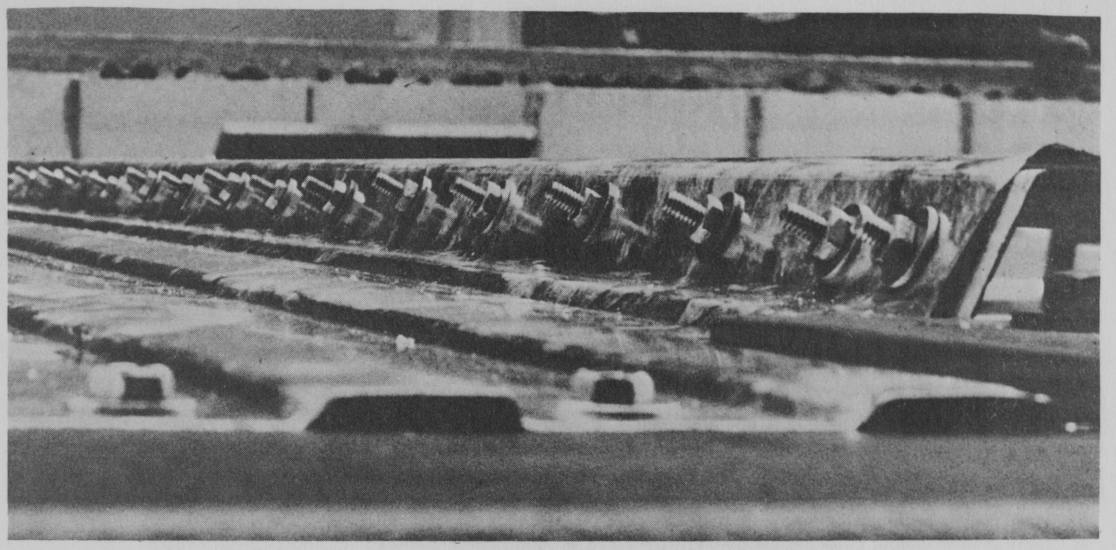

Figure 46 Butlerib Panel Edge Fasteners.

Figure 47 Butlerib Panel 15 feet wide and 13.58 feet long after Buckling.

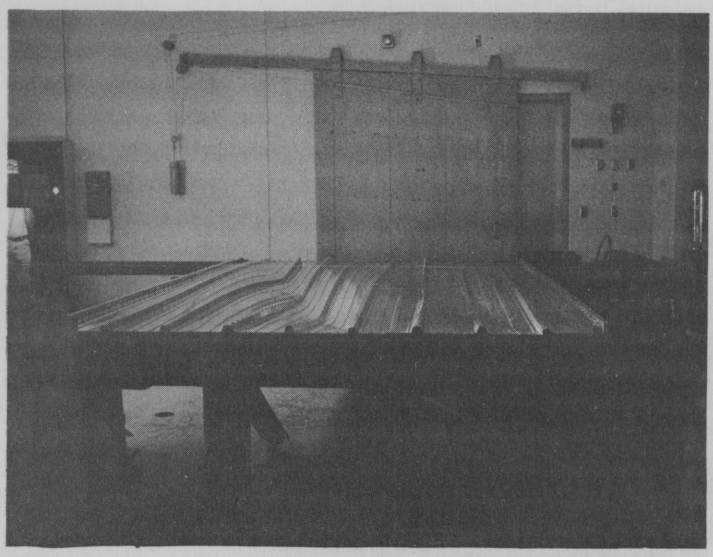

Figure 48. Butlerib Panel 9 feet wide and 13.58 feet long after Buckling.

Figure 49. Butlerib Panel 9 feet wide and 9.58 feet long after Buckling.

Figure 50. Butlerib Panel 15 feet wide and 9.58 feet long after Buckling.

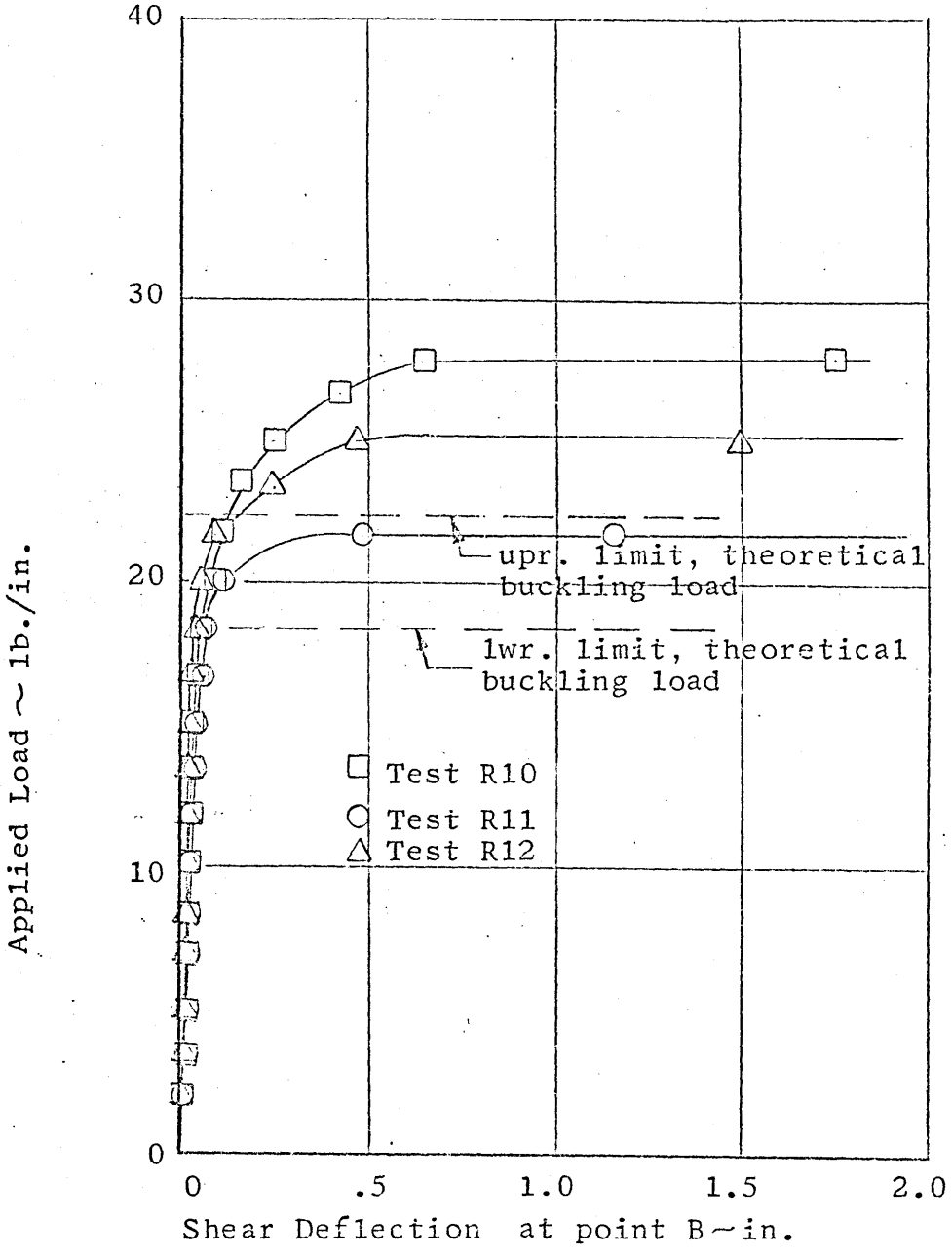

Figure 51. Load versus shear deflection at point B, Butlerib Panel, a = 15 ft, b = 13.58 feet.

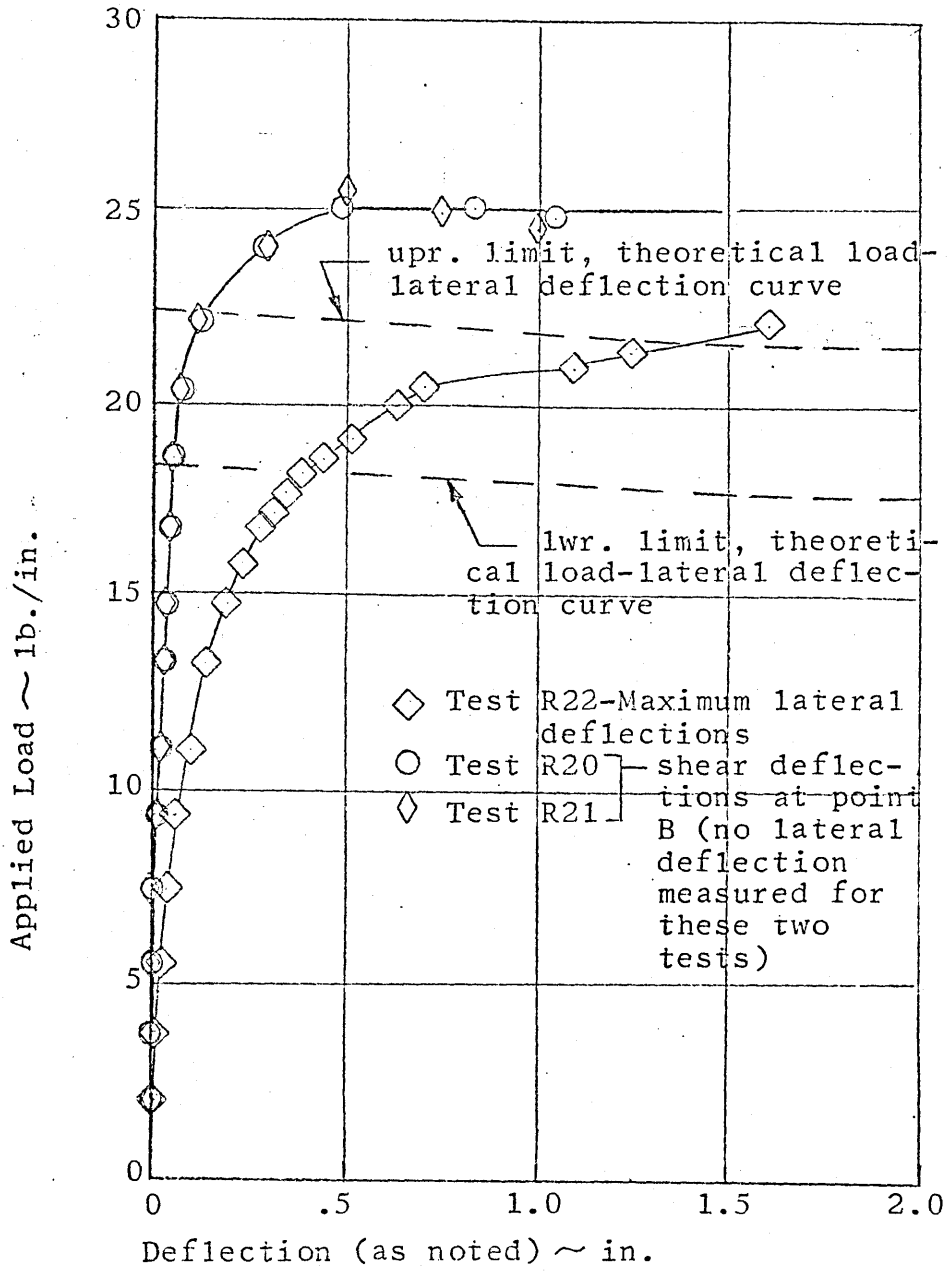

Figure 52. Load versus lateral and shear deflections, Butlerib Panel, a = 9 feet, b = 13.58 feet.

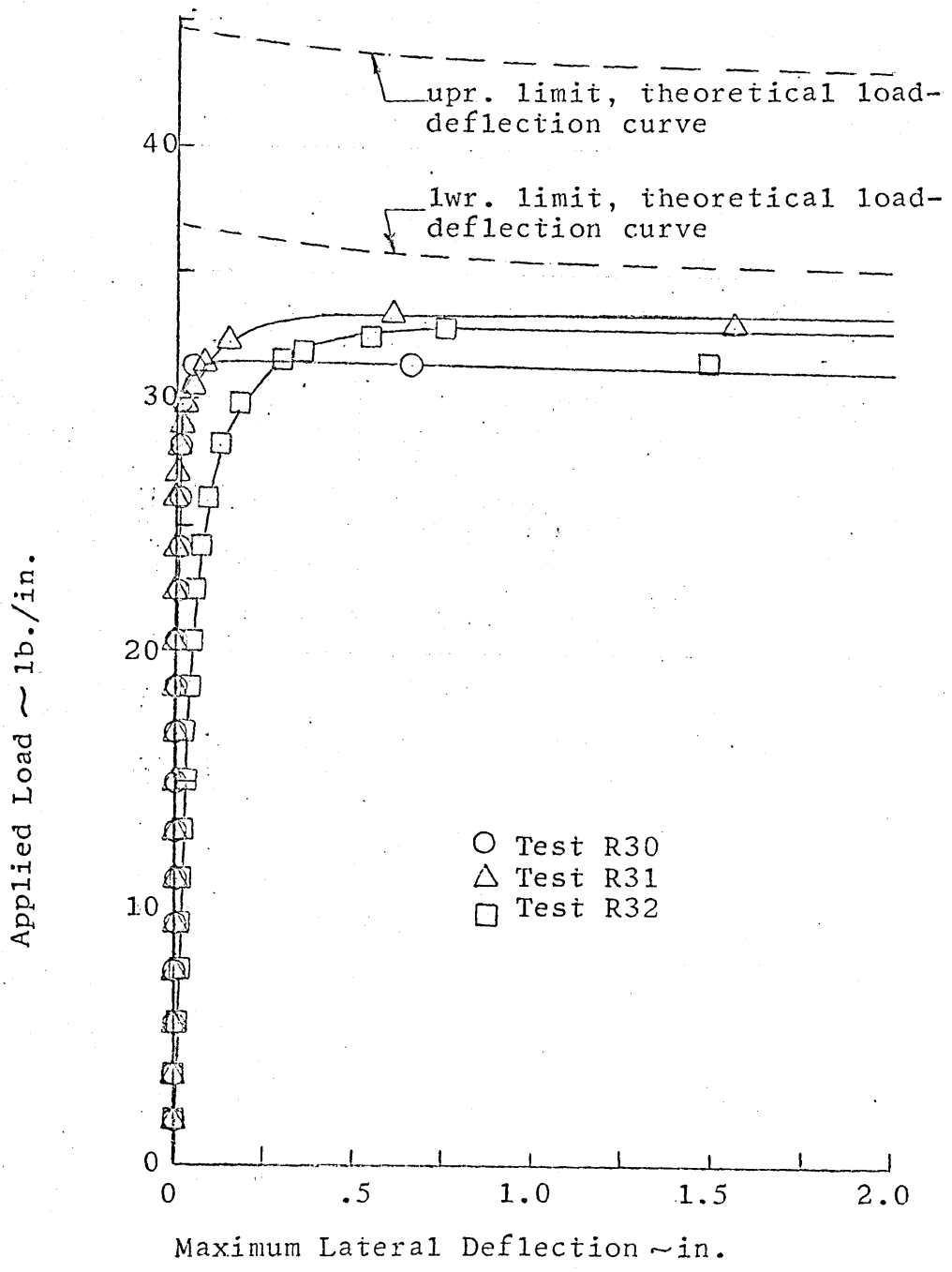

Figure 53. Load versus maximum lateral deflection, Butlerib Panel, a = 9 feet, b = 9.58 feet.

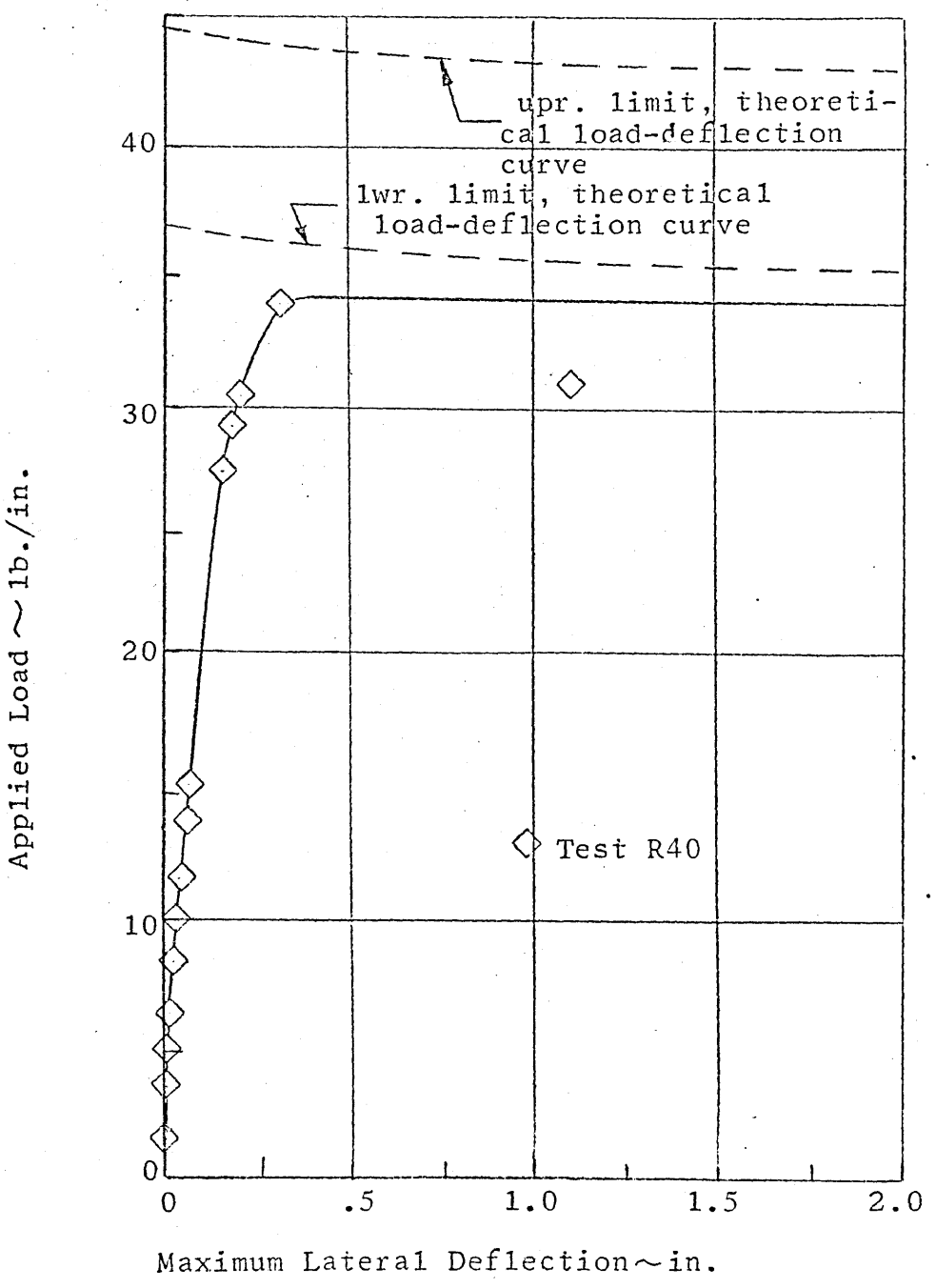

Figure 54. Load versus maximum lateral deflection, Butlerib Panel, a = 15 feet, b = 9.58 feet.

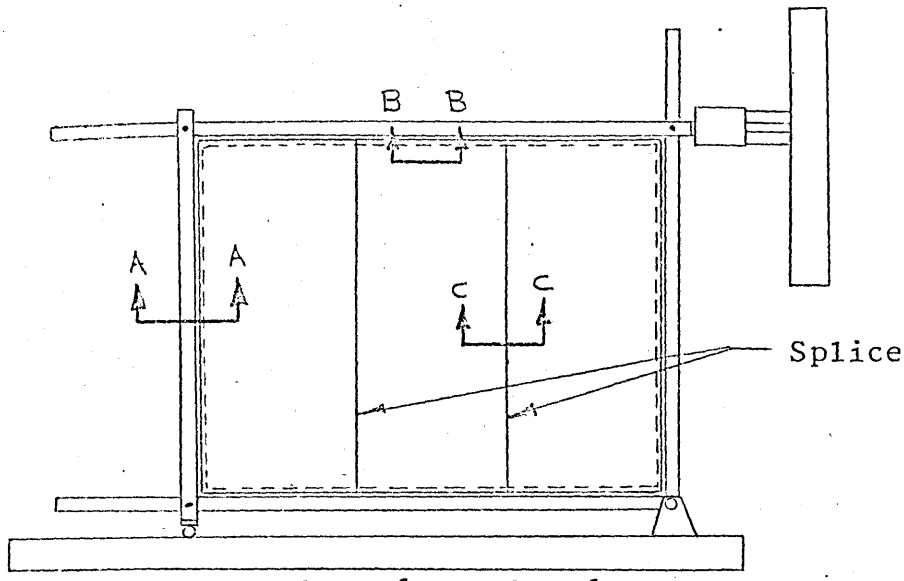

Plan View of testing frame.

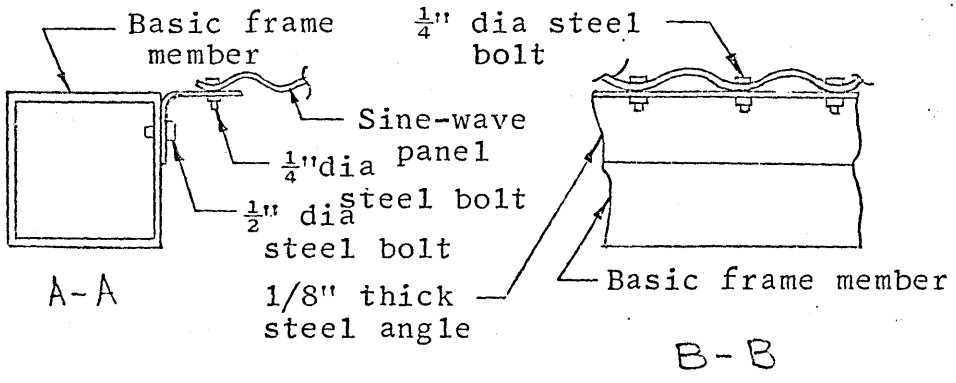

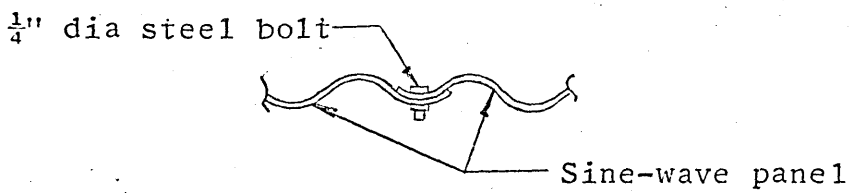

C-C

Figure 55. Sine-wave panel edge and splice attachments.

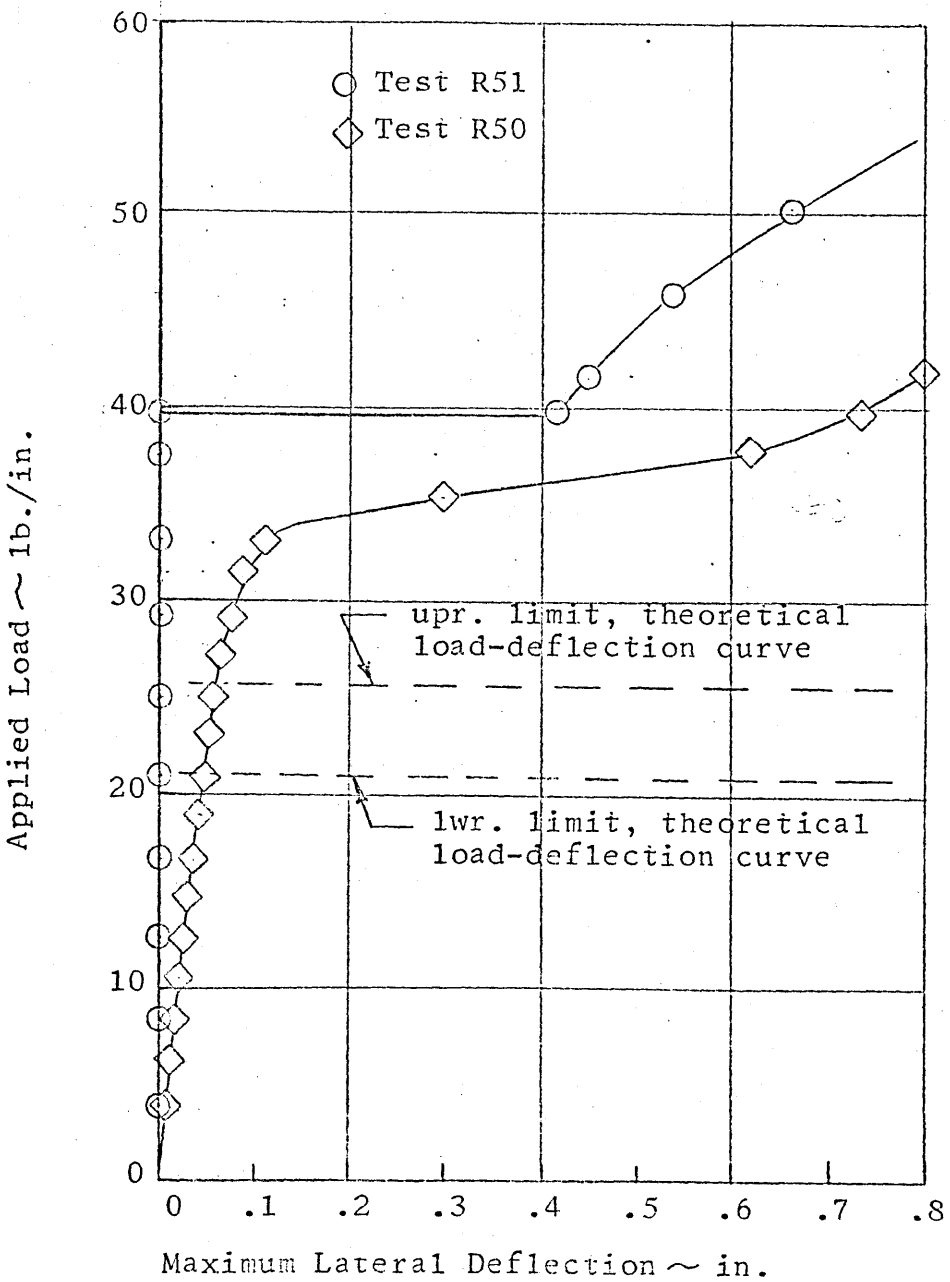

Figure 56. Load versus maximum lateral deflection, Sine-wave Panels, 20 gage steel.

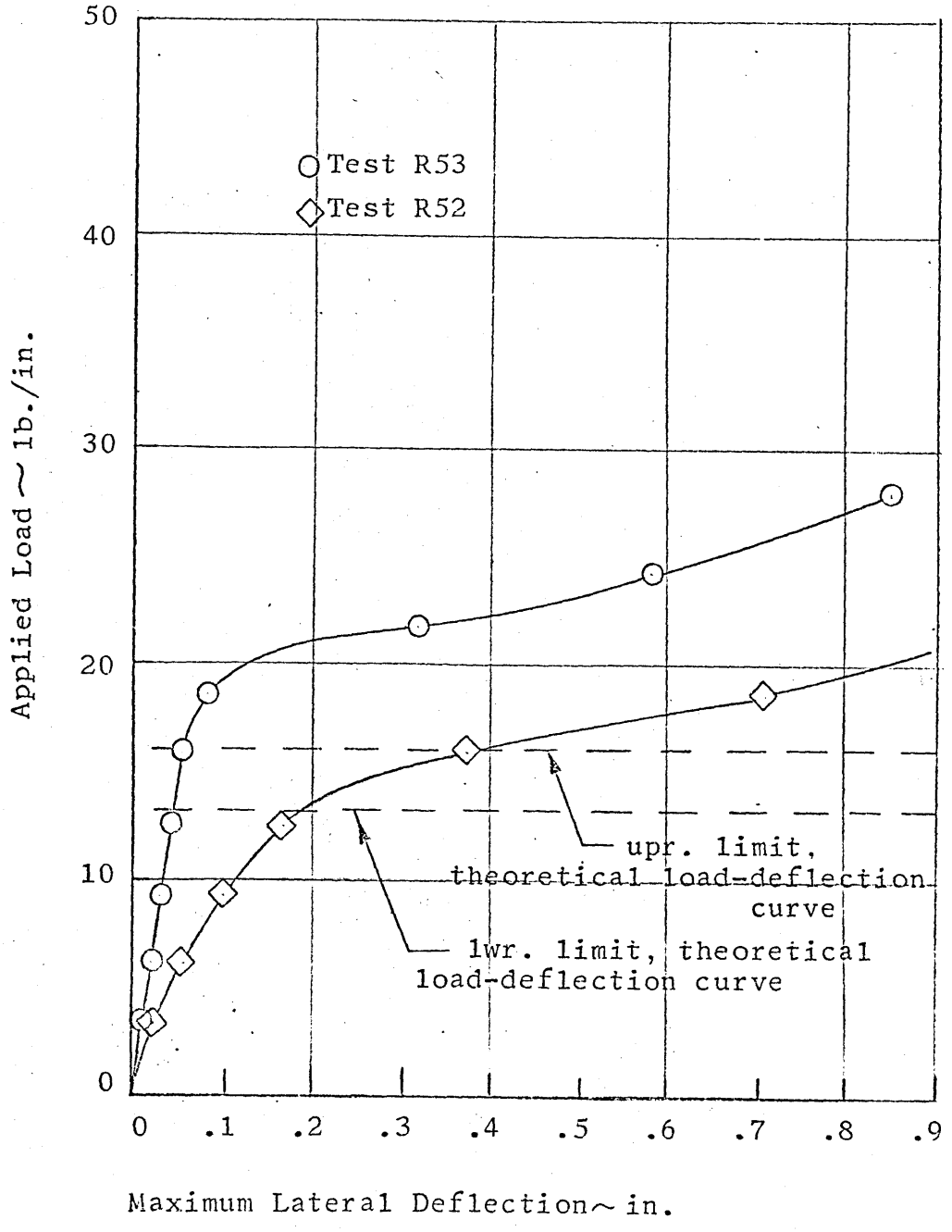

Figure 57. Load versus maximum lateral deflection, Sine-wave Panels, 24 gage steel.

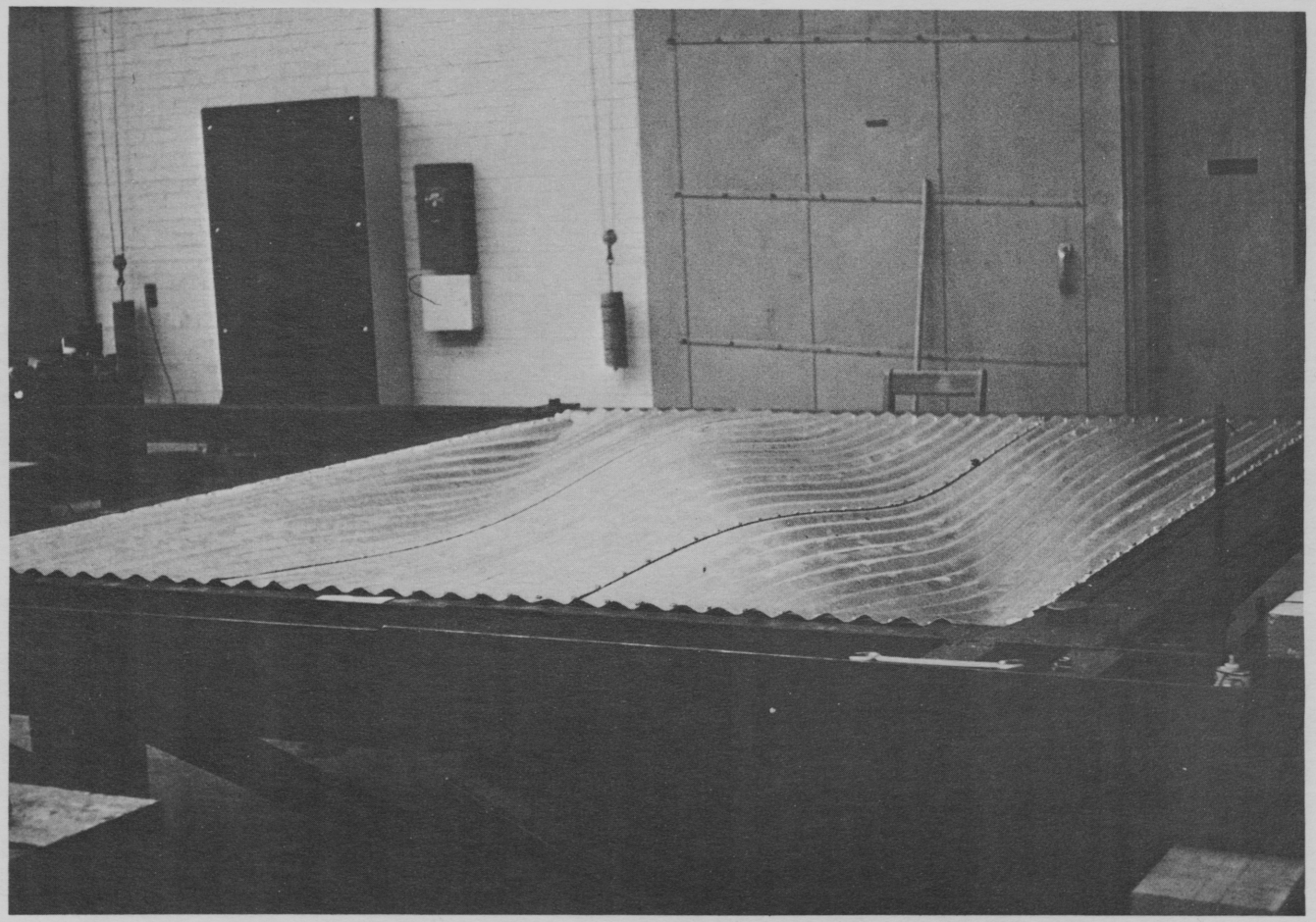

Figure 58. Sine-wave Panel after Buckling.

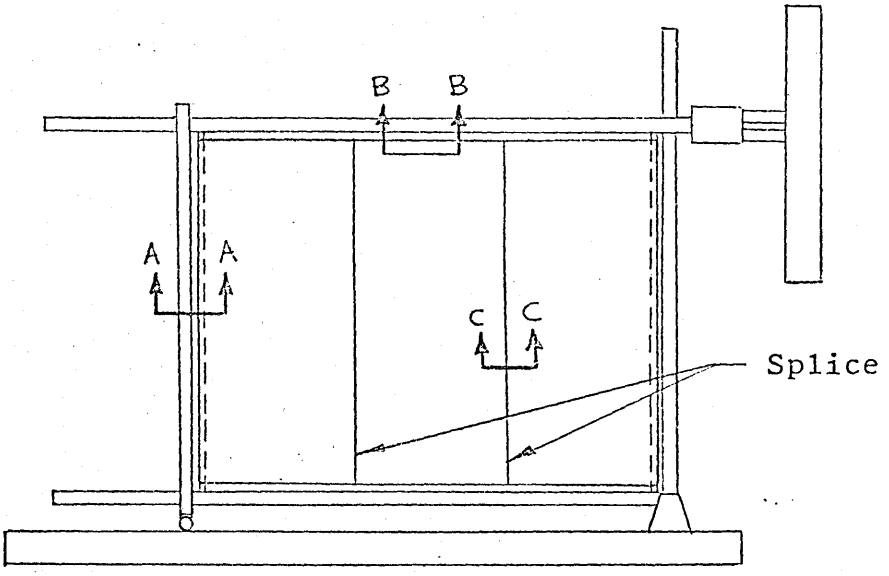

Plan View of testing frame

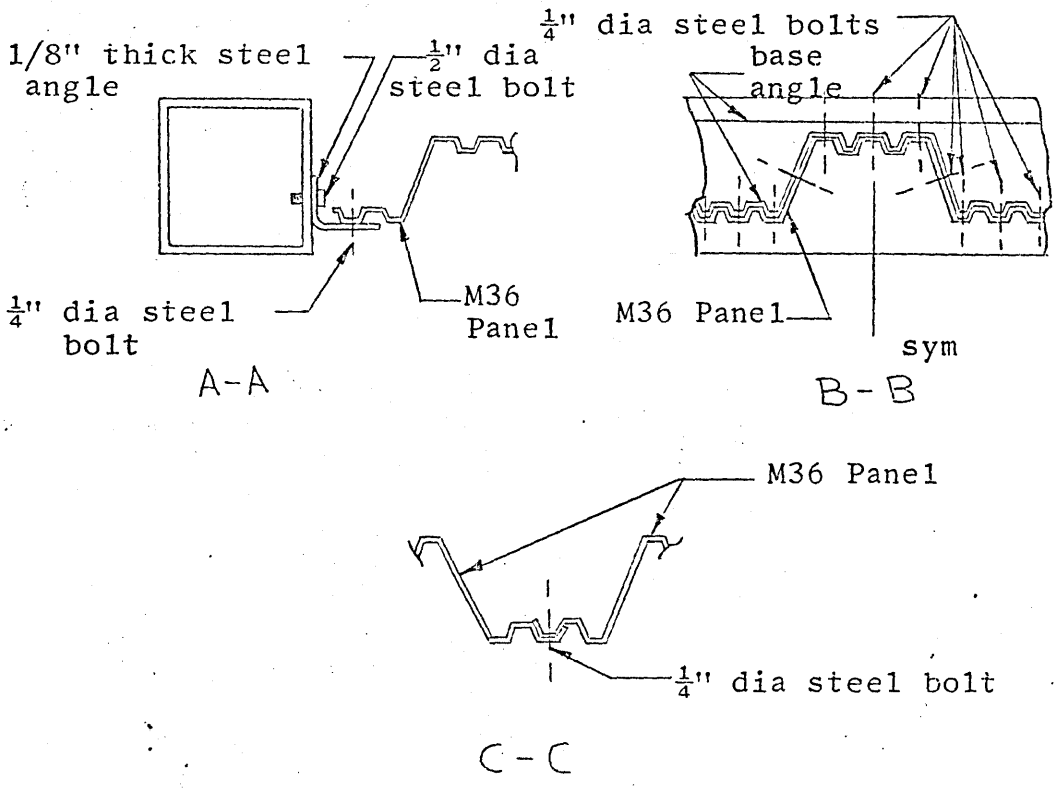

Figure 59. M36 Panel edge and splice attachments.

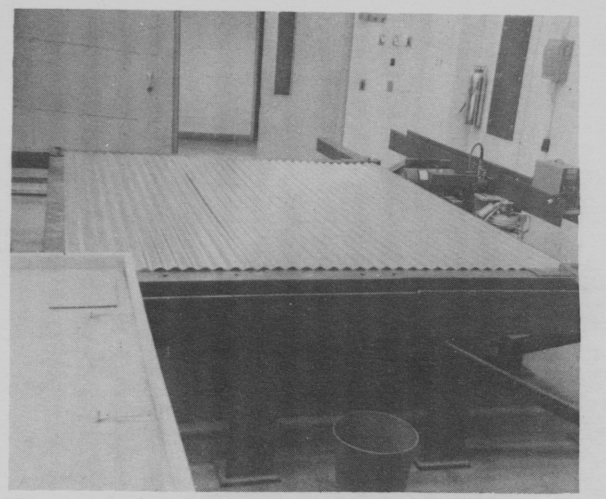

Figure 60. Sine-wave Panel Before Testing.

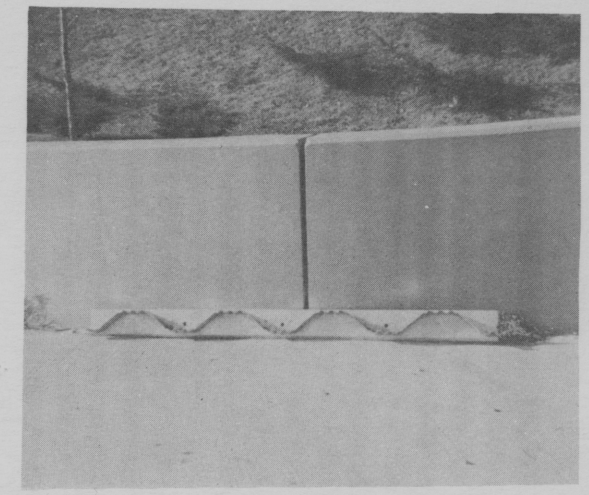

Figure 61. M36 Base Angle.

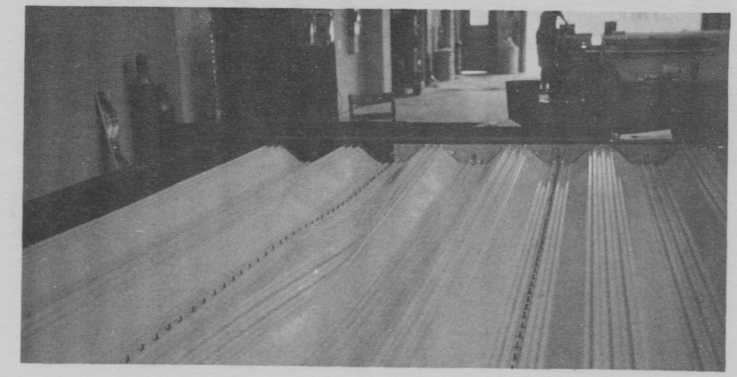

Figure 62. M36 Panel 9 feet wide and 12 feet long after Buckling.

TABLES

TABLE 1

DETERMINANT OF COEFFICIENTS DEFINING THE BUCKLING LOAD WITH M,N = 1 THROUGH 7

Coefficients of A_{pq}, p,q = 1 → 7

M	N	A_{11}	A_{22}	A_{13}	A_{31}	A_{33}	A_{24}	A_{42}	A_{44}	A_{15}	A_{35}	A_{51}	A_{53}	A_{55}
1	1	k_{11}/P_{CR}	-.444	0	0	0	-.178	-.178	-.712	0	0	0	0	0
2	2		k_{22}/P_{CR}	.800	.800	-1.44	0	0	0	.318	-.571	.318	-.571	-.227
1	3			k_{13}/P_{CR}	0	0	-1.14	.320	.457	0	0	0	0	0
3	1				k_{31}/P_{CR}	0	.320	-1.14	.457	0	0	0	0	0
3	3					k_{33}/P_{CR}	2.06	2.06	-3.94	0	0	0	0	0
2	4						k_{24}/P_{CR}	0	0	1.48	-2.67	.127	.817	-1.06
4	2							k_{42}/P_{CR}	0	.127	.817	1.48	-2.67	-1.06
4	4								k_{44}/P_{CR}	.592	3.81	.592	3.81	-4.93
1	5									k_{15}/P_{CR}	0	0	0	0
3	5										k_{35}/P_{CR}	0	0	0
5	1											k_{51}/P_{CR}	0	0
5	3												k_{53}/P_{CR}	0
5	5													k_{55}/P_{CR}

NOTE: These values not shown since this is a symmetric matrix.

TABLE 1 (continued)

M	N	A_{26}	A_{46}	A_{62}	A_{64}	A_{66}	A_{17}	A_{37}	A_{57}	A_{71}	A_{73}	A_{75}	A_{77}
1	1	-.114	-.048	-.114	-.048	-.029	0	0	0	0	0	0	0
2	2	0	0	0	0	0	.207	-.374	-.148	.207	-.374	-.148	-.097
1	3	-.445	-.178	.206	-.294	-.115	0	0	0	0	0	0	0
3	1	.206	-.294	-.445	-.178	-.115	0	0	0	0	0	0	0
3	3	.800	-1.14	.800	-1.14	-.445	0	0	0	0	0	0	0
2	4	0	0	0	0	0	.565	-1.02	-.403	.083	.534	-.692	-.264
4	2	0	0	0	0	0	.083	.534	-.692	.565	-1.02	-.403	-.264
4	4	0	0	0	0	0	.226	1.45	-1.89	.226	1.45	-1.89	.720
1	5	-1.82	-.728	.082	.381	-.488	0	0	0	0	0	0	0
3	5	3.28	-4.68	.317	1.48	-1.82	0	0	0	0	0	0	0
5	1	.082	.381	-1.82	-7.28	-4.88	0	0	0	0	0	0	0
5	3	.317	1.48	3.28	-4.68	-1.82	0	0	0	0	0	0	0
5	5	1.30	6.07	1.30	6.07	-7.43	0	0	0	0	0	0	0
2	6	k_{26}/P_{CR}	0	0	0	0	2.15	-3.88	-1.54	.053	.208	.850	-1.01
4	6		k_{46}/P_{CR}	0	0	0	.863	5.55	-7.85	.146	.567	.850	-2.74
6	2			k_{62}/P_{CR}	0	0	.053	.208	.850	2.15	-3.88	-1.54	-1.01
6	4				k_{64}/P_{CR}	0	.146	.567	2.31	.863	5.55	-7.85	-2.74
6	6	NOTE: These values not shown				k_{66}/P_{CR}	.544	2.15	8.81	.544	2.15	8.81	-10.4
1	7	since this is a symmetric					k_{17}/P_{CR}	0	0	0	0	0	0
3	7	matrix.						k_{37}/P_{CR}	0	0	0	0	0
5	7								k_{57}/P_{CR}	0	0	0	0
7	1									k_{71}/P_{CR}	0	0	0
7	3										k_{73}/P_{CR}	0	0
7	5											k_{75}/P_{CR}	0
7	7												k_{77}/P_{CR}

TABLE 2

DETERMINANT OF COEFFICIENTS DEFINING THE BUCKLING LOAD WITH M = 1 THROUGH 18, N = 1,2

Coefficients of A_{pq}, p = 1→18, q = 1 and 2

M	N	A_{11}	A_{22}	A_{31}	A_{42}	A_{51}	A_{62}	A_{71}	A_{82}	A_{91}	$A_{10,2}$	$A_{11,1}$	$A_{12,2}$	$A_{13,1}$
1	1	k_{11}/P_{CR}	-.444	0	-.178	0	-.114	0	-.085	0	-.067	0	-.056	0
2	2		k_{22}/P_{CR}	.800	0	.318	0	.207	0	.156	0	.125	0	.105
3	1			k_{31}/P_{CR}	-1.14	0	-.445	0	-.291	0	-.220	0	-.177	0
4	2				k_{42}/P_{CR}	1.48	0	.565	0	.369	0	.279	0	.227
5	1					k_{51}/P_{CR}	-1.82	0	-.684	0	-.445	0	-.337	0
6	2						k_{62}/P_{CR}	2.15	0	.800	0	.518	0	.391
7	1							k_{71}/P_{CR}	-2.67	0	-.915	0	-.590	0
8	2								k_{82}/P_{CR}	2.83	0	1.03	0	.661
9	1									k_{91}/P_{CR}	-3.16	0	-1.14	0
10	2										$k_{10,2}/P_{CR}$	3.49	0	1.25
11	1											$k_{11,1}/P_{CR}$	-3.83	0
12	2												$k_{12,2}/P_{CR}$	4.17
13	1													$k_{13,1}/P_{CR}$

NOTE: These values not shown since this is a symmetric matrix.

TABLE 2 (continued)

DETERMINANT OF COEFFICIENTS DEFINING THE BUCKLING LOAD WITH M = 1 THROUGH 18. N=1,2

Coefficients of A_{pq}, p = 1→18, q = 1 and 2

M	N	$A_{14,2}$	$A_{15,1}$	$A_{16,2}$	$A_{17,1}$	$A_{18,2}$
1	1	-.048	0	-.042	0	-.037
2	2	0	.090	0	.080	0
3	1	-.150	0	-.130	0	-.115
4	2	0	.191	0	.166	0
5	1	-.273	0	-.231	0	-.201
6	2	0	.318	0	.269	0
7	1	-.445	0	-.361	0	-.306
8	2	0	.497	0	.403	0
9	1	-.730	0	-.549	0	-.444
10	2	0	.800	0	.600	0
11	1	-1.37	0	-.869	0	-.647
12	2	0	1.48	0	.940	0
13	1	-4.50	0	-1.60	0	-1.01
14	2	$k_{14,2}/P_{cR}$	4.83	0	1.70	0
15	1		$k_{15,2}/P_{cR}$	-5.17	0	-1.82
16	2			$k_{16,2}/P_{cR}$	5.50	0
17	1				$k_{17,1}/P_{cR}$	-5.82
18	2					$k_{18,2}/P_{cR}$

NOTE: These values not shown since this is a symmetric matrix.

TABLE 3

IDENTIFICATION OF TESTS

Panel Configuration	Test Numbers	Panel Dimensions (feet) a	b
M36	R1 R2	3.0	8.0
M36	R3	6.0	12.0
M36	R4	9.0	12.0
Butlerib	R10 R11 R12	15.0	13.58
Butlerib	R20 R21 R22	9.0	13.58
Butlerib	R30 R31 R32	9.0	9.58
Butlerib	R40	15.0	9.58
Sine-wave (20 gage mat'l)	R50 R51	8.0	9.58
Sine-wave (24 gage mat'l)	R52 R53	8.0	9.58

TABLE 4
CONVERGENCE OF BUCKLING LOAD FOR
BUTLERIB AND SINE-WAVE PANELS

Number of terms in series	Buckling Load $\sim \pi^2/m$											
	Butlerib a=15', b=13.58'		Butlerib a=9', b=13.58		Butlerib a=9', b=13.58'		Butlerib a=15', b=9.58'		Sine-Wave a=8', b=9.58'		Sine-Wave a=8'. b=9.58	
	h = .0191"	h = .0217"	h = .0191"	h = .0217"	h = .0191"	h = .0217"	h = .0191"	h = .0217"	h = .0191"	h = .0217"	h = .0191"	h = .0217"
2	153.3	174.1	91.9	104.5	261.9	298.3	436.5	495.5	55.2	63.0	41.4	47.2
4	48.8	56.9	29.9	34.3	83.6	95.4	138.7	157.5	22.5	27.1	14.8	17.4
6	29.2	33.4	20.1	23.7	50.9	58.6	81.6	92.8	20.9	25.5	12.7	15.4
8	21.8	25.3	18.2	22.0	39.7	46.8	58.3	66.6	20.8	25.4	12.6	15.4
10	18.8	22.3	18.1	21.9	36.2	43.6	46.5	53.6	20.8	25.4	12.6	15.4
12	17.8	21.5	18.1	21.9	35.8	43.5	40.1	47.3	20.8	25.4	12.6	15.4
14	17.8	21.5	18.1	21.9	35.8	43.5	36.9	45.0				
16	17.8	21.5	18.1	21.9	35.8	43.5	35.6	43.1				
18	17.8	21.5	18.1	21.9	35.8	43.5	35.5	43.0				

TABLE 5

PREDICTED BUCKLING LOADS FOR THE BUTLERIB AND SINE-WAVE PANELS DERIVED FROM THE SINGLE TERM APPROXIMATION w.

Panel Identification	Panel Dimensions a(ft)	b(ft)	Thickness inches	Buckling Load (lb/in)
Butlerib	15	13.58	.0191 .0217	18.3 22.3
Butlerib	9	13.58	.0191 .0217	18.4 22.3
Butlerib	9	9.58	.0191 .0217	36.8 44.8
Butlerib	15	9.58	.0191 .0217	36.8 44.7
Sine-Wave	8	9.58	.0363 .0411	21.0 25.4
Sine-Wave	8	9.58	.0243 .0277	12.6 15.4

TABLE 6

IDENTIFICATION OF EQUIPMENT

Load Cell - Baldwin-Lima-Hamilton Corporation, Electronics and Instrumentation Division, Waltham, Massachusetts, SR-4 Load Cell, Type u-1, capacity 100,000 pounds, Serial No. 10937

Recorder - Gilmore Industries, Cleveland, Ohio, Model 170, Serial 369.

Hydraulic Jacks - Blackhawk Mfg. Co., Milwaukee, Wisconson, Capacity 20 tons, Model R251, Serials A891994 and A707601.

Pressure Cylinder - Sprague Engr. Corporation, Gardena, California, Model No. S-216-DR-60, Serial No. R-60-5-64, Date 6-19-64, Max. Press. 6600 psi.

Gage D_1 - L. S. Starrett Co., Athol., Mass., No. 25-T6, .0001", KU No. 2216-4632-80.

Gage D_2 - L. S. Starrett Co., Athol., Mass., No. 25-F, .001", KU No. 2216-4632-02.

Gage D_3 - B. C. Ames Co., Waltham, Mass., .001", No. 4224, KU No. 2235-4632-020.

Gage D_4 - L. S. Starrett Co., Athol., Mass., No. 25-5, .001", KU No. 2216-4632-04.

Gage D_5 - B. C. Ames Co., Waltham, Mass., .001", No. 4224, KU No. 2235-4632-019.

TABLE 7

Data From Test R10, Butlerib, a = 15 ft, b = 13.58 ft.

Load (lbs)	Shear (lbs/ft)	Gage Deflections (in)				Shear Deflection(in)
		D_1	D_2	D_3	D_4	
350.	23.	0.0008	0.0018	0.023	0.0141	0.0066
610.	41.	0.0055	0.0038	0.037	0.0183	0.0098
900.	60.	0.0124	0.0065	0.056	0.0228	0.0149
1210.	81.	0.0189	0.0093	0.076	0.0278	0.0207
1500.	100.	0.0233	0.0109	0.092	0.0318	0.0266
1810.	121.	0.0276	0.0127	0.108	0.0368	0.0316
2100.	140.	0.0316	0.0139	0.123	0.0408	0.0376
2410.	161.	0.0362	0.0157	0.141	0.0459	0.0443
2700.	180.	0.0403	0.0170	0.158	0.0501	0.0515
3010.	201.	0.0447	0.0183	0.178	0.0548	0.0612
3300.	220.	0.0486	0.0197	0.199	0.0592	0.0725
3600.	240.	0.0525	0.0213	0.227	0.0642	0.0903
3900.	260.	0.0558	0.0230	0.264	0.0691	0.1174
4200.	280.	0.0597	0.0253	0.325	0.0742	0.1672
4500.	300.	0.0634	0.0286	0.428	0.0791	0.2585
4800.	320.	0.0669	0.0336	0.598	0.0839	0.4155
4820.	321.	0.0691	0.0375	0.738	0.0855	0.5479
4990.	333.	0.0698	0.0399	0.833	0.0855	0.6398
5010.	334.	0.0698	0.0399	1.938	0.0855	1.7448

TABLE 8

Data From Test R11, Butlerib, a = 15 ft, b = 13.58 ft.

Load (lbs)	Shear (lbs/ft)	Gage Deflections (in)				Shear Deflection (in)
		D_1	D_2	D_3	D_4	
300.	20.	0.0027	0.0018	0.021	0.0109	0.0058
600.	40.	0.0098	0.0050	0.043	0.0183	0.0103
900.	60.	0.0163	0.0078	0.064	0.0248	0.0157
1210.	81.	0.0215	0.0103	0.084	0.0311	0.0219
1500.	100.	0.0257	0.0120	0.100	0.0361	0.0273
1800.	120.	0.0299	0.0136	0.116	0.0410	0.0326
2100.	140.	0.0344	0.0153	0.133	0.0458	0.0387
2400.	160.	0.0386	0.0168	0.150	0.0501	0.0456
2700.	180.	0.0432	0.0185	0.170	0.0549	0.0546
3010.	201.	0.0477	0.0201	0.190	0.0597	0.0638
3250.	217.	0.0499	0.0212	0.207	0.0628	0.0745
3310.	221.	0.0523	0.0223	0.235	0.0660	0.0959
3600.	240.	0.0558	0.0243	0.273	0.0702	0.1243
3900.	260.	0.0593	0.0273	0.346	0.0752	0.1859
4050.	270.	0.0608	0.0293	0.410	0.0777	0.2441
4000.	267.	0.0608	0.0298	0.440	0.0778	0.2736
4200.	280.	0.0625	0.0304	0.653	0.0810	0.4811
4090.	273.	0.0628	0.0366	0.690	0.0804	0.5124
4300.	287.	0.0641	0.0408	0.833	0.0817	0.6488
4060.	271.	0.0632	0.0418	0.880	0.0787	0.6987
4210.	281.	0.0641	0.0468	1.050	0.0804	0.8614
4010.	267.	0.0632	0.0479	1.097	0.0782	0.9103
4230.	282.	0.0643	0.0538	1.300	0.0806	1.1042
3730.	249.	0.0613	0.0548	1.347	0.0754	1.1585
4170.	278.	0.0632	0.0718	1.945	0.0804	1.7333

TABLE 9

Data From Test R12, Butlerib, a = 15 ft, b = 13.58 ft.

Load (lbs)	Shear (lbs/ft)	Gage Deflections (in)				Shear Deflection (in)
		D_1	D_2	D_3	D_4	
310.	21.	0.0029	0.0024	0.025	0.0159	0.0043
600.	40.	0.0099	0.0056	0.046	0.0235	0.0078
900.	60.	0.0166	0.0082	0.067	0.0302	0.0130
1200.	80.	0.0221	0.0106	0.085	0.0359	0.0175
1500.	100.	0.0261	0.0123	0.099	0.0412	0.0207
1800.	120.	0.0301	0.0142	0.114	0.0459	0.0252
2100.	140.	0.0344	0.0157	0.129	0.0504	0.0299
2430.	162.	0.0391	0.0175	0.146	0.0558	0.0351
2700.	180.	0.0431	0.0188	0.160	0.0603	0.0394
3000.	200.	0.0476	0.0204	0.177	0.0651	0.0456
3300.	220.	0.0514	0.0223	0.194	0.0694	0.0527
3600.	240.	0.0550	0.0238	0.214	0.0738	0.0631
3900.	260.	0.0583	0.0256	0.250	0.0787	0.0893
4230.	282.	0.0621	0.0308	0.433	0.0850	0.2573
4500.	300.	0.0653	0.0383	0.667	0.0897	0.4762
4270.	285.	0.0638	0.0479	0.945	0.0884	0.7478
4520.	301.	0.0679	0.0696	1.720	0.0904	1.4960

TABLE 10

Data From Test R20, Butlerib, a = 9 ft, b = 13.58 ft.

Load (lbs)	Shear (lbs/ft)	Gage Deflections (in)				Shear Deflection (in)
		D_1	D_2	D_3	D_4	
210.	23.	0.0017	0.0009	0.014	0.0021	0.0069
400.	44.	0.0060	0.0039	0.032	0.0057	0.0097
600.	67.	0.0111	0.0071	0.058	0.0129	0.0135
800.	89.	0.0162	0.0099	0.081	0.0177	0.0188
1000.	111.	0.0210	0.0128	0.101	0.0219	0.0223
1200.	133.	0.0241	0.0148	0.118	0.0251	0.0272
1400.	156.	0.0271	0.0167	0.134	0.0284	0.0318
1600.	178.	0.0298	0.0184	0.150	0.0316	0.0367
1800.	200.	0.0327	0.0200	0.166	0.0348	0.0417
2000.	222.	0.0354	0.0219	0.185	0.0378	0.0497
2200.	244.	0.0382	0.0246	0.216	0.0410	0.0681
2410.	268.	0.0410	0.0276	0.298	0.0442	0.1369
2610.	290.	0.0439	0.0331	0.458	0.0467	0.2808
2720.	302.	0.0457	0.0389	0.645	0.0481	0.4542
2740.	304.	0.0466	0.0510	1.045	0.0481	0.8339
2660.	296.	0.0461	0.0542	1.205	0.0116	1.0482

TABLE 11

Data From Test R21, Butlerib, a = 9 ft, b = 13.58 ft

Load (lbs)	Shear (lbs/ft)	Gage Deflections (in)				Shear Deflection (in)
		D_1	D_2	D_3	D_4	
200.	22.	0.0016	0.0010	0.013	0.0018	0.0062
400.	44.	0.0053	0.0035	0.030	0.0052	0.0098
600.	67.	0.0103	0.0062	0.050	0.0087	0.0146
800.	89.	0.0158	0.0093	0.074	0.0139	0.0191
1000.	111.	0.0206	0.0123	0.097	0.0183	0.0252
1200.	133.	0.0235	0.0140	0.112	0.0216	0.0287
1400.	156.	0.0263	0.0159	0.127	0.0248	0.0325
1600.	178.	0.0291	0.0172	0.143	0.0279	0.0382
1800.	200.	0.0318	0.0189	0.158	0.0307	0.0429
2000.	222.	0.0344	0.0208	0.174	0.0331	0.0492
2200.	244.	0.0372	0.0221	0.193	0.0357	0.0586
2400.	267.	0.0400	0.0249	0.272	0.0385	0.1256
2600.	289.	0.0428	0.0309	0.478	0.0405	0.3154
2750.	306.	0.0445	0.0369	0.675	0.0420	0.4985
2690.	299.	0.0444	0.0428	0.935	0.0418	0.7494
2650.	294.	0.0444	0.0488	1.198	0.0396	1.0065
2610.	290.	0.0442	0.0630	1.675	0.0418	1.4572

TABLE 12

DATA FROM TEST R22, BUTLERIB, a = 9 ft, b = 13.58 ft.

Load (lbs)	Shear (lbs/ft)	Gage Deflections (in)				Shear Deflection (in)	Lateral Deflection (in) $\sim D_5$
		D_1	D_2	D_3	D_4		
200.	22.	0.0003	0.0005	0.013	0.0015	0.0090	0.003
400.	44.	0.0036	0.0031	0.030	0.0047	0.0128	0.008
600.	67.	0.0076	0.0054	0.048	0.0080	0.0177	0.021
800.	89.	0.0128	0.0085	0.073	0.0135	0.0233	0.039
1010.	112.	0.0181	0.0115	0.097	0.0191	0.0275	0.063
1200.	133.	0.0214	0.0134	0.113	0.0224	0.0316	0.096
1400.	156.	0.0242	0.0153	0.129	0.0253	0.0369	0.134
1600.	178.	0.0267	0.0172	0.145	0.0276	0.0431	0.190
1700.	189.	0.0279	0.0178	0.154	0.0291	0.0474	0.231
1800.	200.	0.0292	0.0186	0.163	0.0305	0.0515	0.276
1850.	206.	0.0298	0.0191	0.168	0.0311	0.0537	0.304
1900.	211.	0.0304	0.0194	0.172	0.0319	0.0554	0.340
1950.	217.	0.0311	0.0200	0.178	0.0326	0.0587	0.380
2000.	222.	0.0318	0.0203	0.185	0.0340	0.0620	0.439
2050.	228.	0.0326	0.0208	0.192	0.0347	0.0662	0.517
2100.	233.	0.0332	0.0211	0.200	0.0352	0.0722	0.592
2150.	239.	0.0339	0.0217	0.212	0.0359	0.0813	0.635
2200.	244.	0.0346	0.0224	0.226	0.0366	0.0924	0.704
2250.	250.	0.0349	0.0230	0.244	0.0372	0.1080	1.092
2300.	256.	0.0355	0.0238	0.269	0.0377	0.1302	1.282
2400.	267.	0.0372	0.0261	0.340	0.0387	0.1940	1.599
2500.	268.	0.0385	0.0291	0.420	0.0400	0.2659	1.856
2600.	289.	0.0396	0.0312	0.493	0.0408	0.3328	2.041
2700.	300.	0.0411	0.0345	0.615	0.0418	0.4460	2.238
2650.	294.	0.0416	0.0422	0.875	0.0379	0.6997	
2800.	311.	0.0436	0.0581	1.420	0.0241	1.2387	
2880.	320.	0.0444	0.0636	1.675	0.0150	1.4989	

TABLE 13
DATA FROM TEST R30, BUTLERIB,
a = 9 ft, b = 9.58 ft

Load (lbs)	Shear (lbs/ft)	Gage Deflections (in)				Shear Deflection (in)	Lateral Deflection~D_5 (in)
		D_1	D_2	D_3	D_4		
200.	22.	0.0008	0.0000	0.011	0.0012	0.0087	0
400.	44.	0.0034	0.0003	0.022	0.0032	0.0141	0
600.	67.	0.0078	0.0008	0.035	0.0058	0.0191	0
800.	89.	0.0132	0.0033	0.056	0.0097	0.0270	0
1000.	111.	0.0187	0.0060	0.070	0.0139	0.0274	0.002
1200.	133.	0.0229	0.0076	0.083	0.0171	0.0305	0.005
1400.	156.	0.0255	0.0087	0.094	0.0193	0.0351	0.008
1600.	178.	0.0281	0.0099	0.106	0.0218	0.0400	0.011
1800.	200.	0.0309	0.0112	0.117	0.0241	0.0440	0.012
2000.	222.	0.0333	0.0128	0.128	0.0262	0.0482	0.014
2200.	244.	0.0362	0.0137	0.139	0.0282	0.0529	0.015
2400.	267.	0.0390	0.0148	0.150	0.0302	0.0572	0.015
2600.	289.	0.0418	0.0159	0.161	0.0323	0.0615	0.016
2800.	311.	0.0448	0.0172	0.173	0.0347	0.0663	0.016
3000.	333.	0.0479	0.0186	0.187	0.0371	0.0727	0.016
3200.	356.	0.0505	0.0198	0.203	0.0392	0.0820	0.017
3400.	378.	0.0531	0.0219	0.242	0.0414	0.1133	0.046
3400.	378.	0.0535	0.0268	0.340	0.0418	0.2048	0.646
3490.	388.	0.0546	0.0348	0.460	0.0442	0.3116	
3530.	392.	0.0549	0.0368	0.630	0.0452	0.4777	
3590.	399.	0.0560	0.0483	0.900	0.0463	0.7321	
3230.	359.	0.0549	0.0559	1.160	0.0453	0.9858	

TABLE 14
DATA FROM TEST R31, BUTLERIB,
a = 9 ft, b = 9.58 ft

Load (lbs)	Shear (lbs/ft)	Gage Deflections (in)				Shear Deflection (in)	Lateral Deflection~D_5 (in)
		D_1	D_2	D_3	D_4		
200.	22.	0.0006	0.0006	0.009	0.0008	0.0065	0
400.	44.	0.0034	0.0021	0.019	0.0026	0.0098	0
600.	67.	0.0073	0.0038	0.032	0.0048	0.0144	0
800.	89.	0.0126	0.0060	0.050	0.0091	0.0192	0
1000.	111.	0.0181	0.0082	0.066	0.0130	0.0226	-0.001
1200.	133.	0.0224	0.0101	0.081	0.0171	0.0263	-0.004
1400.	156.	0.0254	0.0115	0.093	0.0196	0.0306	-0.004
1600.	178.	0.0281	0.0128	0.103	0.0217	0.0339	-0.004
1800.	200.	0.0305	0.0139	0.114	0.0237	0.0387	-0.004
2000.	222.	0.0333	0.0150	0.124	0.0256	0.0423	-0.004
2200.	244.	0.0360	0.0162	0.134	0.0275	0.0459	-0.004
2400.	267.	0.0388	0.0175	0.145	0.0294	0.0503	-0.004
2600.	289.	0.0416	0.0186	0.157	0.0315	0.0556	0.000
2800.	311.	0.0445	0.0197	0.169	0.0335	0.0610	0.004
2840.	316.	0.0453	0.0200	0.172	0.0340	0.0624	0.004
2890.	321.	0.0458	0.0203	0.175	0.0344	0.0639	0.007
2940.	327.	0.0465	0.0206	0.178	0.0349	0.0653	0.013
2990.	332.	0.0474	0.0209	0.182	0.0355	0.0673	0.013
3040.	338.	0.0478	0.0213	0.185	0.0360	0.0689	0.016
3090.	343.	0.0485	0.0217	0.187	0.0365	0.0690	0.019
3140.	349.	0.0494	0.0220	0.193	0.0370	0.0732	0.024
3190.	354.	0.0500	0.0227	0.198	0.0377	0.0760	0.029
3240.	360.	0.0506	0.0228	0.203	0.0382	0.0796	0.036
3290.	366.	0.0514	0.0230	0.209	0.0388	0.0838	0.046
3340.	371.	0.0518	0.0236	0.215	0.0391	0.0884	0.060
3390.	377.	0.0525	0.0239	0.223	0.0398	0.0945	0.084

TABLE 14 (continued)

3440.	382.	0.0529	0.0244	0.231	0.0401	0.1011	0.107
3490.	388.	0.0535	0.0249	0.243	0.0408	0.1111	0.154
3540.	393.	0.0542	0.0260	0.272	0.0412	0.1376	0.325
3600.	400.	0.0544	0.0276	0.302	0.0419	0.1646	0.597
3530.	392.	0.0544	0.0320	0.440	0.0439	0.2953	1.537
3610.	401.	0.0550	0.0370	0.600	0.0448	0.4479	

TABLE 15
DATA FROM TEST R32, BUTLERIB,
a = 9 ft, b = 9.58 ft.

Load (lbs)	Shear (lbs/ft)	Gage Deflections (in)				Shear Deflection (in)	Lateral Deflection-D_5 (in)
		D_1	D_2	D_3	D_4		
200.	22.	0.0002	0.0002	0.012	0.0030	0.0079	0.002
400.	44.	0.0032	0.0017	0.024	0.0054	0.0122	0.004
600.	67.	0.0069	0.0036	0.036	0.0075	0.0158	0.006
800.	89.	0.0121	0.0057	0.052	0.0100	0.0212	0.008
1000.	111.	0.0176	0.0087	0.072	0.0166	0.0244	0.010
1200.	133.	0.0218	0.0102	0.084	0.0190	0.0275	0.014
1400.	156.	0.0244	0.0115	0.095	0.0213	0.0316	0.019
1600.	178.	0.0270	0.0126	0.105	0.0233	0.0354	0.024
1800.	200.	0.0295	0.0137	0.116	0.0253	0.0401	0.030
2000.	222.	0.0322	0.0150	0.126	0.0273	0.0434	0.036
2200.	244.	0.0351	0.0167	0.138	0.0293	0.0483	0.045
2400.	267.	0.0379	0.0176	0.149	0.0310	0.0532	0.055
2600.	289.	0.0408	0.0186	0.161	0.0331	0.0586	0.069
2800.	311.	0.0435	0.0197	0.173	0.0352	0.0640	0.088
2850.	317.	0.0442	0.0200	0.177	0.0357	0.0665	0.095
2900.	322.	0.0451	0.0205	0.181	0.0363	0.0683	0.102
2950.	328.	0.0457	0.0208	0.184	0.0368	0.0697	0.110
3000.	333.	0.0464	0.0211	0.188	0.0373	0.0721	0.118
3050.	339.	0.0471	0.0216	0.192	0.0378	0.0742	0.129
3100.	344.	0.0475	0.0217	0.197	0.0384	0.0778	0.140
3150.	350.	0.0481	0.0220	0.201	0.0390	0.0801	0.155
3200.	356.	0.0490	0.0224	0.207	0.0394	0.0844	0.171
3250.	361.	0.0495	0.0228	0.213	0.0400	0.0886	0.190
3300.	367.	0.0502	0.0231	0.220	0.0405	0.0940	0.216
3350.	372.	0.0508	0.0236	0.229	0.0412	0.1009	0.247

TABLE 15 (continued)

3400.	378.	0.0513	0.0241	0.238	0.0415	0.1086	0.290
3450.	383.	0.0518	0.0247	0.250	0.0420	0.1186	0.354
3500.	389.	0.0525	0.0260	0.282	0.0424	0.1481	0.545
3550.	394.	0.0531	0.0265	0.305	0.0429	0.1693	0.730
3400.	378.	0.0531	0.0290	0.373	0.0429	0.2345	1.470
3530.	392.	0.0531	0.0326	0.460	0.0431	0.3168	2.870

TABLE 16
DATA FROM TEST R40, BUTLERIB,
a = 15 ft, b = 9.58 ft

Load (lbs)	Shear (lbs/ft)	Gage Deflections (in)				Shear Deflection (in)	Lateral Deflection~ D_5 (in)
		D_1	D_2	D_3	D_4		
310.	21.	0.0021	0.0010	0.012	0.0076	0.0048	0.003
620.	41.	0.0071	0.0032	0.027	0.0150	0.0081	0.009
920.	61.	0.0132	0.0054	0.044	0.0224	0.0114	0.017
1200.	80.	0.0191	0.0076	0.058	0.0283	0.0149	0.023
1500.	100.	0.0257	0.0102	0.075	0.0340	0.0185	0.031
1800.	120.	0.0309	0.0117	0.090	0.0394	0.0235	0.039
2100.	140.	0.0350	0.0134	0.102	0.0444	0.0277	0.048
2510.	167.	0.0401	0.0154	0.121	0.0505	0.0349	0.060
2810.	187.	0.0442	0.0170	0.135	0.0551	0.0405	0.071
3110.	207.	0.0477	0.0183	0.148	0.0595	0.0461	-*
3410.	227.	0.0511	0.0197	0.160	0.0634	0.0519	-
3710.	247.	0.0546	0.0208	0.173	0.0676	0.0577	-
4000.	267.	0.0579	0.0222	0.187	0.0714	0.0638	-
4300.	287.	0.0613	0.0235	0.201	0.0747	0.0721	-
4610.	307.	0.0650	0.0249	0.217	0.0787	0.0797	-
4920.	328.	0.0688	0.0265	0.237	0.0827	0.0919	0.150
5210.	347.	0.0718	0.0279	0.255	0.0858	0.1038	0.180
5510.	367.	0.0750	0.0298	0.283	0.0908	0.1237	0.200
5800.	387.	0.0783	0.0324	0.331	0.0953	0.1634	0.280
5830.	389.	0.0705	0.0375	0.427	0.0987	0.2614	
6100.	407.	0.0800	0.0452	0.625	0.0984	0.4449	1.100

*Dial of Gage D_5 Malfunctioned.

TABLE 17

PREDICTED AND ACTUAL VALUES OF AND

Panel	h (inches)	Predicted Values		Actual Values	
Butlerib a = 15 ft b = 13.58 ft	.0191	3.1^{o}	10	$6.5^{o} \rightarrow 13^{o}$	10
	.0217	3.4^{o}	10		
Butlerib a = 9 ft b = 13.58 ft	.0191	3.1^{o}	6	$6.5^{o} \rightarrow 13^{o}$	6
	.0217	3.4^{o}	6		
Butlerib a = 9 ft b = 9.58 ft	.0191	3.1^{o}	9	$6.5^{o} \rightarrow 13^{o}$	8+
	.0217	3.4^{o}	8		
Butlerib a = 15 ft b = 9.58 ft	.0191	3.1^{o}	15	$6.5^{o} \rightarrow 13^{o}$	14+
	.0217	3.4^{o}	14		
Sine-Wave a = 8 ft b = 9.58 ft	.0363	7.6^{o}	3	$28^{o} \rightarrow 32^{o}$	4
	.0411	8.2^{o}	4		
Sine-Wave a = 8 ft b = 9.58 ft	.0243	6.1^{o}	4	$23^{o} \rightarrow 28^{o}$	4
	.0277	6.6^{o}	4		

TABLE 18
DATA FROM TEST R50, SINE-WAVE,
a = 8 ft, b = 9.58 ft, 20 gage

Load (lbs)	Shear (lbs/ft)	Gage Deflections (in)				Shear Deflection (in)	Lateral Deflection D_5 (in)
		D_1	D_2	D_3	D_4		
300.	38.	0.0012	0.0010	0.034	0.0145	0.0156	0.008
410.	51.	0.0034	0.0020	0.039	0.0163	0.0152	0.008
600.	75.	0.0068	0.0030	0.049	0.0193	0.0170	0.012
800.	100.	0.0106	0.0048	0.058	0.0230	0.0156	0.018
1000.	125.	0.0153	0.0068	0.078	0.0330	0.0160	0.022
1200.	150.	0.0191	0.0085	0.086	0.0353	0.0165	0.026
1410.	176.	0.0237	0.0106	0.098	0.0378	0.0174	0.030
1600.	200.	0.0275	0.0122	0.106	0.0404	0.0176	0.035
1800.	225.	0.0310	0.0137	0.115	0.0431	0.0181	0.041
2000.	250.	0.0341	0.0147	0.123	0.0455	0.0189	0.044
2220.	278.	0.0369	0.0161	0.132	0.0483	0.0191	0.054
2400.	300.	0.0396	0.0169	0.140	0.0507	0.0206	0.057
2600.	325.	0.0424	0.0186	0.147	0.0535	0.0205	0.063
2800.	350.	0.0449	0.0193	0.156	0.0557	0.0225	0.069
3020.	378.	0.0475	0.0205	0.163	0.0581	0.0225	0.082
3200.	400.	0.0499	0.0218	0.171	0.0605	0.0238	0.110
3400.	425.	0.0522	0.0229	0.179	0.0623	0.0260	0.298
3600.	450.	0.0546	0.0241	0.191	0.0646	0.0315	0.626
3800.	475.	0.0571	0.0252	0.201	0.0668	0.0350	0.732
4010.	501.	0.0595	0.0260	0.211	0.0691	0.0398	0.805
4200.	525.	0.0618	0.0270	0.222	0.0711	0.0440	0.864
4400.	550.	0.0642	0.0281	0.231	0.0731	0.0479	0.916
4600.	575.	0.0667	0.0294	0.243	0.0754	0.0521	0.969
4810.	601.	0.0691	0.0306	0.254	0.0813	0.0523	1.014
5000.	625.	0.0713	0.0317	0.266	0.0789	0.0635	1.058
5200.	650.	0.0733	0.0331	0.280	0.0811	0.0712	1.104

TABLE 18 (continued)

5400.	675.	0.0760	0.0342	0.293	0.0827	0.0781	1.139
5610.	701.	0.0783	0.0358	0.310	0.0847	0.0886	1.166
5800.	725.	0.0810	0.0377	0.337	0.0864	0.1087	1.215
6000.	750.	0.0831	0.0392	0.352	0.0882	0.1176	1.244
6210.	776.	0.0854	0.0408	0.372	0.0898	0.1315	1.267
6420.	803.	0.0876	0.0422	0.391	0.0914	0.1447	1.285
6620.	828.	0.0900	0.0437	0.410	0.0933	0.1572	1.308
6810.	851.	0.0923	0.0452	0.428	0.0952	0.1688	1.334
7000.	875.	0.0944	0.0468	0.446	0.0969	0.1808	1.363
7200.	900.	0.0966	0.0481	0.464	0.0986	0.1930	1.400
7410.	926.	0.0991	0.0499	0.485	0.1006	0.2070	1.458
7600.	950.	0.1013	0.0506	0.506	0.1030	0.2221	1.512
7800.	975.	0.1036	0.0531	0.530	0.1055	0.2377	1.567
8000.	1000.	0.1060	0.0549	0.554	0.1084	0.2539	1.641
8210.	1026.	0.1084	0.0564	0.580	0.1109	0.2727	1.720
8400.	1050.	0.1105	0.0578	0.606	0.1134	0.2919	1.791
8600.	1075.	0.1128	0.0597	0.632	0.1158	0.3106	1.878
8800.	1100.	0.1204	0.0616	0.670	0.1190	0.3349	1.989
9010.	1126.	0.1216	0.0629	0.700	0.1214	0.3593	2.101
9210.	1151.	0.1234	0.0659	0.738	0.1156	0.3986	2.167
9610.	1201.	0.1265	0.0694	0.797	0.1175	0.4480	2.468
10000.	1250.	0.1310	0.0757	0.896	0.1208	0.5312	2.664
10410.	1301.	0.1353	0.0841	1.061	0.1247	0.6774	-
10800.	1350.	0.1398	0.0976	1.314	0.1297	0.9042	4.000
10870.	1359.	0.1414	0.1274	1.876	0.1305	1.4302	
10370.	1296.	0.1374	0.1556	2.499	0.1270	2.0280	

TABLE 19

DATA FROM TEST R51, SINE-WAVE,
a = 8 ft, b = 9.58 ft, 20 Gage

Load (lbs)	Shear (lbs/ft)	Gage Deflections (in)				Shear Deflection (in)	Lateral Deflection ~ D_5 (in)
		D_1	D_2	D_3	D_4		
400.	50.	0.0027	0.0024	0.011	0.0047	0.0008	0
800.	100.	0.0091	0.0048	0.027	0.0091	0.0021	0
1210.	151.	0.0171	0.0080	0.046	0.0139	0.0038	0
1600.	200.	0.0260	0.0112	0.066	0.0181	0.0051	0
2000.	250.	0.0322	0.0139	0.092	0.0231	0.0057	0
2410.	301.	0.0377	0.0160	0.098	0.0279	0.0079	0
2800.	350.	0.0430	0.0181	0.119	0.0369	0.0105	0
3200.	400.	0.0477	0.0200	0.134	0.0408	0.0139	0
3600.	450.	0.0525	0.0222	0.150	0.0448	0.0176	0
3830.	479.	0.0553	0.0243	0.167	0.0469	0.0268	0 → 0.420
4000.	500.	0.0572	0.0251	0.185	0.0483	0.0402	0.451
4420.	553.	0.0619	0.0270	0.207	0.0520	0.0508	0.539
4810.	601.	0.0661	0.0294	0.231	0.0552	0.0639	0.645
5200.	650.	0.0708	0.0317	0.259	0.0589	0.0800	0.814
5620.	703.	0.0757	0.0348	0.293	0.0623	0.1013	1.114
6000.	750.	0.0800	0.0370	0.324	0.0653	0.1217	1.351
6410.	801.	0.0847	0.0399	0.356	0.0689	0.1412	1.536
6820.	853.	0.0891	0.0422	0.389	0.0718	0.1636	1.673
7210.	901.	0.0933	0.0446	0.424	0.0744	0.1883	1.791
7600.	950.	0.0977	0.0482	0.462	0.0784	0.2129	1.911
8000.	1000.	0.1023	0.0524	0.508	0.0807	0.2465	2.043
8800.	1100.	0.1113	0.0591	0.619	0.0868	0.3332	2.371
9590.	1199.	0.1226	0.0693	0.805	0.0943	0.4869	2.866
10000.	1250.	0.1264	0.0755	0.926	0.0990	0.5912	3.148
10390.	1299.	0.1307	0.0847	1.094	0.1026	0.7398	3.377
10800.	1350.	0.1352	0.1042	1.433	0.1053	1.0484	
10970.	1371.	0.1362	0.1377	2.239	0.1038	1.8163	

TABLE 20
DATA FROM TEST R52, SINE-WAVE,
a = 8 ft, b = 9.58 ft, 24 gage

Load (lbs)	Shear (lbs/ft)	Gage Deflections (in)				Shear Deflection (in)	Lateral Deflection D_5 (in)
		D_1	D_2	D_3	D_4		
320.	40.	0.0022	0.0011	0.011	0.0017	0.0050	0.020
600.	75.	0.0072	0.0033	0.023	0.0052	0.0064	0.052
890.	111.	0.0129	0.0060	0.039	0.0087	0.0083	0.094
1200.	150.	0.0191	0.0088	0.055	0.0124	0.0103	0.159
1500.	188.	0.0259	0.0118	0.073	0.0163	0.0133	0.367
1800.	225.	0.0309	0.0139	0.092	0.0198	0.0206	0.703
2100.	263.	0.0351	0.0161	0.117	0.0241	0.0338	0.971
2400.	300.	0.0392	0.0184	0.146	0.0289	0.0502	1.069
2700.	338.	0.0431	0.0208	0.186	0.0337	0.0780	1.171
3000.	375.	0.0451	0.0233	0.212	0.0405	0.0910	1.315
3310.	414.	0.0506	0.0257	0.247	0.0435	0.1141	1.452
3600.	450.	0.0540	0.0285	0.286	0.0460	0.1434	1.580
3910.	489.	0.0577	0.0313	0.329	0.0488	0.1760	1.700
4100.	513.	0.0599	0.0334	0.360	0.0502	0.2006	1.874
4400.	550.	0.0630	0.0362	0.407	0.0527	0.2380	1.984
4700.	588.	0.0665	0.0394	0.461	0.0551	0.2820	2.109
5000.	625.	0.0697	0.0433	0.524	0.0576	0.3342	2.255
5300.	663.	0.0734	0.0477	0.600	0.0599	0.3985	2.338
5610.	701.	0.0773	0.0531	0.701	0.0621	0.4867	2.594
5900.	738.	0.0808	0.0595	0.788	0.0641	0.5604	2.874
6210.	776.	0.0849	0.0759	1.216	0.0650	0.9639	3.102
6500.	813.	0.0850	0.1014	1.701	0.0622	1.4223	

TABLE 21
DATA FROM TEST R53, SINE-WAVE,
a = 8 ft, b = 9.58 ft, 24 gage

Load (lbs)	Shear (lbs/ft)	Gage Deflections (in)				Shear Deflection (in)	Lateral Deflection~D_5 (in)
		D_1	D_2	D_3	D_4		
300.	38.	0.0017	0.0001	0.010	0.0017	0.0058	0.008
600.	75.	0.0063	0.0022	0.023	0.0051	0.0075	0.019
900.	113.	0.0122	0.0045	0.037	0.0086	0.0088	0.028
1200.	150.	0.0182	0.0058	0.051	0.0123	0.0108	0.037
1500.	188.	0.0250	0.0093	0.067	0.0159	0.0117	0.049
1810.	226.	0.0304	0.0116	0.082	0.0194	0.0144	0.078
2100.	263.	0.0343	0.0135	0.104	0.0236	0.0252	0.377
2400.	300.	0.0385	0.0156	0.135	0.0333	0.0382	0.584
2700.	338.	0.0422	0.0178	0.162	0.0364	0.0552	0.857
3000.	375.	0.0459	0.0200	0.202	0.0394	0.0852	1.598
3300.	413.	0.0495	0.0224	0.235	0.0423	0.1084	1.755
3600.	450.	0.0531	0.0250	0.274	0.0449	0.1375	1.896
3910.	489.	0.0565	0.0277	0.317	0.0473	0.1710	2.027
4210.	526.	0.0599	0.0305	0.364	0.0501	0.2080	2.158
4500.	563.	0.0632	0.0333	0.417	0.0525	0.2515	2.291
4800.	600.	0.0665	0.0370	0.476	0.0547	0.3002	2.433
5100.	638.	0.0703	0.0411	0.549	0.0569	0.3618	2.596
5400.	675.	0.0738	0.0452	0.630	0.0593	0.4316	2.766
5700.	713.	0.0775	0.0500	0.725	0.0613	0.5148	2.943
6000.	750.	0.0810	0.0590	0.915	0.0626	0.6892	3.027
6300.	788.	0.0844	0.0600	1.125	0.0636	0.8933	3.323

TABLE 22

DATA FROM TEST R1, M36, a = 3 ft, b = 8 ft

Load (lbs)	Shear (lbs/ft)	Gage Deflections (in)				Shear Deflection (in)
		D_1	D_2	D_3	D_4	
570.	190.	.0092	.0000	.071	.0101	.0378
1020.	340.	.0182	.0000	.116	.0210	.0483
1400.	467.	.0240	.0039	.147	.0261	.0525
1800.	600.	.0308	.0039	.179	.0310	.0658
2250.	750.	.0385	.0097	.212	.0351	.0678
2610.	870.	.0442	.0097	.242	.0391	.0824
3020.	1007.	.0510	.0097	.275	.0422	.1007
3410.	1137.	.0576	.0160	.317	.0457	.1132
3800.	1267.	.0635	.0160	.378	.0482	.1619
4200.	1400.	.0700	.0160	.443	.0520	.2110
4600.	1533.	.0760	.0160	.508	.0561	.2599
5000.	1667.	.0822	.0270	.585	.0601	.2961

TABLE 23

DATA FROM TEST R2, M36, a = 3 ft, b = 8 ft

Load (lbs)	Shear (lbs/ft)	Gage Deflections (in)				Shear Deflection (in)
		D_1	D_2	D_3	D_4	
420.	140.	.0029	.0020	.049	.0040	.0317
800.	267.	.0060	.0040	.103	.0149	.0527
1200.	400.	.0094	.0060	.136	.0220	.0610
1620.	540.	.0148	.0080	.175	.0270	.0779
2020.	673.	.0201	.0090	.206	.0310	.0915
2400.	800.	.0253	.0100	.237	.0350	.1053
2810.	937.	.0313	.0110	.268	.0390	.1181
3210.	1070.	.0374	.0120	.302	.0430	.1339
3670.	1223.	.0447	.0140	.341	.0470	.1512
4000.	1333.	.0500	.0150	.371	.0493	.1677
4400.	1467.	.0557	.0160	.410	.0529	.1898
4790.	1597.	.0610	.0170	.453	.0551	.2195
5220.	1740.	.0685	.0190	.512	.0590	.2568

TABLE 24

DATA FROM TEST R3, M36, a = 6 ft, b = 12 ft.

Load (lbs)	Shear (lbs/ft)	Gage Deflections (in)				Shear Deflection (in)
		D_1	D_2	D_3	D_4	
400.	67.	.0018	.0022	.024	.0031	.0116
800.	133.	.0092	.0057	.060	.0088	.0224
1200.	200.	.0153	.0084	.091	.0152	.0297
1600.	267.	.0209	.0102	.125	.0212	.0429
2000.	333.	.0265	.0118	.152	.0269	.0500
2400.	400.	.0335	.0137	.183	.0380	.0492
2800.	467.	.0392	.0153	.217	.0422	.0659
3200.	533.	.0448	.0168	.242	.0445	.0775
3600.	600.	.0502	.0183	.266	.0495	.0833
4000.	667.	.0557	.0199	.289	.0530	.0905
4400.	733.	.0612	.0215	.313	.0562	.0994
4800.	800.	.0664	.0233	.338	.0593	.1093
5200.	867.	.0710	.0250	.363	.0622	.1204
5600.	933.	.0762	.0268	.390	.0651	.1327
6000.	1000.	.0813	.0285	.423	.0683	.1507
6400.	1067.	.0864	.0302	.455	.0711	.1685
6800.	1133.	.0909	.0320	.487	.0737	.1870
7200.	1200.	.0953	.0340	.524	.0771	.2088
7250.	1208.	.0953	.0340	.543	.0771	.2277

TABLE 25

DATA FROM TEST R4, M36, a = 9 ft, b = 12 ft

Load (lbs)	Shear (lbs/ft)	Gage Deflections (in)				Shear Deflection (in)
		D_1	D_2	D_3	D_4	
400.	44.	.0021	.0026	.020	.0038	.0093
810.	90.	.0090	.0061	.050	.0124	.0166
1200.	133.	.0139	.0090	.082	.0244	.0243
1600.	178.	.0185	.0104	.109	.0348	.0312
2000.	222.	.0235	.0116	.133	.0437	.0369
2400.	267.	.0287	.0128	.154	.0502	.0425
2800.	311.	.0339	.0141	.175	.0567	.0479
3200.	356.	.0387	.0153	.195	.0620	.0544
3600.	400.	.0434	.0168	.213	.0671	.0589
4000.	444.	.0476	.0182	.231	.0712	.0653
4410.	490.	.0519	.0201	.248	.0750	.0703
4800.	533.	.0563	.0213	.264	.0788	.0751
5210.	579.	.0603	.0226	.281	.0822	.0817
5600.	622.	.0642	.0238	.297	.0851	.0882
6000.	667.	.0684	.0249	.314	.0891	.0941
6400.	711.	.0727	.0261	.331	.0927	.1002
6800.	756.	.0774	.0272	.353	.0958	.1118
7200.	800.	.0814	.0283	.376	.0991	.1248
7600.	844.	.0860	.0294	.398	.1016	.1372
8000.	889.	.0907	.0305	.426	.1049	.1545
8400.	933.	.0950	.0316	.449	.1093	.1657
8820.	980.	.0997	.0328	.476	.1130	.1814
9200.	1022.	.1050	.0342	.498	.1162	.1918
9630.	1070.	.1097	.0362	.527	.1207	.2074
10000.	1111.	.1157	.0382	.558	.1249	.2241
10230.	1137.	.1157	.0382	.578	.1249	.2439

TABLE 26

H_x, H_y and H_{xy}
FOR BUTLERIB AND SINE-WAVE PANELS

Panel	Thickness h in	H_x in.-lb.	H_y in.-lb.	H_{xy} in.-lb.
Butlerib	.191	14.9	13.5×10^4	31.3
	.0217	21.8	15.3×10^4	45.9
Sine-Wave	.0363	106.2	3.12×10^4	198.2
	.0411	160.6	3.53×10^4	287.7
Sine-Wave	.0243	33.4	2.34×10^4	59.0
	.0277	49.5	2.67×10^4	87.4

TABLE 27

COEFFICIENTS DEFINING THE LOAD VERSUS LATERAL DEFLECTION RELATION FOR THE BUTLERIB AND SINE-WAVE PANELS

Panel Identification	Panel(ft) Dimensions a	b	Thickness h inches	$L = -C_1 P_y + C_2$ C_1	C_2	J	K
Butlerib	15	13.58	.0191	12.4	229	.901	.0220
			.0217	13.3	295	1.131	.0323
Butlerib	9	13.58	.0191	7.47	137	.541	.0132
			.0217	7.96	177	.788	.0194
Butlerib	9	9.58	.0191	11.9	437	4.31	.239
			.0217	9.99	447	3.16	.137
Butlerib	15	9.58	.0191	19.8	728	7.18	.398
			.0217	18.4	819	6.99	.336
Sine-Wave (20 gage)	8	9.58	.0363	3.54	74.1	.096	.00061
			.0411	3.83	96.9	.140	.00091
Sine-Wave (24 gage)	8	9.58	.0243	5.01	61.9	.149	.00187
			.0277	5.43	81.7	.217	.00277

TABLE 28

H_x, H_y, H_{xy} AND BUCKLING LOADS
FOR M36 PANELS

	Panel Size					
	a=3 ft, b=8 ft		a=6 ft, b=12 ft		a=9 ft, b=12 ft	
h ~ in	.0191	.0217	.0191	.0217	.0191	.0217
H_x (#in^2)	14.2	20.8	14.2	20.8	14.2	20.8
H_y (#in^2)	189x10^4	214x10^4	189x10^4	214x10^4	189x10^4	214x10^4
H_{xy} (#in^2)	32.8	48.2	32.8	48.2	32.8	48.2
Limits of Predicted Buckling Load (lb/in)	376	458	167	203	167	203
Actual Buckling Load (lb/in)	144		101		95	

APPENDIX A

APPENDIX A

Because buckling of a corrugated plate in shear was eventually predicted only from a consideration of lateral deflections, i.e. bending, the actual magnitudes of the membrane stress-strain constants E_x, ν_x, ν_y and G_{xy} developed for the orthotropic model were not needed. It has been pointed out that in all cases, the most effective way of determining the magnitude of these constants is by conducting appropriate tests on actual q x q sections taken from the panel in question. However, approximate theoretical expressions have been developed for each of these constants and are presented in this appendix in order that at least order of magnitude estimates may be made for these constants if necessary.

a) Derivation of E_x

First, an expression for the constant E_x is developed. Most corrugated cross-sections can be broken up into a number of components which are either straight or circular segments. Therefore, these are the only two types of segments considered, and any other type which might occur will have to be replaced by an approximate segment made of straight and circular segments or must have a new expression derived for it.

To begin, E_x is defined as

$$E_x = \frac{N_x/h}{\Delta t/q} = \frac{N_x q}{h \Delta t} \qquad \text{(A1)}$$

The term Δ_t is the total deflection of a q x q element in the x direction due to the load N_x. Therefore, to compute E_x, the only term not already available is Δ_t. It is necessary to compute the portion of Δ_t which arises from each component of the corrugation. Castigliano's Theorem is used as given below

$$\Delta_i = \frac{\partial W_i}{\partial P}$$

W_i is the strain energy of the i^{th} component of the corrugation.

The straight segment to be considered is shown in the following sketch:

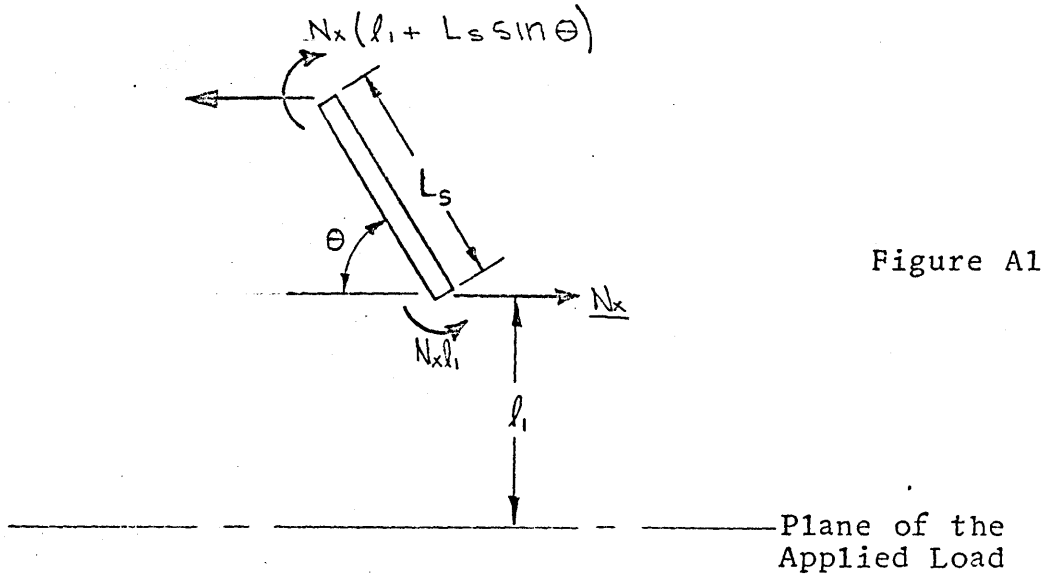

Figure A1

For this segment, the energy due to shear is considered negligible when compared to the bending energy, and therefore the equation for deflection becomes

$$\Delta_{s\ell} = \int_0^{L_s} \frac{P \frac{\partial P}{\partial N_x}}{AE} ds + \int_0^{L_s} \frac{M \frac{\partial M}{\partial N_x}}{EI} ds \qquad \text{(A2)}$$

If it is noted that

$$\left.\begin{aligned} P &= N_x \cos\theta \\ M &= N_x l_1 + N_x (s)(\sin\theta) \end{aligned}\right] \qquad \text{(A3)}$$

the resulting expression for Δ_{si} is obtained as

$$\Delta_{s\ell} = \frac{N_x}{E}\left[\frac{L_s \cos^2\theta}{h} + \frac{12 L_s l_1^2}{h^3} + \frac{12 l_1 L_s^2 \sin\theta}{h^3} + \frac{4 L_s^3 \sin^2\theta}{h^3}\right] \qquad \text{(A4)}$$

The following circular segment is now considered:

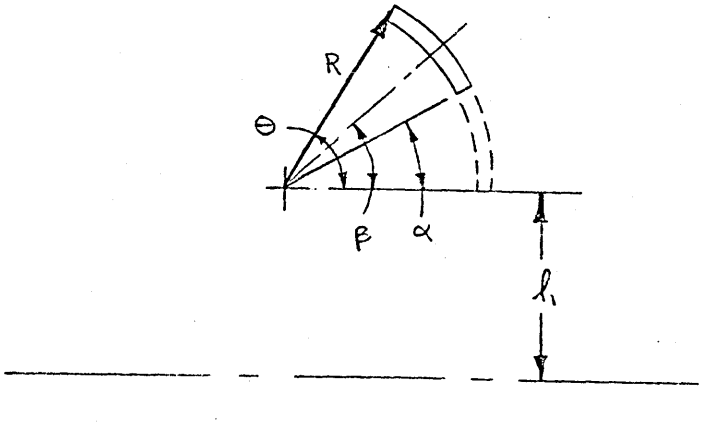

Figure A2

Castigliano's equation assumes the form

$$\Delta_{ci} = \int_\alpha^\theta \frac{P \frac{\partial P}{\partial N_x}}{AE} R\, d\beta + \int_\alpha^\theta \frac{M \frac{\partial M}{\partial N_x}}{EI} R\, d\beta \qquad \text{(A5)}$$

in which $P = N_x \sin\beta$

$$M = N_x \ell_1 + N_x R \sin\beta$$

For this the equation, Δ_{ci} is found to be

$$\Delta_{ci} = \frac{N_x R}{E h}\left[\frac{\beta}{2} - \frac{\sin 2\beta}{4}\right]_{\alpha}^{\Theta} + \frac{12 N_x R}{E h^3}\left[\ell_1^2\beta - 2\ell_1 R \sin\beta + \frac{R^2\beta}{2} - \frac{R^2 \sin 2\beta}{4}\right]_{\alpha}^{\Theta} \qquad \text{(A6)}$$

The equation for Δ_{ci} is left in the above form, since completing the substitution of Θ and α for β only increases the number of terms in the expression and adds nothing to the clarity of the equation.

Now it is possible to solve for Δ_t.

$$\Delta_t = \sum_i \Delta_{si} + \sum_j \Delta_{cj} \qquad \text{(A7)}$$

The subscripts i and j indicate summations over all of the straight and circular segments respectively in the repeating cross-section.

b) Derivation of ν_x and ν_y

The effective Poisson's ratios are computed in the x and y directions. To compute ν_y, N_y is considered to be applied to the q x q element and ν_y is defined as $\Delta_{x_1}/\Delta_{y_1}$, with Δ_{x_1} and Δ_{y_1} the total deflections in the x and y directions respectively. To estimate ν_y, the

following element with $q = \ell_1 + \ell_2 \cos\Theta$ is considered:

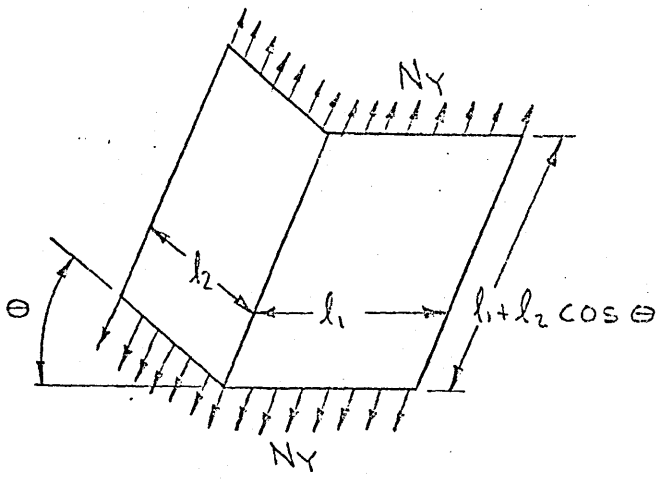

Figure A3

from which the following equations are obtained:

$$\Delta Y_1 = \frac{N_Y}{Eh}\left(\ell_1 + \ell_2 \cos\Theta\right) \tag{A8}$$

$$\Delta X_1 = \frac{\nu N_Y}{Eh}\ell_1 + \frac{\nu N_Y}{Eh}\left(\ell_2\right)\cos\Theta \tag{A9}$$

and it follows that

$$\nu_Y = \Delta x_1 / \Delta Y_1 = \nu \tag{A10}$$

To derive ν_x, N_x is applied to a section from a corrugated plate

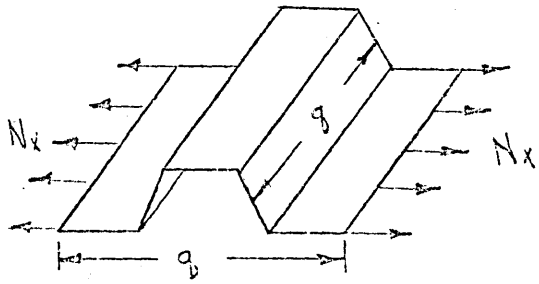

Figure A4

Now ν_x is defined as $\Delta x_1 / \Delta x_2$ with Δy_2 and Δx_2 the total deflections of the above section in the y and x directions respectively. The deflection Δy for any point in the corrugation depends upon the slope of the corrugation at that point, since the axial stress in any component varies with the slope. Therefore, as an estimate Δy_2 is set equal to the Δy in the horizontal components of the corrugation. This leads to

$$\Delta y_2 = \frac{\nu N_x}{E h} q \qquad \text{(A11)}$$

and by definition

$$\Delta x_2 = \frac{N_x}{E_x h} q \qquad \text{(A12)}$$

Thus it follows that

$$\nu_x = \nu \frac{E_x}{E} \qquad \text{(A13)}$$

c) Derivation of G_{xy}

To derive an expression for G_{xy}, it is first noted that for a square isotropic element, the following is obtained

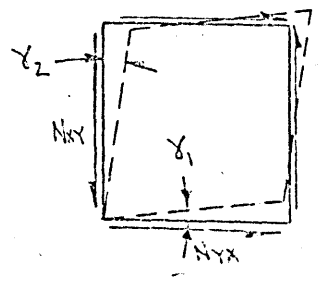

Deflected Shape

Figure A5

and by definition

$$\gamma_{xy} = \gamma_1 + \gamma_2 \qquad \text{(A14)}$$

For this element, it seems obvious that the contributions to γ_{xy} from N_{xy} and N_{yx} must be equal due to equal properties in all directions and the assumption that $N_{xy}=N_{yx}$. Therefore

$$\gamma_1 = \gamma_2 = \gamma_{xy}/2 = N_{xy}/2Gh \qquad \text{(A15)}$$

Then for the orthotropic q x q element, γ_{xy} will still equal $\gamma_1 + \gamma_2$, but γ_1 will no longer equal γ_2. To obtain γ_1 and γ_2 a corrugated element is examined:

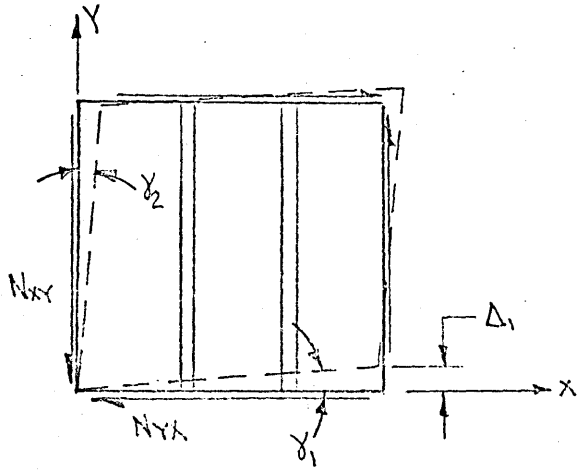

Figure A6

Solving for γ_1, it is first noted that the stress on the x face is N_{xy}/h. Observing that $\gamma_1 = \Delta_1/q$ with Δ_1 equal to the sum of the Δ's for each segment across the corrugations, Δ_1 is found to be

$$\Delta_1 = s\left(\frac{N_{xy}}{h}\right)\left(\frac{1}{2G}\right) \tag{A16}$$

and therefore

$$\gamma_1 = \frac{N_{xy}}{2Gh}\left(\frac{s}{q}\right) \tag{A17}$$

It seems that the best estimate for γ_2 is found by assuming the average stress $\frac{N_{xy}}{h}\left(\frac{q}{s}\right)$ acts over the entire y face. Based upon this assumption

$$\gamma_2 = \frac{N_{xy}}{2Gh}\left(\frac{q}{s}\right) \tag{A18}$$

γ_{xy} is obtained by recalling that

$$\gamma_{xy} = \gamma_1 + \gamma_2$$

$$\gamma_{xy} = \frac{N_{xy}}{2Gh}\left(\frac{q^2+s^2}{qs}\right) = \frac{N_{xy}}{G_{xy}h} \tag{A19}$$

From this equation G_{xy} is defined as

$$G_{xy} = \frac{2qs}{q^2+s^2} \tag{A20}$$

Note that in the preceeding equation if q = s, i.e. a flat plate, G_{xy} is equal to G.

APPENDIX B

a) Computer program used to obtain the buckling load resulting from the use of the infinite series approximation for w.

In determining this buckling load, a computer program is used which obtains the solutions to the matrix equation

$$A - \lambda I = 0$$

in which λ represents the eigenvalues, and I is the identity matrix. To adapt the determinant obtained from equation (53), e.g., Tables 1 or 2, so that it fits the form of equation (B1) the diagonal terms are set equal to zero and all terms in each row are divided by the corresponding values of k_{mn}. It is then seen that $\lambda_i = 1/P_{cr_i}$. The resulting real roots (λ_i) are inverted to obtain P_{cr_i}, and the minimum value of P_{cr_i} is the buckling load of the panel.

This program is designed to handle any basic determinant up to a maximum size of 40 x 40. The size chosen must be recorded in the read statement after item 2 as seen in the listing of the program included herein; e.g., the program listed here is set up to operate on an 18 x 18 basic determinant. The numerator of each term in the basic determinant is read into the matrix A2 and the denominator into the matrix A1. A2 and A1 are combined as one matrix by the program. For each run of this program the number of separate sets of calculations is defined by the term KOUNT.

The program is also designed in such a manner that it starts with the first coefficient listed in the basic determinant and uses as many consecutive coefficients as desired, up to the maximum number given in the basic determinant. The number of terms to be used is identified in the program by N. The N appropriate diagonal terms, i.e. k_{mn}, corresponding to the panel being investigated must also be read into the computer for each separate set of calculations.

A1

```
      DIMENSION A(40,40),RR(40),RI(40),A1(40,40),A2(40,40)
      CALL SETUP(0)
      READ(5,2) KOUNT
    2 FORMAT(2I3)
      READ(5,1)((A2(I,J),A1(I,J),J=1,18),I=1,18)
    1 FORMAT(12F6.0)
      CALL CLOCK(0)
      DO 60 L=1,KOUNT
      READ(5,2)N
   70 READ(5,1)(A2(I,I),A1(I,I),I=1,N)
      DO 40 I=1,N
      DO 40 J=1,N
      A(I,J)=-(A2(I,J)*A1(I,I))/(A1(I,J)*A2(I,I))
   40 IF(ABS(A(I,J)).LT.1.E-10) A(I,J)=0.
      DO 141 KK=1,N
  141 A(KK,KK)=0.
  142 CALL HESSEN(A,N)
      DO 41 I=1,N
      DO 41 J=1,N
   41 IF(ABS(A(I,J)).LT.1.E-10) A(I,J)=0.
      CALL QREIG(A,N,RR,RI,1)
      WRITE(6,3) N
    3 FORMAT(1H0,31H INVERTED EIGENVALUES WITH N = ,I4)
      DO 50 I=1,N
      IF(RI(I).NE.0.) GO TO 50
      RT=1./RR(I)
      WRITE(6,4) RT
    4 FORMAT(1X,F18.9)
   50 CONTINUE
   60 CALL CLOCK(N)
      CALL EXIT
      END
```

```
       HESSEN  DECK,REF
      SUBROUTINE TO PUT MATRIX IN UPPER HESSENBERG FORM.
      SUBROUTINE HESSEN(A,M)
      DIMENSION A(40,40),B(99)
      DOUBLE PRECISION SUM
      IF (M - 2) 30,30,32
   32 DO 40 LC = 3,M
      N = M - LC + 3
      N1 = N - 1
      N2 = N - 2
```

```
      NI = N1
      DIV = ABS(A(N,N-1))
      DO 2 J = 1,N2
      IF(ABS(A(N,J))- DIV) 2,2,1
    1 NI = J
      DIV = ABS(A(N,J))
    2 CONTINUE
      IF(DIV) 3,40,3
    3 IF(NI - N1) 4, 7,4
    4 DO 5 J = 1,N
      DIV = A(J,NI)
      A(J,NI) = A(J,N1)
    5 A(J,N1) = DIV
      DO 6 J = 1,M
      DIV = A(NI,J)
      A(NI,J) = A(N1,J)
    6 A(N1,J) = DIV
    7 DO 26 K = 1, N1
   26 B(K) = A(N,K)/A(N,N-1)
      DO 45 J = 1,M
      SUM = 0.0
      IF (J - N1) 46,43,43
   46 IF(B(J))  41,43,41
   41 A(N,J) = 0.0
      DO 42 K = 1,N1
      A(K,J) = A(K,J) - A(K,N1)*B(J)
   42 SUM = SUM + A(K,J)*B(K)
      GO TO 45
   43 DO 44 K = 1,N1
   44 SUM = SUM + A(K,J)*B(K)
   45 A(N1,J) = SUM
   40 CONTINUE
   30 RETURN
       END



       QRT      DECK,REF
      SUBROUTINE QRT(A,N,R,SIG,D)
      DIMENSION A(40,40),PSI(2),G(3)
      N1 = N - 1
      IA = N - 2
      IP = IA
      IF(N-3) 101,10,60
60    DO 12 J = 3,N1
      J1 = N - J
      IF(ABS(A(J1+1,J1))-D)    10,10,11
   11 DEN = A(J1+1,J1+1)*(A(J1+1,J1+1)-SIG)+A(J1+1,J1+2)*A(J1+2,J1+1)+R
      IF(DEN) 61,12,61
```

A3

```
61    IF(ABS(A(J1+1,J1)*A(J1+2,J1+1)*(ABS(A(J1+1,J1+1)+A(J1+2,J1+2)
     1-SIG)+ABS(A(J1+3,J1+2)))/DEN)-D)  10,10,12
12    IP=J1
10    DO  14  J=1,IP
      J1=IP-J+1
      IF(ABS(A(J1+1,J1))-D)     13,13,14
14    IQ=J1
13    DO  100  I=IP,N1
      IF(I-IP)    16,15,16
15    G(1)=A(IP,IP)*(A(IP,IP)-SIG)+A(IP,IP+1)*A(IP+1,IP)+R
      G(2)=A(IP+1,IP)*(A(IP,IP)+A(IP+1,IP+1)-SIG)
      G(3)=A(IP+1,IP)*A(IP+2,IP+1)
      A(IP+2,IP)=0.0
      GO TO 19
16    G(1)=A(I,I-1)
      G(2)=A(I+1,I-1)
      IF(I-IA)    17,17,18
17    G(3)=A(I+2,I-1)
      GO TO 19
18    G(3)=0.0
  19  XK = SIGN(SQRT(G(1)**2 + G(2)**2 + G(3)**2), G(1))
22    IF(XK)    23,24,23
23    AL=G(1)/XK+1.0
      PSI(1)=G(2)/(G(1)+XK)
      PSI(2)=G(3)/(G(1)+XK)
      GO TO 25
24    AL=2.0
      PSI(1)=0.0
      PSI(2)=0.0
25    IF(I-IQ)    26,27,26
26    IF(I-IP)     29,28,29
28    A(I,I-1)=-A(I,I-1)
      GO TO 27
29    A(I,I-1)=-XK
27    DO 30  J=I,N
      IF(I-IA)  31,31,32
31    C=PSI(2)*A(I+2,J)
      GO TO 33
32    C=0.0
33    E=AL*(A(I,J)+PSI(1)*A(I+1,J)+C)
      A(I,J)=A(I,J)-E
      A(I+1,J)=A(I+1,J)-PSI(1)*E
      IF(I-IA)    34,34,30
34    A(I+2,J)=A(I+2,J)-PSI(2)*E
30    CONTINUE
      IF(I-IA)    35,35,36
35    L=I+2
      GO TO  37
36    L=N
37    DO  40  J=IQ,L
```

```
      IF(I-IA)  38,38,39
38    C=PSI(2)*A(J,I+2)
      GO TO  41
39    C=0.0
41    E=AL*(A(J,I)+PSI(1)*A(J,I+1)+C)
      A(J,I)=A(J,I)-E
      A(J,I+1)=A(J,I+1)-PSI(1)*E
      IF(I-IA)  42,42,40
42    A(J,I+2)=A(J,I+2)-PSI(2)*E
40    CONTINUE
      IF(I-N+3)   43,43,100
43    E=AL*PSI(2)*A(I+3,I+2)
      A(I+3,I)=-E
      A(I+3,I+1)=-PSI(1)*E
      A(I+3,I+2)=A(I+3,I+2)-PSI(2)*E
100   CONTINUE
101   RETURN
       END



       QREIG   DECK,REF
        PROGRAM TO CALL QR TRANSFORMATION, MAXIMUM ITER IS 50.
      SUBROUTINE QREIG(A,M,ROOTR,ROOTI,IPRNT)
      DIMENSION A(40,40),ROOTR(40),ROOTI(40)
      N = M
      IF(IPRNT)  80,81,80
80    WRITE (6,104)
81    ZERO = 0.0
      JJ=1
 177  XNN=0.0
      XN2=0.0
      AA = 0.0
      B = 0.0
      C = 0.0
      DD = 0.0
      R=0.0
      SIG=0.0
      ITER = 0
17    IF(N-2)     13,14,12
13    IF(IPRNT)  82,83,82
82    WRITE (6,105)A(1,1)
83    ROOTR(1) = A(1,1)
      ROOTI(1) = 0.0
 1    RETURN
14    JJ=-1
  12  X = (A(N-1,N-1) - A(N,N))**2
      S = 4.0*A(N,N-1)*A(N-1,N)
      ITER = ITER + 1
```

```
      IF(X .EQ. 0.0 .OR. ABS(S/X) .GT. 1.0E-8) GO TO 15
   16 IF(ABS(A(N-1,N-1))-ABS(A(N,N)))  32,32,31
   31 E = A(N-1,N-1)
      G = A(N,N)
      GO TO 33
   32 G = A(N-1,N-1)
      E = A(N,N)
   33 F = 0.
      H = 0.
      GO TO 24
   15 S = X + S
      X = A(N-1,N-1) + A(N,N)
      IF(S)    18,19,19
19    SQ=SQRT(S)
      F=0.0
      H=0.0
      IF (X) 21,21,22
21    E=(X-SQ)/2.0
      G=(X+SQ)/2.0
      GO TO 24
22    G=(X-SQ)/2.0
      E=(X+SQ)/2.0
      GO TO 24
   18 F = SQRT(-S)/2.0
      E=X/2.0
      G=E
      H=-F
24    IF(JJ)  28,70,70
   70 D = 1.0E-10*(ABS(G) + F)
      IF(ABS(A(N-1,N-2)) .GT. D)  GO TO 26
28    IF(IPRNT)  84,85,84
84    WRITE (6,105)E,F, ITER
      WRITE (6,105)G,H
85    ROOTR(N) = E
      ROOTI(N) = F
      ROOTR(N-1) = G
      ROOTI(N-1) = H
      N=N-2
      IF(JJ)  1,177,177
   26 IF(ABS(A(N,N-1)) .GT. 1.0E-10*ABS(A(N,N)))  GO TO 50
29    IF(IPRNT)  86,87,86
86    WRITE (6,105)A(N,N), ZERO, ITER
87    ROOTR(N) = A(N,N)
      ROOTI(N) = 0.0
      N=N-1
      GO TO 177
50    IF(ABS(ABS(XNN/A(N,N-1))-1.0)-1.0E-6)  63,63,62
62    IF(ABS(ABS(XN2/A(N-1,N-2))-1.0)-1.0E-6)  63,63,700
   63 VQ=ABS(A(N,N-1))-ABS(A(N-1,N-2))
      IF (ITER-15) 53,164,64
```

A6

```
 164 IF(VQ) 165,165,166
 165 R = A(N-1,N-2)**2
     SIG = 2.0*A(N-1,N-2)
     GO TO 60
 166 R = A(N,N-1)**2
     SIG = 2.0*A(N,N-1)
     GO TO 60
64   IF(VQ)   67,67,66
66   IF(IPRNT)  88,85,88
88   WRITE (6,107)A(N-1,N-2)
     GO TO 84
67   IF(IPRNT)  89,87,89
89   WRITE (6,107)A(N,N-1)
     GO TO 86
 700 IF(ITER .GT. 50) GO TO 63
     IF(ITER .GT. 5 ) GO TO 53
 701 Z1=          ((E-AA)**2+(F-B)**2)/(E*E+F*F)
     Z2=       ((G-C)**2+(H-DD)**2)/(G*G+H*H)
     IF(Z1-0.25)  51,51,52
51   IF(Z2-0.25)   53,53,54
53   R=E*G-F*H
     SIG=E+G
     GO TO 60
54   R=E*E
     SIG=E+E
     GO TO 60
52   IF(Z2-0.25) 55,55,601
55   R=G*G
     SIG=G+G
     GO TO 60
 601 R = 0.0
     SIG = 0.0
60   XNN=A(N,N-1)
     XN2=A(N-1,N-2)
     CALL QRT(A,N,R,SIG,D)
     AA=E
     B=F
     C=G
     DD=H
     GO TO 12
104  FORMAT(////1X, 9HREAL PART  6X  14HIMAGINARY PART, 26X
    1  13HTAKEN AS ZERO 6X 4HITER //)
105  FORMAT(1X,E15.8,3X,E15.8, 42X I3)
107  FORMAT(56X  E13.8)
      END
```

b) Computer program used to calculate the coefficients defining the load versus lateral deflection relation.

The computer program listed on the following pages calculates the coefficients L, J and K given in equation (69). These coefficients define the load versus lateral deflection relation of a panel and are identified in the program as follows:

$$J = -XJ$$

$$K = XK$$

$$L = XL(P_y) + XLL$$

The data which must be put into the computer is identified in the following manner:

$$\alpha = ANG$$

$$n = XN$$

$$H_x = HX$$

$$H_y = H$$

$$H_{xy} = HZ$$

$$a = A$$

$$b = B$$

B1

```
      READ(5,100) KOUNT
  100 FORMAT(I3)
      DO 13 J=1,KOUNT
   30 READ(5,1)ANG,XN,HX,H,HZ,A,B
    1 FORMAT(8F10.5)
      PI=3.14159
      PI2=PI**2.
      PI4=PI**4.
      PI6=PI**6.
      PI8=PI**8.
      XN2=XN**2.
      XN4=XN**4.
      XN6=XN**6.
      XN8=XN**8.
      ANG2=ANG**2.
      ANG4=ANG**4.
      ANG6=ANG**6.
      A2=A**2.
      A3=A**3.
      A5=A**5.
      A7=A**7.
      B2=B**2.
      B3=B**3.
      B5=B**5.
      B7=B**7.
      BET=PI2/B2+(ANG2*XN2*PI2)/A2
      XL1=(ANG*XN2*PI2*B)/(4.*A)
      XL2=(HX*XN4*PI4*B)/(8.*A3)
     0XL3=H*((PI4*A)/(8.*B3)+(3.*ANG2*XN2*PI4)/(4.*A*B)+(ANG4*XN4*PI4*B)
     1/(8.*A3))
      XL4=HZ*((XN2*PI4)/(8.*A*B)+(ANG2*XN4*PI4*B)/(8.*A3))
      XL=XL1
      XLL=XL2+XL3+XL4
      XJ1=-(HX*9.*XN6*PI6*B)/(128.*A5)
     0XJ2=H*((3.*ANG2*XN2*PI4*BET)/(16.*A*B)-(BET**2.)*((9.*PI2*A)/(128.
     1*B)+(9.*ANG2*XN2*PI2*B)/(128.*A))-(9.*ANG2*XN2*PI6)/(32.*A*B3)-(9.
     2*ANG4*XN4*PI6)/(32.*A3*B))
      XJ=XJ1+XJ2
      XK1=(HX*15.*XN8*PI8*B)/(256.*A7)
     0XK2=H*((BET**2.)*((15.*A*PI4)/(256.*B3)+(15.*ANG4*XN4*PI4*B)/(256.
     1*A3)+(9.*ANG2*XN2*PI4)/(128.*A*B))-BET*((3.*ANG2*XN2*PI6)/(16.*A*B
     23)+(3.*ANG4*XN4*PI6)/(16.*A3*B))+(15.*ANG2*XN2*PI8)/(64.*A*B5)+(15
     3.*ANG6*XN6*PI8)/(64.*A5*B)+(9.*ANG4*XN4*PI8)/(32.*A3*B3))
      XK=XK1+XK2
      WRITE(6,2) XL
    2 FORMAT(1X, 6H XL = ,F15.5)
```

```
      WRITE(6,3) XL2
    3 FORMAT(1X, 7H XL2 = ,F15.5)
      WRITE(6,4) XL3
    4 FORMAT(1X, 7H XL3 = ,F15.5)
      WRITE(6,5) XL4
    5 FORMAT(1X, 7H XL4 = ,F15.5)
      WRITE(6,6) XLL
    6 FORMAT(1X, 7H XLL = ,F15.5)
      WRITE(6,7) XJ1
    7 FORMAT(1X, 7H XJ1 = ,F15.5)
      WRITE(6,8) XJ2
    8 FORMAT(1X, 7H XJ2 = ,F15.5)
      WRITE(6,9) XJ
    9 FORMAT(1X, 6H XJ = ,F15.5)
      WRITE(6,10) XK1
   10 FORMAT(1X, 7H XK1 = ,F15.5)
      WRITE(6,11) XK2
   11 FORMAT(1X, 7H XK2 = ,F15.5)
      WRITE(6,12) XK
   12 FORMAT(1X, 6H XK = ,F15.5)
   13 CONTINUE
      CALL EXIT
      END
```

c) Computer program used to calculate shear deflections.

The shear deflections are computed by the use of this program in the following manner;

$$\text{Shear deflection} = D_3 - \left[D_1 + (D_2 + D_4)\frac{\ell_1}{\ell_2}\right] - \Delta_B$$

in which D_1, D_2, D_3 and D_4 are gage readings, Δ_B is the bending deflection of the basic frame, and ℓ_1 and ℓ_2 are pin-to-pin dimensions as noted in the following figure:

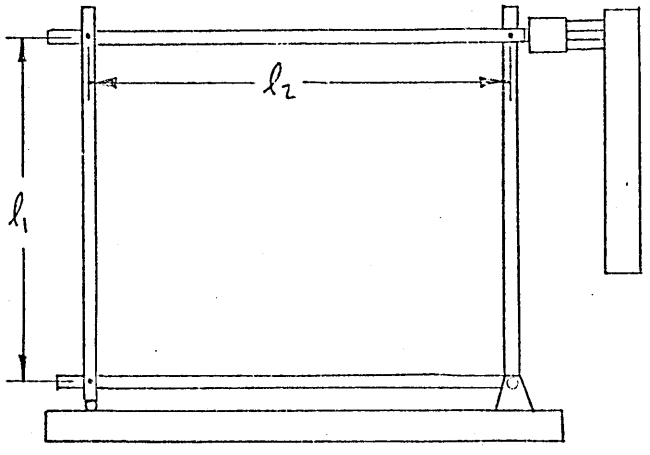

The dimensions ℓ_1 and ℓ_2 corresponding to each panel are listed below:

Panel	ℓ_1 (ft)	ℓ_2 (ft)
Butlerib (9 x 13.58)	14.1875	8.8125
Butlerib (15 x 13.58)	14.1875	14.8125
Butlerib (9 x 9.58)	10.1875	8.8125
Butlerib (15 x 9.58)	10.1875	14.8125
Sine-wave	10.4479	8.8125
M36 (3 x 8)	8.4479	3.7500
M36 (6 x 12)	12.4479	6.7500
M36 (9 x 12)	12.4479	9.7500

The symbols representing the necessary input for the program are defined as follows:

DES = test number

PAN, EL, DESC, RIP = Panel description

A = ℓ_1 (ft.)

C = actual dimension of the panel in the x direction (ft.)

PULT = Ultimate load (lb/10)

NO = number of load readings including the zero reading

B = ℓ_2 (ft.)

P = Applied load (lb/10)

D1, D2, D3, D4 = gage readings (in.)

```
      DIMENSION P(60),D1(60),D2(60),D3(60),D4(60)
    1 READ(2,2)DES,PAN,EL,DESC,RIP,A,C,PULT,NO,B
    2 FORMAT (A4,6X,4A5,3F10.4,I2,8XF10.4)
      READ(2,3)P(1),D1(1),D2(1),D3(1),D4(1)
    3 FORMAT (5F10.4)
      WRITE (3,4)DES,PAN,EL,DESC,RIP
    4 FORMAT (45X19HDIAPHRAGM TEST DATA//28X17HTEST DESIGNATION A4,4X8HP
     1ANEL - 4A5/)
      PULT=(PULT-P(1))*10.
      DELTB=PULT*8.*A*A*A/29500000./B/B/5.522+.00005
      WRITE(3,5)A,B,PULT,DELTB
    5 FORMAT (3X10HLENGTH A =F8.4,16H FT    WIDTH B =F8.4,17H FT    ULT
     1LOAD =F7.0,28H LBS   ULT BEND DEFLECTION =F7.4,3H IN///22X4HLOAD5X
     25HSHEAR12X22HGAUGE DEFLECTIONS - IN10X5HSHEAR/78X10HDEFLECTION//21
     3X5H(LBS)3X8H(LBS/FT)6X2HD18X2HD28X2HD38X2HD46X4H(IN)/)
      DO 10 I=2,NO
      READ(2,3)P(I),D1(I),D2(I),D3(I),D4(I)
      PC=(P(I)-P(1))*10.
      SC=PC/C+.5
      D1C=D1(1)-D1(I)
      D2C=D2(I)-D2(1)
      D3C=D3(I)-D3(1)
      D4C=D4(1)-D4(I)
      IF(D2C)6,9,9
    6 D2C=-D2C
    9 DELTT=D3C-(D1C+(D2C+D4C)*A/B)
      DELTB=PC*8.*A*A*A/29500000./B/B/5.522
      DELTS=DELTT-DELTB+.00005
   10 WRITE(3,11)PC,SC,D1C,D2C,D3C,D4C,DELTS
   11 FORMAT (19XF7.0,F10.0,2F10.4,F10.3,2F10.4)
      WRITE(3,12)
   12 FORMAT (1H1)
      GO TO 1
      END
```